universität wien

DISSERTATION / DOCTORAL THESIS

Titel der Dissertation /Title of the Doctoral Thesis

„Regulation of Stem Cell Lineages“

verfasst von / submitted by

Merve Deniz Abdusselamoglu

angestrebter akademischer Grad / in partial fulfilment of the requirements for the degree of

Doctor of Philosophy (PhD)

Wien, 2019 / Vienna, 2019

Studienkennzahl lt. Studienblatt / degree programme code as it appears on the student record sheet:	UA 794 685 490
Dissertationsgebiet lt. Studienblatt / field of study as it appears on the student record sheet:	Molekulare Biologie / Molecular Biology
Betreut von / Supervisor:	Mag. Dr. Jürgen A. Knoblich

Regulation of Stem Cell Lineages

By

Merve Deniz Abdusselamoglu

Acknowledgements

I would like to express my gratitude to my supervisor Juergen A Knoblich who gave me this chance to work in this fantastic scientific environment, guided me through PhD, and always reminded me the big picture.

I would like to thank my PhD committee, Julius Brennecke, Luisa Cochella and Thomas Hummel, for guiding me through my project but always giving me useful advice.

I would like to thank all past and current member of Knoblich lab I shared my time and enthusiasm in science with. It is always a nurturing environment.

Thank you to Elif Eroglu, who started this project and showed me how to dissect larval brain for the first time.

Thank you to Francois Bonnay who shared the same desk with me as well as his endless knowledge in Drosophila. Many times, you were the helping hand I needed.

Thank you to Sebastian Wissel, who is the best partner in crime.

Thank you, Christopher Esk for always being the best bay buddy ever.

Thank you, Josh Bagley for being such a great friend but also a much-needed mentor in every aspect of life.

A big thank you to Dominik Lindenhofer who was there with me all the time when I needed a distraction.

Thank you to Lisa Landskron, Veronica Krenn, Hilary Gustafson, Daniel Reumann, Tom Kruitwagen, Jaydeep Sidhaye, Sunanjay Bajaj, Oliver

Eichmuller, Camilla Bosone and Shan Bian for the fun we had together and the conversations about science.

A big thank you to my best friend Robin Burns for always being there for me and being the best person to share every experience with.

I would like to also thank to my great friends, Marialaura, Hagar, Lily, Pooja, Duygu, Mary, Julien. Your friendships are the best thing I gained from my time in Vienna.

Canim kedim Miss Piggy, bana bu zorlu yolda hayat arkadasi oldugun ve her zaman yuzumu guldurdugun icin tesekkurler. Iyiki varsin.

Canim Ailem, Annem Buket ve Babam Sükrü, sizler olmadan yasadiklarimin hicbiri gerceklesmezdi. Hem varliginiz ile hem de sonsuz desteginiz ile beni buralara getirdiniz. Sizlere minnetarim. Hersey icin tesekkurler. Ayrica tum aileme, Anneannem, Babaannem, Dedelerim, Amcam, Dayim ver Yengelerime cok teşekkür ederim.

Canim, biricik kardesim Cemre. Sadece bu PhD degil hersey seninle daha guzel. Hersey bitip herkes gittiginde yine ikimizin beraber olacagini bilmek dunyanin en guzel duygusu. Seni cok seviyorum.

Table of Contents

1. SUMMARY **4**

2. ZUSAMMENFASSUNG **6**

3. INTRODUCTION **9**

3.1. DEVELOPMENT OF DROSOPHILA CENTRAL NERVOUS SYSTEM 9
3.2. TWO TYPES OF NEUROBLAST LINEAGES IN DROSOPHILA LARVAL BRAIN 13
3.3. TEMPORAL PATTERNING IN *DROSOPHILA* NEURAL STEM CELLS AND PROGENITORS 15
3.4. ASYMMETRIC CELL DIVISION OF NEUROBLASTS 19
3.5. ENSURING LINEAGE PROGRESSION – CELL FATE DETERMINANTS AND BEYOND 21
3.6. *DROSOPHILA* AS A BRAIN TUMOR MODEL 26
3.7. TRITHORAX- AND POLYCOMB-GROUP PROTEINS 28

4. AIM AND STRUCTURE OF THIS THESIS **30**

5. CHAPTER 1: THE TRANSCRIPTION FACTOR ODD-PAIRED REGULATES TEMPORAL IDENTITY IN TRANSIT-AMPLIFYING NEURAL PROGENITORS VIA AN INCOHERENT FEED-FORWARD LOOP **31**

5.1. PROLOGUE 31

6. CHAPTER 2: DYNAMICS OF ACTIVATING AND REPRESSIVE HISTONE MODIFICATIONS IN *DROSOPHILA* NEURAL STEM CELL LINEAGES AND BRAIN TUMORS **72**

6.1. PROLOGUE 72
6.2. INTRODUCTION 73
6.3. RESULTS 76
6.4. DISCUSSION 89
6.5. MATERIALS AND METHODS 91
6.6. REFERENCES 97
6.7. SUPPLEMENTARY FILES 102

7. DISCUSSION **109**

8. REFERENCES **110**

1. Summary

To achieve the complex structure of our brains, which drive our impressive cognitive and motor functions, a limited number of neural stem cells (NSCs) proliferate to generate a diverse pool of neurons and glia during development. These NSCs undergo symmetric and asymmetric cell divisions and are regulated both spatially and temporally to initiate lineages. During the lineage progression, cell fate decisions are made by gene expression programs to ensure correct development. Once a cell identity is established, its maintenance is assured by epigenetic mechanisms. Understanding the mechanisms that control the fate decisions and their maintenance is crucial to understand development and the causes of stem cell originated tumors.

Drosophila neural stem cells, called neuroblasts (NBs), are a well-established model system for stem cell biology. In larval brain, there are two types of NBs: while type I NBs divide asymmetrically to give rise a ganglion mother cell (GMC), which ultimately divides to generated two differentiated cells, type II NBs instead divide asymmetrically to generate intermediate neural progenitors (INPs), a transit amplifying cell population. INPs also undergo asymmetric cell division five to six times to give rise to an INP and a GMC, that divides one more time to generate neurons or glial cells. While it has been shown that NBs employ temporal patterning, a phenomenon where a NSC can generate diverse neurons in chronological order, in type II lineages, it has been shown that INPs also undergo temporal patterning by successively expressing Dichaete (D), grainyhead (grh) and eyeless (ey). Previously we have shown that the chromatin remodeling complex subunit Osa, and its direct target hamlet (ham) are crucial for the initiation and the progression of temporal patterning, respectively. However, the involvement of other factors and how these transitions in the patterning is achieved still remains largely unknown. In the first chapter of this thesis, we first developed a FACS-based method in order to isolate three distinct temporal states of INPs. Using transcriptomic analysis, we identified the factor odd-paired (opa), which is direct target of Osa, as a key regulator of D-to-grh transition. We

showed that opa is required for repression of D expression. Together with D and opa, Osa forms an incoherent feed-forward loop (FFL), and a new mechanism that results in successive expression of temporal identities.

During the lineage progression of NSCs, with each division, a cell fate decision has to be made depending on transcriptional programs. These programs define the cellular identities. To ensure the correct spatial and temporal gene expression of these programs, epigenetic mechanisms acts as cell's memory. While Trithorax (TrxG) group proteins are evolutionary conserved regulators of gene activation, their antagonists are Polycomb (PcG) group proteins. These regulators exert their function via histone modifications. Thus, investigating the histone landscape during development is crucial to understand functional specialization of cells. In the second chapter of this thesis, we developed a method to track in vivo changes of histone modifications upon differentiation as well as between two different NB populations, and their tumorigenic counterparts. We have analyzed genes that are specific to type II NB, and genes required for tumor formation. We also showed that type II NBs requires Polycomb repressive complex 2 (PRC2) to maintain their self-renewal potential.

Collectively, these data demonstrate yet again that *Drosophila* NB is a well-established system to study stem cell biology. During lineage progression, transcriptional programs regulate the cell fate decisions, which are assured by epigenetic mechanisms that act as cell's memory. Understanding how these transcriptional programs are established, and how they are maintained is crucial in order to understand the complexity of brain structure.

2. Zusammenfassung

Um die komplexe Struktur unseres Gehirns zu erreichen, die unsere beeindruckenden kognitiven und motorischen Funktionen antreibt, vermehrt sich eine begrenzte Anzahl neuronaler Stammzellen (NSCs), um während der Entwicklung einen vielfältigen Pool von Neuronen und Glia zu bilden. Diese NSCs durchlaufen symmetrische und asymmetrische Zellteilungen und werden sowohl räumlich als auch zeitlich reguliert, um eine zusammengehörende Reihe von differenzierten Zellen zu initiieren. Während dieses Differenzierungsprozesses werden die Entscheidungen über das Zellschicksal durch Genexpressionsprogramme getroffen, um eine korrekte Entwicklung zu gewährleisten. Sobald eine Zellidentität etabliert ist, wird ihr Erhalt durch epigenetische Mechanismen sichergestellt. Das Verständnis der Mechanismen, welche das Genprogamm der Zelle und deren Aufrechterhaltung steuern, ist entscheidend für das Verständnis der Gehirnentwicklung und der Ursachen von jenen Tumoren, die durch Stammzellen entstehen.

Die neuronalen Stammzellen von *Drosophila*, die sogenannten Neuroblasten (NBs), sind ein etabliertes Modellsystem für die Stammzellbiologie. Im Larvenhirn gibt es zwei Arten von NBs: Während sich die NBs des Typs I asymmetrisch teilen, um eine Ganglienmutterzelle (GMC) zu erzeugen, die sich letztendlich in zwei differenzierte Zellen teilt, teilen sich die NBs des Typs II asymmetrisch, um intermediäre neuronale Vorläufer (INPs), eine transitverstärkende Zellpopulation, zu erzeugen. INPs durchlaufen auch eine asymmetrische Zellteilung fünf- bis sechsmal, sodass ein INP und ein GMC entstehen, die sich noch einmal teilen, um Neuronen oder Gliazellen zu erzeugen. Während gezeigt werden konnte, dass NBs zeitliche Musterung verwenden, ein Phänomen, bei dem ein NSC verschiedene Neuronen in chronologischer Reihenfolge erzeugen kann, wurde in Typ-II-Differenzierungen gezeigt, dass INPs auch zeitliche Musterung durchlaufen, indem sie Dichaete (D), Grainhead (grh) und eyeless (ey) nacheinander exprimieren. Zuvor haben wir gezeigt, dass das Chromatin,

das die komplexe Untereinheit Osa umgestaltet, und sein direkter Zielort hamlet (ham) für die Einleitung bzw. das Fortschreiten der zeitlichen Musterung entscheidend sind. Die Einbeziehung anderer Faktoren und wie diese Übergänge in der Musterung erreicht werden, ist jedoch noch weitgehend unbekannt. Im ersten Kapitel dieser Arbeit, entwickelten wir zunächst eine FACS-basierte Methode, um drei verschiedene zeitliche Zustände von INPs zu isolieren. Mit Hilfe der transkriptomischen Analyse identifizierten wir den Faktor odd-paired (opa), der ein direktes Ziel von Osa ist, als einen Schlüsselregulator für den Übergang von D zu grh. Wir haben gezeigt, dass Opa für die Unterdrückung der D-Expression erforderlich ist. Zusammen mit D und opa bildet Osa eine inkohärente Feed-Forward-Schleife (FFL) und einen neuen Mechanismus, der zu einer sukzessiven Expression zeitlicher Identitäten führt.

Während der Linienentwicklung der NSCs muss bei jeder Division eine Zellschicksalentscheidung in Abhängigkeit von den Transkriptionsprogrammen getroffen werden. Diese Programme definieren die zellulären Identitäten. Um die korrekte räumliche und zeitliche Genexpression dieser Programme zu gewährleisten, fungieren epigenetische Mechanismen als Gedächtnis der Zelle. Während die Familie der Trithorax (TrxG) Proteine evolutionär konservierte Regulatoren der Genaktivierung sind, sind ihre Antagonisten die Familie Polycomb (PcG) Proteine. Diese Regler üben ihre Funktion über Histonmodifikationen aus. Daher ist die Untersuchung der Histonlandschaft während der Entwicklung entscheidend für das Verständnis der funktionellen Spezialisierung von Zellen. Im zweiten Kapitel dieser Arbeit, entwickelten wir eine Methode zur Verfolgung in vivo Änderungen von Histon-Modifikationen nach der Differenzierung sowie zwischen zwei verschiedenen NB-Populationen, und ihre tumorigenen Gegenstücke. Wir haben Gene analysiert, die spezifisch für Typ II NB sind, und Gene, die für die Tumorbildung benötigt werden. Wir zeigten auch, dass Typ II NBs den repressiven Polycomb-Komplex 2 (PRC2) benötigen, um ihr Selbsterneuerungspotenzial zu erhalten.

Zusammengenommen zeigen diese Daten einmal mehr, dass *Drosophila* NB ein etabliertes System zur Untersuchung der

Stammzellbiologie ist. Während der Progression der Linie regulieren Transkriptionsprogramme die Entscheidungen des Zellschicksals, die durch epigenetische Mechanismen gewährleistet werden, die als Gedächtnis der Zelle fungieren. Das Verständnis, wie diese Transkriptionsprogramme etabliert sind und wie sie gepflegt werden, ist entscheidend, um die Komplexität der Gehirnstruktur zu verstehen.

3. Introduction

In order to achieve highly complex cognitive and motor functions, our brains are composed of thousands of networks containing vast arrays of functionally and morphologically distinct neurons and glia cells. During central nervous system (CNS) development, limited pool of neural stem cells (NSCs) undergo repeated symmetric and/or asymmetric cell divisions. These NSCs are regulated spatially and temporally to generate an enormous number of the aforementioned diverse set of cells. Gene expression programs are required to determine cell fate decisions and must be maintained during lineage progression. Thus, understanding the maintenance and decision behind a cell fate is an exciting field in brain development with many burning questions.

Drosophila melanogaster has been a favorable model system to understand and dissect mechanisms that underlie brain development (Brand & Livesey, 2011; Homem & Knoblich, 2012). The availability of genetic tools along and the simplicity of its development has together made *Drosophila melanogaster* an instrumental organism in furthering neural stem cell biology. The NSCs of *Drosophil*a undergo asymmetric cell division which generates progeny that can be readily identified by their marker expression and birth order (Brand & Livesey, 2011; Reichert, 2011; Weng & Lee, 2011). The following introduction will therefore a provide necessary background on the development of *Drosophila* CNS and will further describe the mechanisms behind their cell fate decisions and maintenance.

3.1. Development of Drosophila central nervous system

The life cycle of *Drosophila* consists of four successive stages: egg, larva, pupa and adult (Figure 1). Upon fertilization, chorion, a protective envelope, covers the embryo. In the first instar, larvae hatch from the eggs and grow rapidly in order to transition to the next stages of larval development; the second and the third instar. In the pupal stage, due to the

pupal case, pupa is stationary, and undergoes metamorphosis into the adult fly (Jennings, 2011). The developmental period of a fly is about 10 days at 25°C, while the average lifespan of an adult fly is about 50 days. Importantly, both of these time-frames are temperature-dependent (Linford, Bilgir, Ro, & Pletcher, 2013).

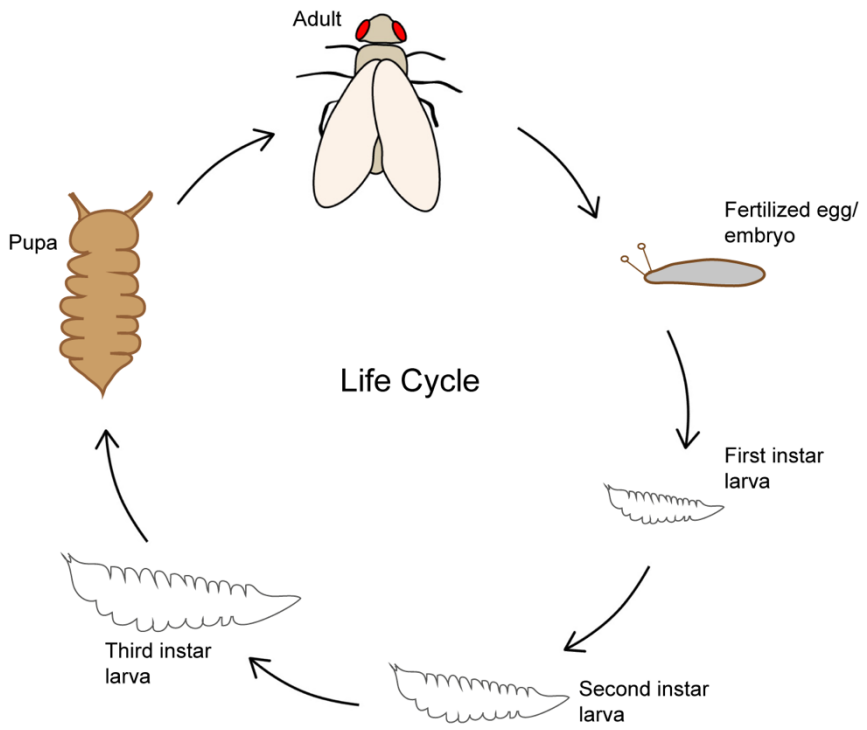

Figure 1. Life cycle of *Drosophila*.

Life cycle of *Drosophila* consists of four successive stages: Embryo – Larva – Pupa – Adult.

During the development of a fly brain, all neurons and glia cells arise from neural stem cells called neuroblasts (NBs), in two consecutive waves (White & Kankel, 1978) (Figure 2). During embryogenesis, neuroblasts reside in the ventrolateral region of embryo in a neuroepithelium, where they delaminate from, and start dividing (Homem & Knoblich, 2012) (Figure 3A). These embryonic NBs are specified via restriction of pro-neural genes to individual cells by Notch/Delta signaling (Artavanis-Tsakonas & Simpson, 1991). After delamination, NBs start dividing asymmetrically to generate one cell with the capacity of self-renewal and another, smaller cell called ganglion

mother cell (GMC). GMCs divide one more time to give rise to two post-mitotic neurons or glia cells (Skeath & Thor, 2003; Wu, Egger, & Brand, 2008). In this first wave of neurogenesis, NBs divide asymmetrically twelve times, and they are incapable of growing after each division, which causes them to shrink progressively (Fuse, Hisata, Katzen, & Matsuzaki, 2003). Meanwhile, they express transient low level of Prospero (Lai & Doe, 2014), a protein which represses self-renewal and cell-cycle genes (Choksi et al., 2006). Thus, at the end of embryogenesis, these small NBs enter quiescence (Prokop & Technau, 1991) and remain inactive via Salvador/Hippo/Warts signaling (Ding, Weynans, Bossing, Barros, & Berger, 2016). These quiescent NBs are mainly arrested in G2 phase, though some of them are in G0 phase (Otsuki & Brand, 2018).

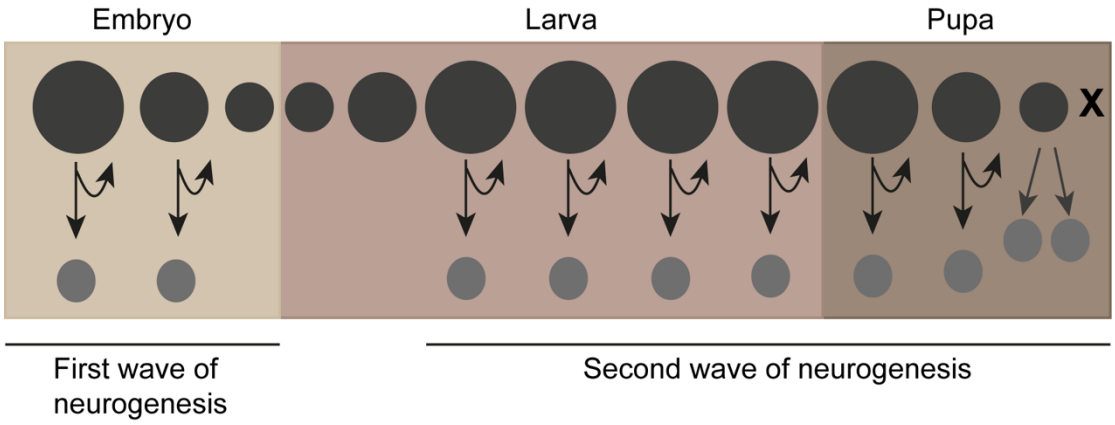

Figure 2. Neurogenesis in *Drosophila*.

Neurogenesis in *Drosophila* happens in two waves. Schematic of neuroblasts (in dark gray) producing differentiated progeny (in light gray) from embryonic to pupal stages. During embryogenesis, dividing NBs shrink with each division, resulting in them to enter quiescence. Upon larval feeding, NBs regrow and start proliferating to give rise to 90% of the adult brain. Finally, in pupal stages, NBs shrink with each division and ultimately disappear.

Early after larval hatching, larval feeding starts, which triggers the regrowth of NBs and resumes their proliferation (Figure 2). Upon food-uptake, the Target of Rapamycin (TOR) pathway is activated in the fat body, a mammalian liver-like tissue (Colombani et al., 2003; Sousa-Nunes, Yee, &

Gould, 2011). After TOR activation, signals from fat body stimulate glial cells in order to initiate insulin-like peptides secretion (Chell & Brand, 2010). Meanwhile, food uptake leads to the inactivation of Hippo pathway, subsequently resulting in the translocation of Yorkie, a transcriptional coactivator leading to neuroblast cell growth and proliferation (Ding et al., 2016). In contrast to embryonic NBs, post-embryonic NBs re-grow to their original size after each division. This allows them to divide multiple times to constitute 90% of cells of the adult CNS (Homem & Knoblich, 2012; Truman & Bate, 1988).

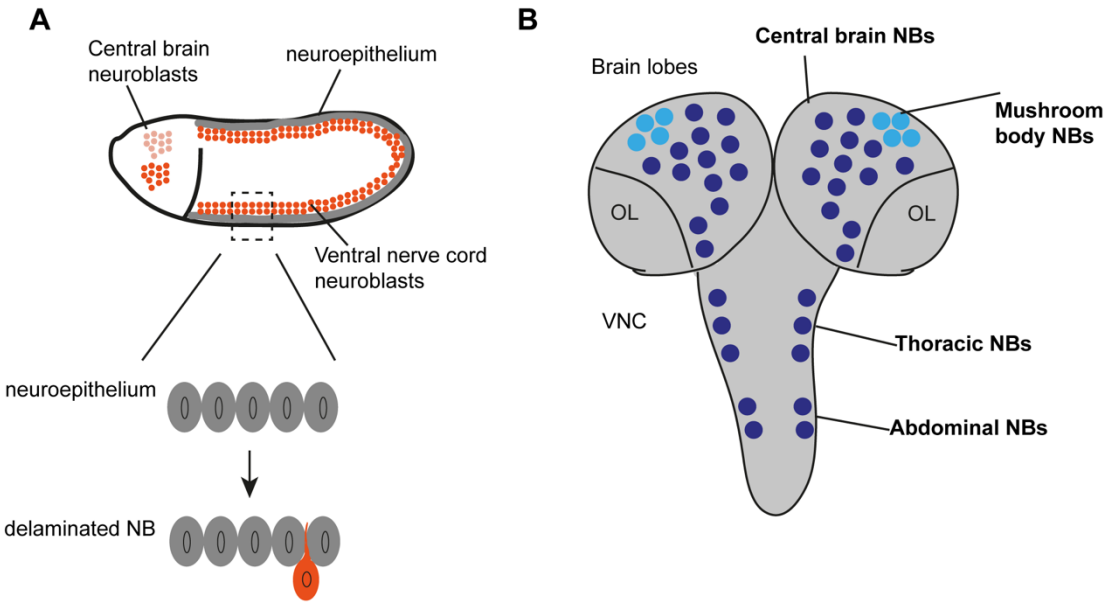

Figure 3. *Drosophila* brain development.

(A) Neuroblasts delaminate from the neuroepithelium in *Drosophila* embryo. **(B)** Larval brain consists of two brain lobes including optic lobes (OL) and the ventral nerve cord (VNC). There are different types of NBs in the larval brain.

The larval brain consists of two lobes with optic lobes and a ventral nerve cord (VNC) (Figure 3B). In each lobe, there are four mushroom body (MB) NBs, optic lobe (OL) NBs, type I and type II NBs exist, whereas there are thoracic and abdominal NBs are in the VNC (Figure 3B). Each of these distinct NB populations disappear at different developmental stages (Homem

et al., 2014; Maurange, Cheng, & Gould, 2008b; Siegrist, Haque, Chen, Hay, & Hariharan, 2010).

3.2. Two types of neuroblast lineages in Drosophila larval brain

The larval brain of *Drosophila* is largely composed of type I and type II NBs. As this thesis focuses on these two NBs, their lineage progression will be discussed in detail here.

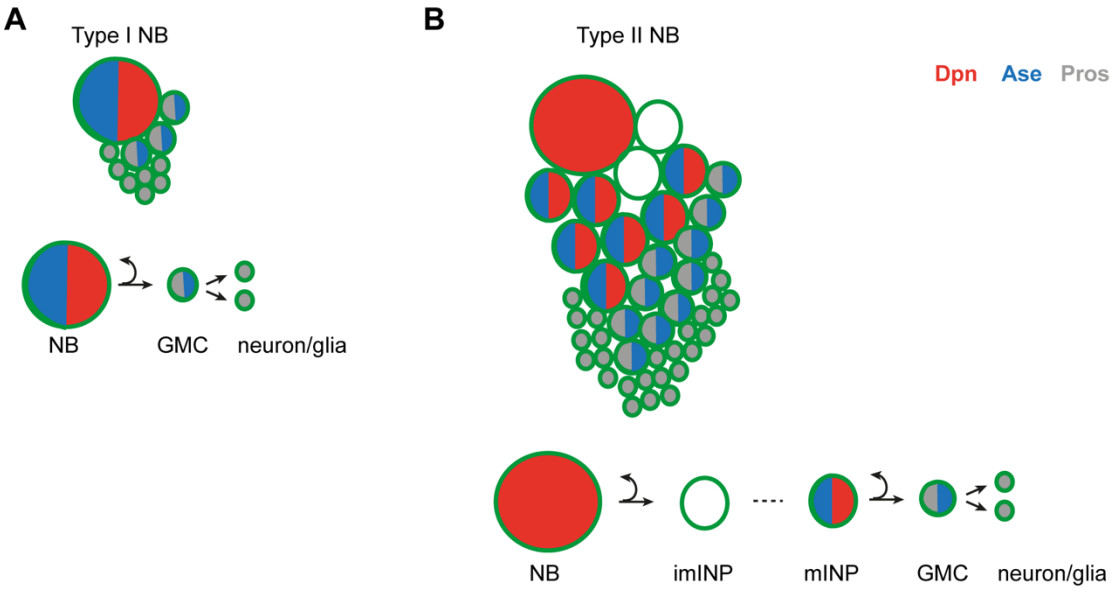

Figure 4. Neuroblast lineages of the *Drosophila* larval CNS.

(A) Type I NB lineage is shown in detail. These NBs divide asymmetrically to give rise to GMC, which divides on more time to generate neurons/ glia cells. Asense (Ase), Deadpan (Dpn) and Prospero (Pros) were depicted. **(B)** Type II NB lineage is shown. Unlike type I, these lineages have transit amplifying cell population called intermediate neural progenitors (INPs), that undergo maturation.

Type I and type II NBs can be distinguished depending on the marker expression patterns, their location in the brain, and their lineage architecture (Homem & Knoblich, 2012). Per lobe, around 85 type I NBs per lobe constitute the majority of central brain (Ito & Hotta, 1992), while there are only

8 type II NBs (Bello, Izergina, Caussinus, & Reichert, 2008; Boone & Doe, 2008; Bowman et al., 2008). In parallel to embryonic NBs, type I NBs divide asymmetrically to produce one larger cell with a self-renewal capacity, and a smaller GMC that divides one more time and generates two post-mitotic neurons and glia cells (Figure 4A). Type I NBs express key self-renewal transcription factors (TFs), such as Deadpan (Dpn), Helix-loop-helix mγ (HLHmγ), and Klumpfuss (Klu) along with Asense (Ase) (Bello et al., 2008; Berger et al., 2012; Boone & Doe, 2008; Bowman et al., 2008; San-Juán & Baonza, 2011; Xiao, Komori, & Lee, 2012; Zacharioudaki, Magadi, & Delidakis, 2012). In addition to these markers, type I NBs also have low levels of Prospero present in their cytoplasm (Bello et al., 2008; Boone & Doe, 2008; Bowman et al., 2008).

In contrast to type I NB, type II NBs have a more complex lineage structure (Figure 4B). They divide asymmetrically to generate a transit amplifying cell population called intermediate neural progenitors (INPs) (Bello et al., 2008; Boone & Doe, 2008; Bowman et al., 2008). At first, these immature INPs (imINPs) are in a cell cycle arrest, which later undergo maturation program to become mature INPs (mINPs). Post maturation, mINPs can asymmetrically divide between 5-6 times giving rise to GMCs, which then generate neurons/ glia cells through a final cell divison. While type II NBs are generated later in the embryo as in stage 12, their identity is specified via EGFR signaling (Álvarez & Díaz-Benjumea, 2018; Walsh & Doe, 2017). The progeny from type II NBs is integrated into the adult neuropile structure, called central complex (Bayraktar, Boone, Drummond, & Doe, 2010; Izergina, Balmer, Bello, & Reichert, 2009; Viktorin, Riebli, Popkova, Giangrande, & Reichert, 2011). Similar to type I NBs, type II NBs also express Dpn, HLHmγ and Klu. In contrast to type I, the Ets TF Pointed is exclusively expressed in type II NBs, where it represses the expression of Ase (Zhu, Barshow, Wildonger, Jan, & Jan, 2011). During the maturation of INPs, imINPs first turn on Ase expression, which is then followed by Dpn expression. In addition, INPs also express TF Earmuff (Erm) (Janssens et al., 2017; Weng, Golden, & Lee, 2010). In both lineages, GMCs can be identified by nuclear TF Prospero

(Pros) and Ase, neurons are characterized by the expression of Pros as well as the RNA-binding protein embryonic lethal abnormal vision (elav) {Campos:td}. It has been recently shown that the type II NB identity is established by the SET1/MLL protein Trithorax via TF buttonhead and Sp1 (Álvarez & Díaz-Benjumea, 2018; Komori, Xiao, Janssens, Dou, & Lee, 2014a; Xie et al., 2014), where a NB can generate INPs. Due to the combination of all these markers, cell size and the lack of cell migration during larval brain development (Dumstrei, Wang, & Hartenstein, 2003), each cell type can be identified, which allows for a detailed investigation into stem cell biology.

In the pupal stages, both NBs undergo a metabolic switch from glycolysis to oxidative phosphorylation to uncouple cell growth and cell cycle progression. Thus, NBs start to shrink after each cell division (Homem et al., 2014), This process is mediated by ecdysone hormone and mediator complex. Ultimately, these shrunken NBs terminally differentiate because of the accumulation of Pros in the nucleus (Maurange, Cheng, & Gould, 2008a). It has been recently shown that the levels of two RNA-binding protein, IGF-II mRNA-binding protein (Imp) and Syncrip (Syp) play a role in the NB decommissioning (Yang et al., 2017). For instance, the levels of Imp in mushroom body (MB) NBs decline slower compared to other NBs, which results in MB NBs to continue proliferation. It has been also suggested that MB NBs can avoid decommissioning via uncoupling proliferation from dietary amino acids by expressing Eyeless (ey) (Sipe & Siegrist, 2017), unlike type I and type II NBs.

3.3. Temporal patterning in *Drosophila* neural stem cells and progenitors

How can this seemingly homogenous population of neural stem cells produce high levels of neural diversity? Morphogen gradients and their signaling cascades provide spatial information to NSCs to generate neural diversity (Bhat, 1999; Dessaud, McMahon, & Briscoe, 2008; Xin Li et al., 2013). However, it has been shown that when progenitors are cultured *in*

vitro, they were still capable of generating diverse neuron types in chronological order, suggesting an intrinsic mechanism is involved (Gaspard et al., 2008; Naka, Nakamura, Shimazaki, & Okano, 2008). Other than spatial information, NSCs employ temporal patterning (also known as 'temporal clock'), a phenomenon where NSCs acquire new features to give rise to different types of progeny over time. *Drosophila* NBs also undergo temporal patterning in order to determine their age or temporal identity, which defines the fate of the progeny.

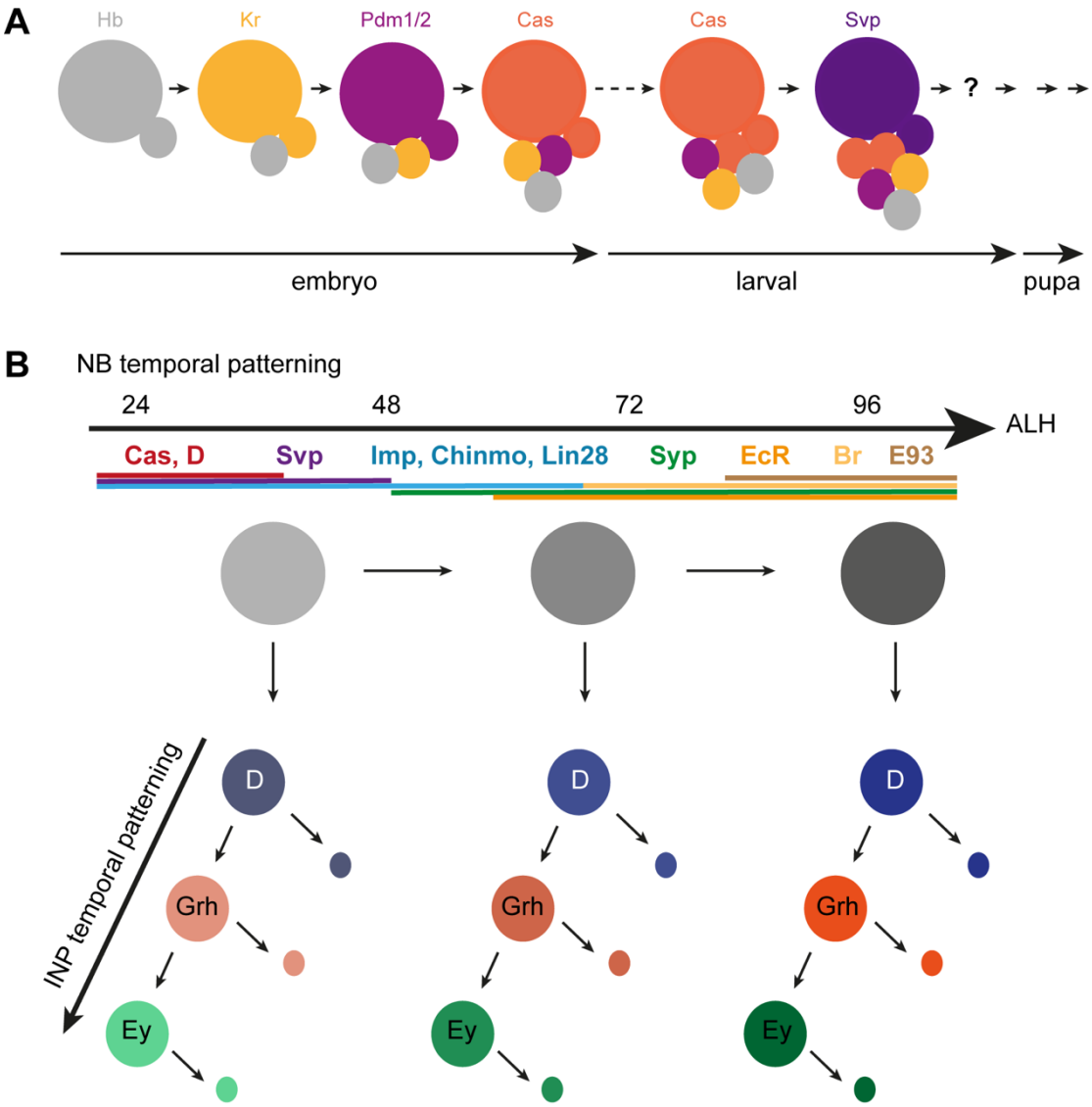

Figure 5. Temporal patterning during *Drosophila* CNS development.
(A) During embryonic and larval stages, NBs express a set of TFs sequentially, which are inherited by their progeny to define neuronal fates. Adapted from Homem et al., 2012. **(B)** The combination of NB temporal clock, together with INP temporal clock, generates great diversity in the progeny. Adapted from (Holguera & Desplan, 2018).

During embryogenesis, NBs follow a cascade of transcription factors (TFs) sequentially to define the competence of NBs: Hunchback (Hb) – Kruppel (Kr) – POU domain protein 1 and 2 (Pdm1/2) – Castor (Cas) (Baumgardt, Karlsson, Terriente, Díaz-Benjumea, & Thor, 2009; Grosskortenhaus, Pearson, Marusich, & Doe, 2005; Grosskortenhaus, Robinson, & Doe, 2006; Isshiki, Pearson, Holbrook, & Doe, 2001) (Figure 5A). The progenies of the NBs maintain the expression of the TFs that is present at the time of their birth. Most of the transitions from one identity to another is regulated via feedback and feed-forward loops. However, the first transition from Hb to Kr requires cytokinesis, suggesting that the number of NB divisions play a role in timing the temporal identity of NBs (Grosskortenhaus et al., 2005). Meanwhile TF Seven-up (Svp) suppresses Hb further transcriptionally (Kanai, Okabe, & Hiromi, 2005; Mettler, Vogler, & Urban, 2006). The subsequent transitions are independent of cell cycle, since these transitions occur even in G2- arrested NBs (Grosskortenhaus et al., 2005). Recently, it has been demonstrated that *hb* gene is initially transcriptionally downregulated, which was followed by the re-localization of *hb* locus to nuclear periphery, silencing it permanently (Kohwi, Lupton, Lai, Miller, & Doe, 2013). Additionally, another study also demonstrated that the Polycomb repressor complex is regulating the competence window to Kr (Touma, Weckerle, & Cleary, 2012). These findings together demonstrate that temporal patterning is regulated in a more complex manner than mere transcriptional on/off switches since chromatin reorganization clearly plays a role.

In the larval brain, NBs express Cas and Svp in the first 48 hours after larval hatching (Bayraktar & Doe, 2013; Homem et al., 2014; Maurange, Cheng, & Gould, 2008b). While the early-born neurons express TF Chinmo,

the late-born neurons are smaller in size and are positive for Broad-Complex (Br-C) (Maurange, Cheng, & Gould, 2008b). Larval NBs also express two RNA-binding proteins, IGF-II mRNA-binding protein (Imp) and Syncrip (Syp) in an opposing gradient manner (Z. Liu et al., 2015). For mushroom body NBs, these two RNA-binding proteins control the expression of Chinmo post-transcriptionally in order to establish a temporal gradient that specifies neuronal fates (Dillard, Narbonne-Reveau, Foppolo, Lanet, & Maurange, 2018; Z. Liu et al., 2015; Zhu et al., 2006).

On top of its complex lineage architecture, type II NBs also have a complex temporal patterning, employing the process in a two-dimensional manner (Bayraktar & Doe, 2013; Syed, Mark, & Doe, 2017) (Figure 5B). In type II NB lineages, younger NBs express Cas, Dichaete (D), Svp, Chinmo, Imp and Lin28. While Cas, D and Svp expression lasts up to 48 hours after larval hatching (ALH), Imp, Chinmo and Lin28 expression gradually decreases 48 h post ALH. This is complementary to increasing Syp levels beginnning at 48 h ALH, followed by the expression of ecdysone receptor (EcR), triggered by Svp. Expression of EcR renders NBs susceptible to ecdysone signaling, thus, NBs transition from early (Chinmo/ Imp/ Lin28) to late (Broad/ Syp/ Ecdysone-induced protein 93F (E93)) states (Syed et al., 2017). In addition to NB temporal patterning, transit-amplifying cells in these lineages (INPs) are also temporally patterned. INPs express three TFs sequentially: Dichaete (D) – Grainyhead (grh) – Eyeless (ey) (Bayraktar & Doe, 2013). Transitions in INP temporal patterning has been suggested to work in 'feedforward activation and feedback repression' mechanism (Bayraktar & Doe, 2013; Doe, 2017). However, how these transitions are achieved remain elusive. In conclusion, the combination of NB temporal identity, together with INP temporal identity, is required to achieve neuronal diversity. For example, 'young' (D^+) INPs born from late temporal state NBs give rise to Brain-specific homeobox $(Bsh)^+$ neurons. Meanwhile, 'old' (ey^+) INPs from early temporal identity NBs produce Reversed polarity $(Repo)^+$ glial cells (Bayraktar & Doe, 2013). However, how and if these two temporal clocks regulate each other remains unknown.

3.4. Asymmetric cell division of neuroblasts

One of the key features of stem cells is the ability to divide asymmetrically in order to generate two daughter cells with different fates. While this process can be achieved stochastically, by extrinsic signals or intrinsic cues, *in vitro* live cell imaging experiments of NBs illustrated that different cell fates are established via an intrinsic mechanism in NB divisions (Broadus & Doe, 1997; Ceron, Tejedor, & Moya, 2006; Homem, Reichardt, Berger, Lendl, & Knoblich, 2013). Indeed, NBs rely on the asymmetric segregation of cell fate determinants to generate progeny with different cell fates. This process is achieved in a stepwise fashion: 1) establishment of axis polarity, 2) alignment of mitotic spindle in line with axis polarity, and 3) asymmetric localization and differential segregation of cell fate determinants (Juergen A Knoblich, 2010) (Figure 6).

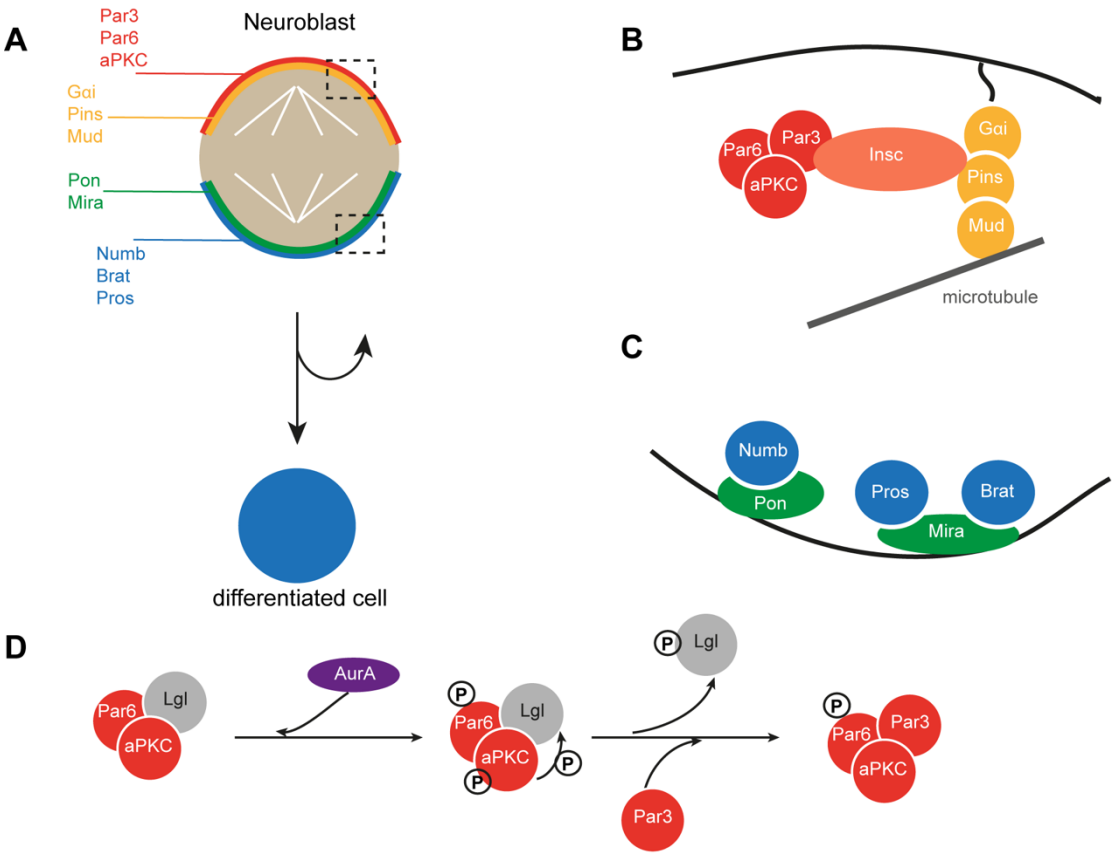

Figure 6. The asymmetric cell division machinery.

(A) A cartoon depiction of NB dividing asymmetrically. The Par complex localizes to apical side, leading localization of cell fate determinants basally. **(B)** Orientation of mitotic spindle via Gαi/ Pins/ Mud complex. **(C)** The cell fate determinants Numb, Brat and Pros localize basally through their adaptor proteins Pon and Mira, respectively. **(D)** A cartoon depicting the dynamics of the Par complex through cell division. (Adapted from Lisa Landskron).

Early in development, when embryonic NBs delaminate from neuroectoderm, they inherit an apical-basal polarity (Rebollo, Roldán, & Gonzalez, 2009). Afterwards, centrosomes act as the apical reference for subsequent cell divisions (Rebollo et al., 2007; Rusan & Peifer, 2007). Molecularly, the Partitioning defective (Par) complex, composed of Par3 (Bazooka), Par6 and atypical protein kinase (aPKC), establishes polarity by localizing to the apical side of the cell (Figure 6A).

After axis polarity has been established, mitotic spindle is oriented via the adaptor protein Inscuteable (Insc) (Kraut, Chia, Jan, Jan, & Knoblich, 1996). Insc bridges the Par complex with that of Gαi /Partner of Insc (Pins) /mushroom body defect (Mud) complex (Kraut et al., 1996; Schaefer, Petronczki, Dorner, Forte, & Knoblich, 2001; Schaefer, Shevchenko, & Knoblich, 2000). Gαi is required to tether the complex to plasma membrane, while Pins is required for the localization of Insc. Mud attaches the complex to the astral microtubules in order to orient the spindle poles along the axis polarity (Bowman, Neumueller, Novatchkova, Du, & Knoblich, 2006; Izumi, Ohta, Hisata, Raabe, & Matsuzaki, 2006; Siller, Cabernard, & Doe, 2006) (Figure 6B).

Finally, cell fate determinants localize and hence segregate asymmetrically. During interphase, all three cell fate determinants, Numb, Brain tumor (Brat), and Prospero (Pros), are localized uniformly to the cell cortex. During mitosis, the Par complex directs cell fate determinants to basal pole via an interplay between kinases and phosphatases, particularly via serine/threonine kinase aPKC. While in interphase, aPKC is in a complex with Par6 along with cytoskeleton protein lethal (2) giant larvae (Lgl), which causes a reduced substrate specificity of aPKC (Wirtz-Peitz, Nishimura, & Knoblich,

2008). However, once NB enters mitosis, another serine/threonine kinase Aurora A (AurA) phosphorylates Par6 triggering conformational changes in aPKC, that ultimately phosphorylates Lgl (Figure 6D). Thus, while Lgl is released from the complex (Jörg Betschinger, Mechtler, & Knoblich, 2003), Par3 takes its place to link Numb to aPKC, subsequently leading to phosphorylation of Numb by aPKC (Smith et al., 2007; Wirtz-Peitz et al., 2008). Phosphorylated Numb is then released from apical side, where it was hitherto associated with cell membrane via its positively charged amino-terminus (J A Knoblich, Jan, & Jan, 1997), and localizes to the basal pole via its adapter protein Partner of Numb (Pon) (Haenfler, Kuang, & Lee, 2012; Lu, Rothenberg, Jan, & Jan, 1998). Moreover, Polo kinase phosphorylates Pon in order to restrict them to basal pole via liquid-liquid phase separation mechanism (Shan et al., 2018; Hongyan Wang, Ouyang, Somers, Chia, & Lu, 2007). Meanwhile, aPKC phosphorylates another direct substrate Miranda (Mira), which results in its localization to basal side together with its cargo proteins Brat and Pros (Atwood & Prehoda, 2009) (Figure 6C-D).

Once the cell division is complete, in order to restore protein localization, protein phosphatase 4 (PP4) dephosphorylates Mira (Sousa-Nunes, Chia, & Somers, 2009) and protein phosphatase 2 (PP2) dephosphorylates Par6 to inactivate aPKC (Ogawa, Ohta, Moon, & Matsuzaki, 2009). Thus, through this intricate asymmetric cell division machinery, two daughter cells with different fates are generated.

3.5. Ensuring lineage progression – cell fate determinants and beyond

Once asymmetric cell division is achieved, the Par complex is inherited by the apical larger cell to maintain the neuroblast identity, whereas the cell fate determinants are segregated into smaller, basal cell. Nevertheless, the question remains - how do these factors, Numb, Brat and Pros, function to ensure lineage directionality?

In *Drosophila* sensory organ precursors (SOP), Numb was the first identified asymmetrically segregating protein between daughter cells (Rhyu,

Jan, & Jan, 1994). Later, it was demonstrated that Numb localizes asymmetrically in NBs, too (Jürgen A Knoblich, Jan, & Jan, 1995; Spana, Kopczynski, Goodman, & Doe, 1995). In the larval brain, loss of Numb in NBs leads to ectopic NB formation and failure to generate differentiating progeny (Lee, Andersen, Cabernard, Manning, Tran, Lanskey, et al., 2006a; Hongyan Wang et al., 2006). On molecular level, Numb has been shown to act as a tissue-specific inhibitor of Notch pathway (Le Borgne, Bardin, & Schweisguth, 2005; Mummery-Widmer et al., 2009; Rhyu et al., 1994; Skeath & Doe, 1998). Numb binds to AP-2 complex via the endocytic protein α - Adaptin (Berdnik, Török, González-Gaitán, & Knoblich, 2002; Song & Lu, 2012). This binding causes the endocytosis of Notch receptor, culminating in its degradation and the pathway is repressed in Numb-inheriting cells (Berdnik et al., 2002; Santolini et al., 2000). Another endocytic role of Numb occurs in SOP cells where Numb inhibits the recycling of Sanpodo, which is required for Notch signaling (Cotton, Benhra, & Le Borgne, 2013; Couturier, Mazouni, & Schweisguth, 2013; O'Connor-Giles & Skeath, 2003). In type II NBs, loss of Notch signaling diminishes type II lineages completely. In accordance with this, loss-of-function of Numb results in imINPs to revert back to supernumerary NBs due to the failed repression of Notch (Bowman et al., 2008; Farnsworth, Bayraktar, & Doe, 2015; Weng et al., 2010; Xiao et al., 2012; Zacharioudaki et al., 2012).

Pros is another cell fate determinant that is a homeodomain TF. This TF is in cytoplasm of NBs, where it is inactive. Upon its translocation to the nucleus in GMCs via its adaptor protein Miranda, it acts as a transcriptional activator and repressor (Ikeshima-Kataoka, Skeath, Nabeshima, Doe, & Matsuzaki, 1997; Jürgen A Knoblich et al., 1995; Shen, Jan, & Jan, 1997; Spana et al., 1995). GMCs fail to repress NB genes in *pros* mutant embryos, while pros-depleted NBs overproliferate (Bello, Reichert, & Hirth, 2006; Joerg Betschinger, Mechtler, & Knoblich, 2006; Bowman et al., 2008; Choksi et al., 2006; Lee, Wilkinson, Siegrist, Wharton, & Doe, 2006c). Pros binds near self-renewal and cell cycle progression genes to repress, whereas it binds to differentiation genes to activate them. Some of the targets of Pros includes

Cyclin E, Mira, Insc, Glial cells missing (gcm) and *Twin of eyeless (toy)* (Choksi et al., 2006).

Another cell fate determinant is Brat, belonging to TRM-NHL protein family (Tocchini & Ciosk, 2015). It binds to 3'-UTR of mRNAs to act as a translational repressor. Brat functions as a growth regulator in many tissues via suppressing dMyc and Mad (Joerg Betschinger et al., 2006; Harris, Pargett, Sutcliffe, Umulis, & Ashe, 2011). While, in the embryo, Brat regulates neuronal differentiation (Joerg Betschinger et al., 2006), in larval brain, Brat-depletion causes NB overgrowth at the expense of neurons (Arama, Dickman, Kimchie, Shearn, & Lev, 2000; Bello et al., 2006; Joerg Betschinger et al., 2006; Lee, Wilkinson, Siegrist, Wharton, & Doe, 2006c). Interestingly, loss of Brat induces tumors only in the CNS {Frank:vb}. Brat acts together with its partner proteins, Nanos and Pumilio, during embryogenesis in order to suppress the translation of hunchback {Sonoda:2001kb}. In ovaries, Brat works with Pumilio to repress dMyc and Mad in order to lower Dpp responsiveness to promote differentiation (Harris et al., 2011). In contrast, Brat acts independently of Nanos and Pumilio to repress src64B translation in axon bundle stabilization (Marchetti, Reichardt, Knoblich, & Besse, 2014). In type II NBs, Brat has been shown to inhibit Wnt signaling via Apc2, a component of Armadillo degradation complex, in order to specify imINP identity (Komori, Xiao, McCartney, & Lee, 2014b).

Interestingly, type II NBs do not express Pros, unlike type I NBs.Thus, after asymmetric cell division, type II NBs only segregate Numb and Brat, whereas type I NBs segregate all three determinants (Bayraktar et al., 2010; Bello et al., 2008; Boone & Doe, 2008; Bowman et al., 2008). In type II lineages, Pros expression start in INPs, and then segregated into GMCs together with Numb and Brat (Figure 7A). Loss-of-function of any of these three determinants cause tumor formation. While *pros* mutant type I NBs cannot specify GMC identity, which results in overgrowth, *numb* or *brat* mutants causes failure in INP-identity specification. Because of mis-specified identities, smaller daughter cells fail to repress neuroblast markers, ultimately giving rise to supernumerary NBs (Bowman et al., 2008) (Figure 7B).

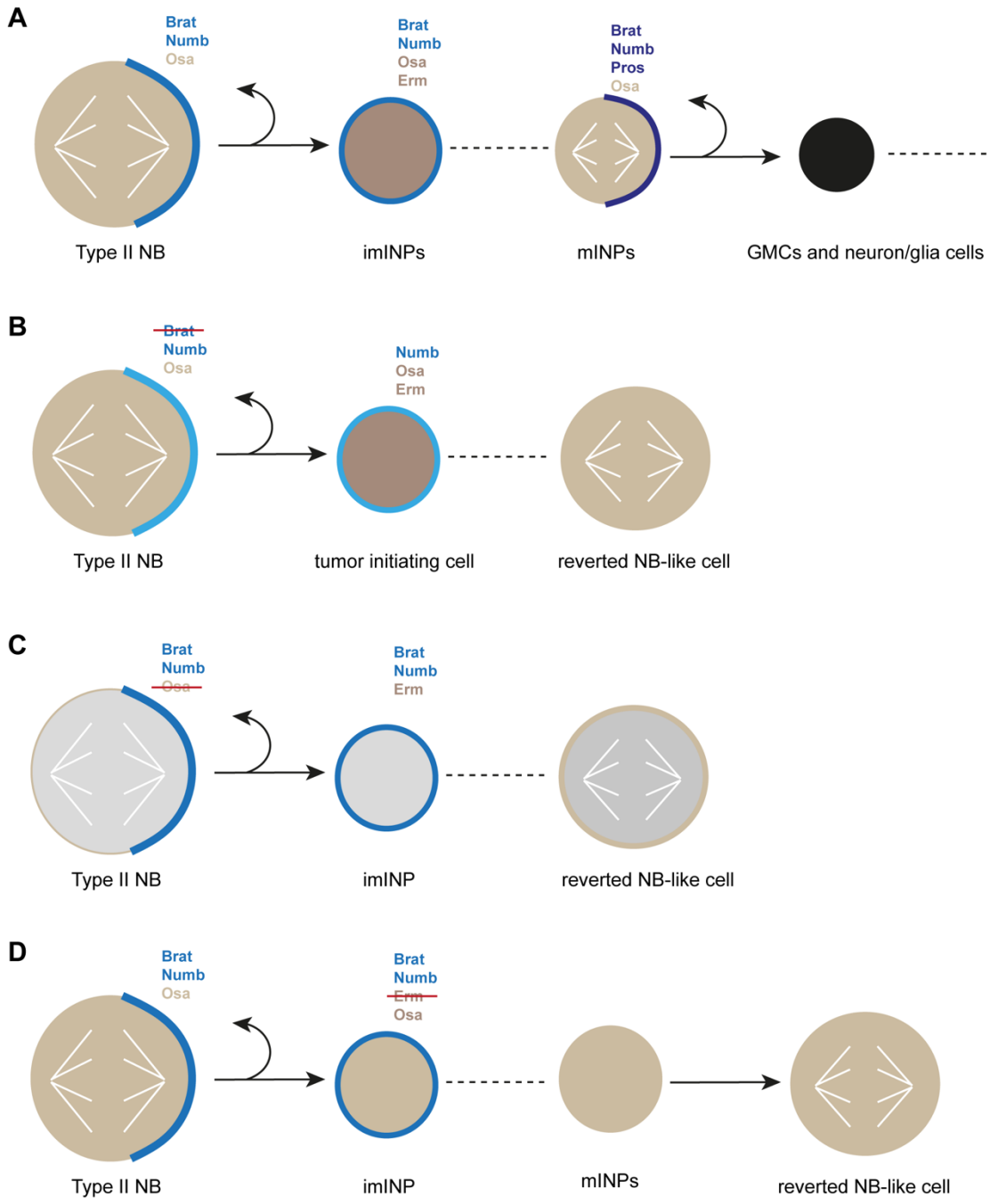

Figure 7. Mechanisms ensuring correct lineage progression in type II lineages.

(A) A cartoon depiction of a wild-type type II NB. NB divides to segregates Brat and Numb to INPs. In INPs, a restriction program starts through Osa and Erm. **(B)** When Brat is depleted, INPs revert back to NB-state to form tumors. **(C)** When Osa is depleted, restrictive program in INPs fail to be initiated. **(D)** When Erm is depleted, INPs first mature and then dedifferentiate into tumor NBs.

In addition to these three cell fate determinants, both NBs and their newly generated small progeny should maintain and stabilize their identities (Figure 7C-D). It has been suggested that a transcriptional network is regulating the self-renewal capacity of NBs, including TFs Dpn, HLHmγ and Klu (Berger et al., 2012; Xiao et al., 2012; Zacharioudaki et al., 2012). Interestingly, TF Nervous fingers 1 (Nerfin-1) has been shown to maintain the differentiated state, and loss of Nerfin-1 causes neurons to revert back to NB state (Froldi et al., 2015; Xu et al., 2017). In type II lineages, after cell division, newly born imINPs express Brat and Numb to antagonize this self-renewal network (Janssens et al., 2017; 2014). But INPs re-enter proliferation by resuming the expression of these three TFs (Berger et al., 2012). But then how do INPs have less self-renewal capacity than NBs, if they express the same set of self-renewal genes? This suggests that there is a program restricting the self-renewal capacity of INPs. For example, TF Earmuff (Erm) is required for correct lineage progression (Figure 7C). Erm depleted mINPs revert back to the supernumerary type II NB state. Interestingly, these INPs can still go through maturation before they become ectopic NBs (Weng et al., 2010). In a newborn INP, once the self-renewal factors are downregulated, Erm is activated rapidly through its poised enhancer. In type II NBs, Rpd3, a histone deacetylase, represses *erm* together with Dpn, HLHmγ and Klu. After the asymmetric cell division, self-renewal genes are downregulated, which leads to alleviation of Rpd3-mediated repression, enabling histone-acetylation-driven activation of *erm* (Janssens et al., 2017). In addition, Erm has been shown to work together with HDAC3 and SWI/SNF chromatin remodeling complex in INPs to limit their self-renewal capacity (Janssens et al., 2014; Koe et al., 2014). Furthermore, loss of Osa, a SWI/SNF complex subunit, causes INPs to revert back to ectopic NBs (Neumüller et al., 2011) (Figure 7D). In INPs, Osa starts a transcriptional program by directly binding TSS of a set of TFs, including Hamlet. Hamlet is a Prdm protein that restricts the self-renewal capacity of INPs (Eroglu et al., 2014). Furthermore, Mi-2/NuRD ATP remodeling complex has been shown to act on

decommissioning of stem cell enhancers to maintain differentiated state of their progeny (Zacharioudaki, Falo Sanjuan, & Bray, 2019).

In type II lineages, Notch signaling has been shown to ensure correct progression. Notch signaling is active in type II NBs and mINPs, while it is shutdown in imINPs. Loss of Notch leads to ectopic Erm expression in NBs and loss of type II lineages (Xiaosu Li, Xie, & Zhu, 2016). Recently, Notch has been proposed to ensure lineage directionality via an asymmetric amplification loop with the Super elongation complex (SEC) (K. Liu et al., 2017). While Notch induces SEC expression in NBs exclusively, SEC promotes the expression of Notch target genes, forming a feedback loop. After cell division, asymmetrically segregated Numb in imINPs downregulate Notch signaling, enabling Erm activation. In mINPs, Erm is downregulated, allowing Notch expression, but this time without SEC expression, which acts as an amplifier. Consistently, overexpression of SEC in mINPs causes tumor formation (K. Liu et al., 2017). Recently, Integrator complex has also been shown to ensure lineage directionality by preventing dedifferentiation of INPs via regulating Erm expression (Zhang et al., 2019).

3.6. *Drosophila* as a brain tumor model

Drosophila CNS also serves as a great model system to study tumorigenesis. Three different types of tumors can occur in the *Drosophila* CNS. These are glia-derived tumors, excess proliferation of neuroepithelial cells in the optic lobe, and finally defective asymmetric cell division-originated tumors. In larval glial cells, co-activation of PI3K and EGFR-Ras causes overproliferation and give rise to glioma-like tumors (Read, 2011; Read, Cavenee, Furnari, & Thomas, 2009). Meanwhile, an example of optic lobe tumor is *lethal (3) malignant brain tumor (l(3)mbt)* mutants arising from neuroepithelium (Gateff, Löffler, & Wismar, 1993). Finally, defects in asymmetric cell division and thus, failure to stabilize restriction of self-renewal in the progenitors result in tumor formation. Most of key components of asymmetric cell division machinery also identified as tumor suppressors. Among these genes are *lethal giant larvae (lgl)* and *discs large (dlg)* (Gateff,

1994; Watson, Justice, & Bryant, 1994; Wright, 1987) are the first ones to be identified. Mutations in other asymmetric cell division genes, such as *brat, numb, pros, pins, mud* or *AurA* results in brain tumors, and studied extensively (Bello et al., 2006; Joerg Betschinger et al., 2006; Bowman et al., 2006; 2008; Caussinus & Gonzalez, 2005; Lee, Andersen, Cabernard, Manning, Tran, Lanskey, et al., 2006a; Lee, Robinson, & Doe, 2006b; Hongyan Wang et al., 2006). In addition, it has been shown recently that genes downstream of segregating determinants act as potential tumor suppressors (Eroglu et al., 2014; Janssens et al., 2014; Koe et al., 2014; Weng et al., 2010; Zhu et al., 2011). Recently, it has been shown that long non-coding RNA cherub segregates asymmetrically and thus, high levels of it accumulates in emerging tumor NBs, which results in transformation of stem cells into malignant cells.

These tumor models are not merely the overproliferation of NBs, but indeed a detailed tumor formation and propagation. For example, brat or numb mutant NBs initially produce less progeny compared to wild-type counterparts. This is due to cell cycle arrest at G2 phase. After 48 hours of tumor induction, tumor NBs overcome this and overproliferate at the expense of the neurons (Bowman et al., 2008). Recently, it has been shown that long non-coding RNA cherub segregates asymmetrically to accumulate in the newly emerging tumor NBs, which results in transformation of stem cells into malignant cells, suggesting a critical role in tumor transformation (Landskron et al., 2018). Furthermore, the pieces of mutant larval brains can be injected into the abdomen of adult host flies, where they grow 100-fold bigger than the original tumor and metastasize (Caussinus & Gonzalez, 2005). Thus, *Drosophila* provides an excellent model system to study tumor formation and metastasis.

3.7. Trithorax- and Polycomb-Group Proteins

Evolutionary conserved Trithorax group (TrxG) and Polycomb group (PcG) genes were first identified in *Drosophila* as the activator and repressor of homeotic gene (HOX) expression, respectively. The first discovered PcG gene, Polycomb (Pc) was shown to repress HOX in embryo. Pc loss caused anterior embryonic segments to transform into posterior ones (Lewis, 1978). In contrast, Trithorax (first TrxG gene) mutants cause the transformation into more anterior segments {Ingham:1983fl}. These proteins are suggested to act as a cellular memory system, since even after their initial transcriptional regulators are gone, both PcG and TrxG proteins are required to maintain HOX gene expression (Ingham, 1985). However, studies over the last decades proved that PcG and TrxG proteins are more than mere regulators of HOX gene expression but they regulate many cellular processes (Schuettengruber, Bourbon, Di Croce, & Cavalli, 2017).

Polycomb response elements (PREs) and Trithorax response elements (TREs) target these complexes to chromatin to regulate epigenetic landscape. The functional diversity of these complexes relies on the various compositions of the complexes. For example, PcG proteins can be found in Polycomb repressive complex 1 (PRC1) and Polycomb repressive complex 2 (PRC2) (Figure 8). The core component of PRC2 is Enhancer of zeste (*E(z)*), which is a histone methyltransferase. Thus, PRC2 exerts its function via trimethylating lysine 27 of histone H3. Other components of PRC2 includes *Esc, Su(z)12* and *Caf1-55* (Kassis, Kennison, & Tamkun, 2017). Meanwhile PRC1 components are *Pc, Psc, Ph* and *Sce*. Pc contains a chromodomain that allows its binding to methylated histones, while Sce has H2A ubiquitin-ligase activity, and required for the H2AK118ub histone mark (Hengbin Wang et al., 2004a). In addition, Pho repressive complex (PhoRC) acts as the recruiter, since it does contain Pho, which binds to PREs (Brown, Mucci, Whiteley, Dirksen, & Kassis, 1998). Thus, it has been proposed that PcG-mediated repression works in a sequential manner: First Pho binds to PREs and recruits PRC2, which exerts its mark on histones (H3K27me3). This mark is then recognized via Pc, leading to PRC1 recruitment (L. Wang et al., 2004b).

However, recently it has been shown that these complexes can act independently as well (Kassis et al., 2017).

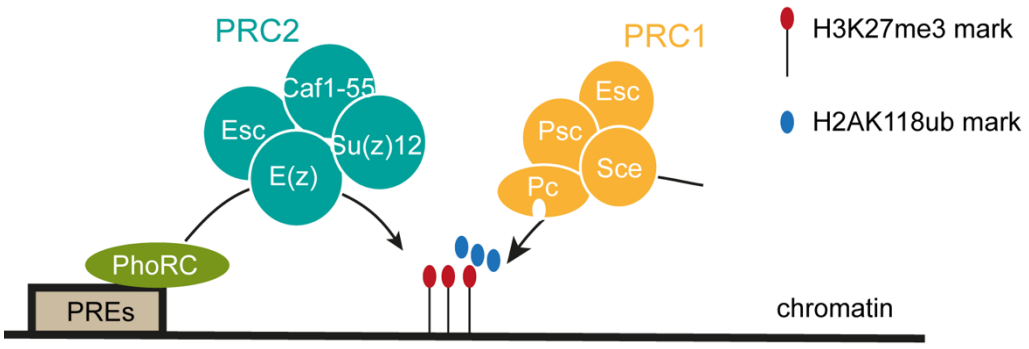

Figure 8. Polycomb group proteins act in complexes.

PcG proteins act in complexes, such as Polycomb repressive complex 1 and Polycomb repressive complex 2. Both complexes have core components, including catalytic enzymes, *E(z)* and *Sce*. These enzymes can modify histones covalently.

On the other hand, TrxG proteins are a heterogenous group with wide array of functions in transcriptional activation. Some of the TrxG complexes include ATP-dependent chromatin remodeling while, some functions via covalent modifications of histones (Schuettengruber et al., 2017). For instance, SWI/SNF complex is an ATP-dependent chromatin remodeler, which regulates chromatin structure of genes implicated in proliferation, cell signaling, and cell cycle (Kadoch & Crabtree, 2015). Another group of TrxG complexes include histone modifying activities, such as histone acetylation and methylation. For instance, TrxG gene *trx,* encodes a protein with a SET domain that is required for H3K4me3 mark (Kassis et al., 2017; Schuettengruber, Chourrout, Vervoort, Leblanc, & Cavalli, 2007). The dynamics of these histone modifications reflect the transcriptional state of the genes.

4. Aim and structure of this thesis

This thesis is written in the cumulative format based on two manuscripts that are presented as chapters of the result part of this thesis.

Chapter 1:

Chapter 1 describes a novel mechanism of temporal patterning in transit amplifying cell population of *Drosophila* larval brain, which is composed of three proteins in an incoherent feedforward loop (FFL) in order to achieve successive expression of temporal identities.

Chapter 2:

Chapter 2 describes our efforts to investigate epigenetic landscape of distinct neural stem cell (NSC) types and their progenies in *Drosophila* larval brain.

5. Chapter 1: The transcription factor odd-paired regulates temporal identity in transit-amplifying neural progenitors via an incoherent feed-forward loop

5.1. Prologue

In order to generate vast arrays of diverse neurons, neural progenitors undergo temporal patterning. This evolutionarily conserved process is also observed in Drosophila transit-amplifying cell population known as intermediate neural progenitors (INPs), where successive expression of Dichaete (D), Grainyhead (grh), and eyeless (ey) specify neuronal fates. However, it remains elusive how the transitions from one temporal state to another are achieved. Here, we developed an unbiased method to isolate distinct states of temporal identities. Using transcriptomic analysis, we identified the factor odd-paired (opa), which is direct target of Osa, as a key regulator of D-to-grh transition. We showed that opa is required for repression of D expression. Together with D and opa, Osa forms an incoherent feed-forward loop (FFL), resulting in successive expression of temporal identities.

This manuscript is published in eLife on July 22, 2019. DOI: 10.7554/eLife.46566

Authors:
Merve Deniz Abdusselamoglu, Elif Eroglu, Thomas R Burkard, Jürgen A Knoblich*
* Corresponding author

Author Contributions:
M.D.A. conceptualized, designed, performed, interpreted experiments and wrote the manuscript. E.E. conceptualized and performed experiments, T. R. B. conducted all bioinformatic analyses. J.A.K. supervised the project and wrote the manuscript.

eLIFE elifesciences.org

RESEARCH ARTICLE

The transcription factor odd-paired regulates temporal identity in transit-amplifying neural progenitors via an incoherent feed-forward loop

Merve Deniz Abdusselamoglu, Elif Eroglu†, Thomas R Burkard, Jürgen A Knoblich*

IMBA – Institute of Molecular Biotechnology of the Austrian Academy of Science, Vienna Biocenter (VBC), Vienna, Austria

Abstract Neural progenitors undergo temporal patterning to generate diverse neurons in a chronological order. This process is well-studied in the developing *Drosophila* brain and conserved in mammals. During larval stages, intermediate neural progenitors (INPs) serially express Dichaete (D), grainyhead (Grh) and eyeless (Ey/Pax6), but how the transitions are regulated is not precisely understood. Here, we developed a method to isolate transcriptomes of INPs in their distinct temporal states to identify a complete set of temporal patterning factors. Our analysis identifies odd-paired (opa), as a key regulator of temporal patterning. Temporal patterning is initiated when the SWI/SNF complex component Osa induces D and its repressor Opa at the same time but with distinct kinetics. Then, high Opa levels repress D to allow Grh transcription and progress to the next temporal state. We propose that Osa and its target genes opa and D form an incoherent feedforward loop (FFL) and a new mechanism allowing the successive expression of temporal identities.

DOI: https://doi.org/10.7554/eLife.46566.001

***For correspondence:** juergen.knoblich@imba.oeaw.ac.at

Present address: †Department of Cell and Molecular Biology (CMB), Karolinska Institutet, Stockholm, Sweden

Competing interests: The authors declare that no competing interests exist.

Funding: See page 22

Received: 04 March 2019
Accepted: 12 June 2019
Published: 22 July 2019

Reviewing editor: K VijayRaghavan, National Centre for Biological Sciences, Tata Institute of Fundamental Research, India

© Copyright Abdusselamoglu et al. This article is distributed under the terms of the Creative Commons Attribution License, which permits unrestricted use and redistribution provided that the original author and source are credited.

Introduction

During brain development, neural stem cells (NSCs) generate large numbers of highly diverse neuronal and glial cells in chronological order (***Cepko et al., 1996***; ***Gao et al., 2014***; ***Greig et al., 2013***; ***Holguera and Desplan, 2018***). Through a phenomenon known as temporal patterning, NSCs acquire properties that change the fate of their progeny over time (***Kohwi et al., 2013***; ***Mattar et al., 2015***; ***Okamoto et al., 2016***). Importantly, temporal patterning of NSCs is an evolutionary conserved process and has been observed across species ranging from insects to mammals (***Alsiö et al., 2013***; ***Livesey and Cepko, 2001***; ***Toma et al., 2014***). During mammalian brain development, neural progenitors in the central nervous system (CNS) undergo temporal patterning by relying on both extrinsic as well as progenitor-intrinsic cues. Wnt7, for example, is an extracellular ligand required for the switch from early to late neurogenesis in cortical progenitors (***Wang et al., 2016***), Ikaros (the ortholog of the Drosophila Hunchback), in contrast, is an intrinsic factor specifying early-born neuronal fates (***Mattar et al., 2015***). Like Ikaros, intrinsic temporal identity factors in vertebrates are often homologous to factors described in *Drosophila* (***Naka et al., 2008***; ***Ren et al., 2017***; ***Syed et al., 2017***). How these factors are involved in neuronal fate specification and how they are regulated remain unknown.

Drosophila has been crucial to understanding stem cell biological mechanisms and in particular distinct temporal patterning processes (***Homem and Knoblich, 2012***). During embryonic neurogenesis, *Drosophila* NSCs, called Neuroblasts (NBs), undergo temporal patterning through a cascade of

eLife digest The brain consists of billions of neurons that come in a range of shapes and sizes, with different types of neurons specialized to perform different tasks. Despite their diversity, all of these neurons originate from a single population known as neural stem cells. As the brain develops, each neural stem cell divides to produce two daughter cells: one remains a stem cell, which can then divide again, and the other becomes a neuron.

A longstanding question in developmental biology is how a limited pool of neural stem cells can generate so many different types of neurons. The answer seems to lie in a process known as temporal identity, whereby neural stem cells of different ages give rise to different types of neurons. This requires neural stem cells to keep track of their own age, but it is still unclear how they can do so.

Abdusselamoglu et al. have now uncovered part of the underlying mechanism behind temporal identity by studying fruit flies, an insect in which the early stages of brain development are similar to the ones in mammals. A method was developed to sort fly neural stem cells into groups based on their age. Comparing these groups revealed that a protein called Opa make neural stem cells switch from being 'young' to being 'middle-aged'. Another protein, Osa activates Opa, which in turn represses a protein called Dichaete. As Dichaete is mainly active in young neural stem cells, the actions of Osa and Opa push neural stem cells into middle age.

Fruit flies are therefore a valuable system with which to study the mechanisms that regulate neural stem cell aging. Revealing how the brain generates different types of neurons could help us study the way these cells organize themselves into complex circuits. This knowledge could then be harnessed to understand how these processes go wrong and disrupt development.

DOI: https://doi.org/10.7554/eLife.46566.002

transcription factors (***Isshiki et al., 2001***). During larval neurogenesis, NB temporal patterning relies on opposing gradients of two RNA-binding proteins (***Liu et al., 2015***; ***Syed et al., 2017***). Temporal patterning is also seen in intermediate neural progenitors (INPs), the transit-amplifying progeny of a discrete subset of larval NBs called type II NBs (***Bayraktar and Doe, 2013***). Once they arise from an asymmetric division of a type II NB, newborn INPs undergo several maturation steps before they resume proliferation: they first turn on earmuff (erm), and Asense (ase), and finally Deadpan (Dpn) expression to become mature INPs (mINP) (***Bello et al., 2008***; ***Boone and Doe, 2008***; ***Bowman et al., 2008***; ***Janssens et al., 2014***; ***Walsh and Doe, 2017***). Then mINPs divide 3–6 times asymmetrically to generate ganglion mother cells (GMCs), which in turn divide to generate a pair of neurons or glia. Analogous to embryonic NBs (***Isshiki et al., 2001***), recent reports suggest that a transcription factor cascade regulates temporal patterning of INPs (***Bayraktar and Doe, 2013***). Indeed, the sequential expression of Dichaete (D), Grainyhead (Grh) and Eyeless (Ey) is required to generate different neurons: D^+ INPs produce Brain-specific homeobox $(Bsh)^+$ neurons, while Ey^+ INPs produce Toy^+ neurons (***Bayraktar and Doe, 2013***).

The three temporal identity factors are regulated through various regulatory interactions (***Bayraktar and Doe, 2013***; ***Doe, 2017***): D is necessary, but not sufficient, for activating Grh. Grh instead is required for repression of D and activation of Ey (***Bayraktar and Doe, 2013***). Therefore, INP temporal patterning is thought to be regulated by a 'feedforward activation and feedback repression' mechanism (***Figure 1A***). Intriguingly however, INP temporal patterning also critically requires the SWI/SNF chromatin remodeling complex subunit Osa (***Eroglu et al., 2014***). Although Osa is not considered a specific temporal identity factor, it is required to initiate temporal patterning by activating the initial factor D. While the Osa target gene hamlet is required for the Grh-to-Ey transition (***Eroglu et al., 2014***), regulation of the first transition is less well understood. This result suggests that in addition to feedforward activation and feedback repression, temporal switch genes are required to ensure correct INP temporal patterning. Nevertheless, D and ham double knock down (k.d.) phenotypes do not recapitulate the complete loss of temporal patterning initiation observed in Osa-depleted type II NB lineages, suggesting the contribution of additional unidentified factors.

Here, we describe a FACS-based method to isolate INPs from three different temporal identities. By comparing the transcriptomic profiles of each set of INPs, we identify odd-paired (opa), a

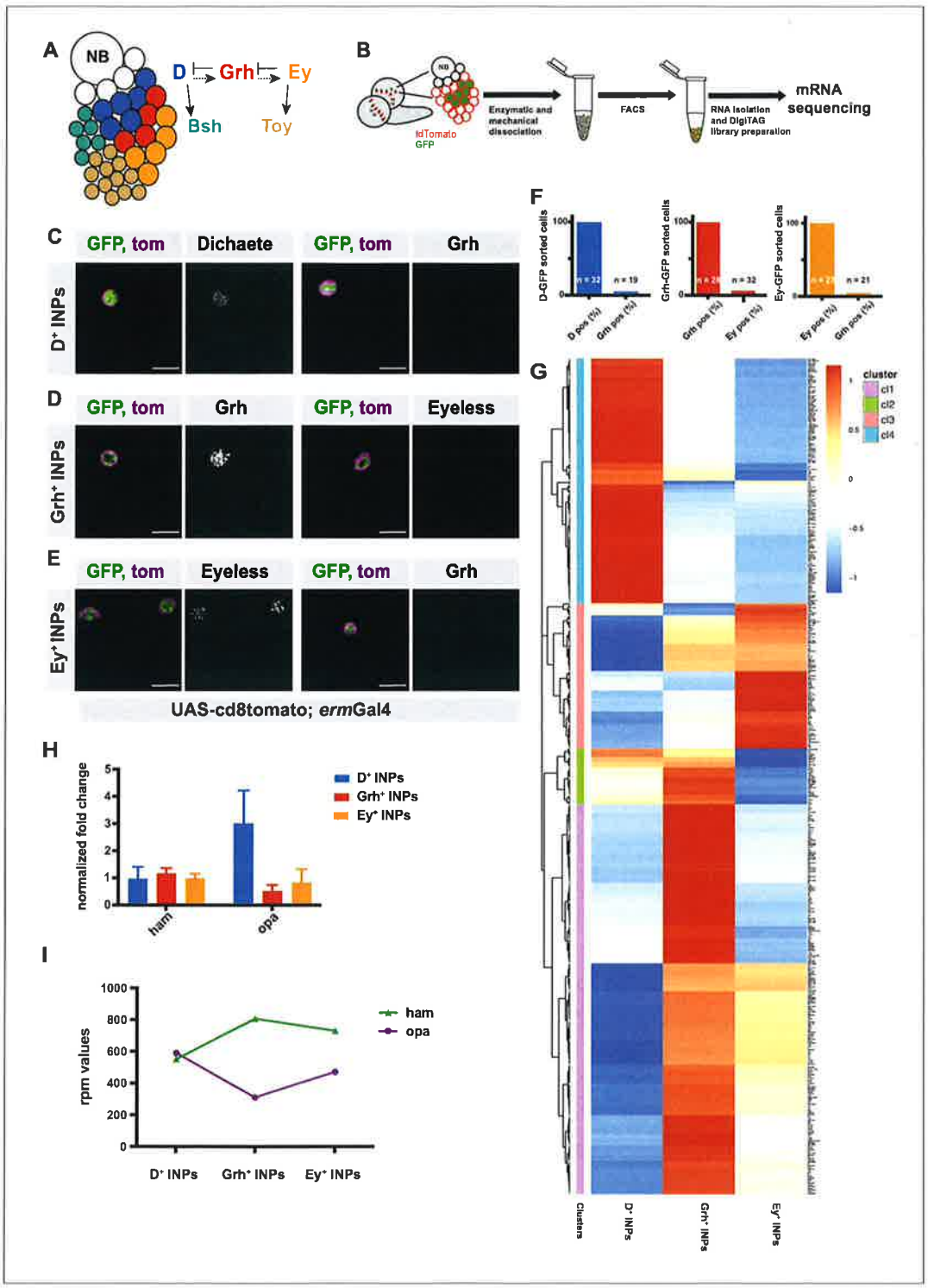

Figure 1. Transcriptomic analysis of temporally staged-INPs. (**A**) Cartoon depicting a typical type II neuroblast of larval *Drosophila* brain; NB and imINPs (empty circles) are followed by mINPs and neurons, GMCs omitted for simplicity. INPs are temporally patterned with Dichaete (blue), Grainyhead (red), and Eyeless (orange), and neurons are Bsh (green) or Toy (brown) positive. Summary of the regulation of temporal identity factors, and their progeny. (**B**) Cartoon illustrating the strategy used to isolate temporally-staged INPs. (**C–E**) D-, Grh and Ey-GFP FACS-sorted cells are stained

Figure 1 continued on next page

Figure 1 continued

for D and Grh (**C**), Grh or Ey (**D–E**), GFP-tagging temporal identity factors (in green, D or, Grh or Ey), tdTomato tagging the membrane of INPs (magenta), antibody staining (gray) scale bar 10 µm, (induced with ermGal4, marked with membrane bound tdTomato). (**F**) Graphs showing the percentage of temporal identity positive cells in D-, Grh- or Ey-GFP FACS sorted cells. n numbers are depicted on the graphs. (**G**) Hierarchical clustering analysis of gene log2fc between three different temporally-staged INP populations. (H) qPCR analysis of opa and ham expression levels in FACS-sorted D^+, Grh^+ and Ey^+ INPs. Data are mean ± SD, n = 3, genes were normalized to Act5c, and then the average expression levels, Delta-Delta Ct method is used. (I) Graph showing the rpm levels of opa and ham between different INP temporal stages.

DOI: https://doi.org/10.7554/eLife.46566.003

The following source data and figure supplements are available for figure 1:

Source data 1. Quantification of temporally FACS-sorted INPs for temporal markers (***Figure 1F***).

DOI: https://doi.org/10.7554/eLife.46566.006

Source data 2. qPCR data (***Figure 1H***).

DOI: https://doi.org/10.7554/eLife.46566.007

Source data 3. Rpm levels of opa and ham genes in three different temporal states of INPs (***Figure 1I***).

DOI: https://doi.org/10.7554/eLife.46566.008

Figure supplement 1. INPs can be FACS-sorted depending on their temporal identity.

DOI: https://doi.org/10.7554/eLife.46566.004

Figure supplement 1—source data 1. Quantification of number of INPs in three different temporal states versus their GFP-tagged counterparts (***Figure 1—figure supplement 1A***).

DOI: https://doi.org/10.7554/eLife.46566.009

Figure supplement 1—source data 2. Quantification of FACS-sorted INPs Dpn staining positivity (***Figure 1—figure supplement 1D***).

DOI: https://doi.org/10.7554/eLife.46566.010

Figure supplement 1—source data 3. qPCR data (***Figure 1—figure supplement 1E***).

DOI: https://doi.org/10.7554/eLife.46566.011

Figure supplement 1—source data 4. Rpm levels of genes in three different temporal states of INPs (***Figure 1—figure supplement 1F***).

DOI: https://doi.org/10.7554/eLife.46566.012

Figure supplement 2. Temporally sorted INPs are pure populations.

DOI: https://doi.org/10.7554/eLife.46566.005

transcription factor whose expression is enabled by direct binding of Osa to its TSS, as a regulator of temporal patterning and repressor of D. Though Osa enables both D and Opa expression, Opa's slower activation kinetics allow D to function in a short time window before being repressed by Opa. This mode of action resembles an incoherent feedforward-loop (FFL) motif, where an upstream gene directly activates the target gene, meanwhile indirectly repressing it by activating its repressor (***Alon, 2007***; ***Mangan and Alon, 2003***). Thus, we uncover a novel mechanism controlling temporal patterning during neurogenesis.

Results

Transcriptome analysis of distinct INP temporal states

To obtain a comprehensive list of temporally regulated genes in INPs, we used FACS to purify INPs at each of their three temporal states: D^+, Grh^+ and Ey^+ (***Figure 1B***). For this, we generated fly lines expressing tdTomato under an INP specific promoter (erm-Gal4 >CD8::tdTomato) and expressing GFP-fusions of one of the temporal identity factors (D-GFP, Grh-GFP and Ey-GFP, ***Figure 1—figure supplement 1A***). Although D-GFP flies were generated with CRISPR/Cas9 method to knock-in GFP into the endogenous locus, Grh-GFP and Ey-GFP flies were generated as BAC clones insertions (***Spokony and White, 2012***). To test if extra copies from BAC clones cause overexpression effects, numbers of each temporal state were quantified in control versus GFP-tagged brains (***Figure 1—figure supplement 1A***). After dissection and dissociation of third instar larval brains, GFP-positive INP populations ($D\text{-}GFP^+$, $Grh\text{-}GFP^+$ and $Ey\text{-}GFP^+$) were identified (***Figure 1B*** and ***Figure 1—figure supplement 1B***) as the largest cells with highest GFP and tdTomato expression (***Figure 1—figure supplement 1B***). Using immunofluorescence (IF), these cells were verified to be mature INPs (***Figure 1—figure supplement 1C-D***). All sorted cells within the INP populations expressed Dpn, indicating a 100% mature INP identity, while unsorted cells showed a mixture of Dpn^+ and Dpn^- cells (***Figure 1—figure supplement 1C-D***). We validated the temporal identity of the progenitors by

performing IF for their respective temporal identity markers (***Figure 1C–F*** and ***Figure 1—figure supplement 2***). Importantly, each GFP$^+$ sorted INP population was 100% positive for its respective temporal marker (***Figure 1F***). In contrast, the unsorted cells consisted of mixed cell populations containing various temporal identities (***Figure 1—figure supplement 2B***). Lastly, we tested for the presence of sorted cells expressing markers of two temporal identities, which reflects transition states of INP temporal patterning as occurs in vivo. Analyzing Grh IF on D-GFP$^+$ and Ey-GFP$^+$ sorted cells, and Ey IF on Grh-GFP$^+$ sorted cells revealed that sorted populations contained only 4–6% of such double-positive cells (***Figure 1C–F***, and ***Figure 1—figure supplement 2A-C***), suggesting we can isolate almost pure populations of different temporal states. Collectively, we established the genetic tools and methodology to precisely sort INPs into separate populations according to their three distinct temporal states.

Since our stringent FACS sorting conditions led to low RNA yields, we generated cDNA libraries using DigiTag (***Landskron et al., 2018***; ***Wissel et al., 2018***). With this RNA sequencing strategy, we found 458 genes expressed differently between D$^+$ and Grh$^+$ INPs, and 466 genes between Grh$^+$ and Ey$^+$ INPs (FDR 0.05, log2foldchange > 1, and Rpm (reads per million mapped reads)>10 in one of three samples/D$^+$, Grh$^+$ or Ey$^+$ INPs). Hierarchical clustering identified genes specifically expressed in certain temporal states, and therefore potentially involved in temporal patterning (***Figure 1G***). First, we confirmed the quality of our dataset by examining the transcriptional changes of temporal identity genes with quantitative PCR (qPCR) (***Figure 1—figure supplement 1E***). As expected, each temporal state had high expression levels of their own temporal identity genes. Second, we confirmed the expression of known temporal identity genes (***Figure 1—figure supplement 1F***). FACS-purified Grh$^+$ INPs expressed high levels of Ey mRNA. However, immunofluorescent analysis showed that Grh$^+$ INPs expressed only low levels of Ey protein, suggesting that post-transcriptional modifications regulate the Grh-to-Ey transition (***Figure 1C–F*** and ***Figure 1—figure supplement 1F***). Third, we performed GO-term analysis on the identified gene clusters. Genes upregulated in D$^+$ INPs showed enrichment for mitochondrial translation, cellular nitrogen compound metabolic process and gene expression (***Figure 1—figure supplement 2D***). Genes upregulated in Grh +INPs were enriched for protein binding and system development (***Figure 1—figure supplement 2E***). Finally, genes upregulated in Ey +INPs were enriched for neurogenesis and sequence-specific DNA binding (***Figure 1—figure supplement 2F***). Interestingly, we observed that the glial identity-promoting factor glial cell missing (gcm) and cell cycle inhibitor dacapo (dap) were upregulated in Ey$^+$ INPs (***Figure 1G—figure supplement 1F***). These observations support previous findings indicating that INPs begin producing glia cells instead of neurons during their later cell divisions, and that Ey is required for cell cycle exit (***Baumgardt et al., 2014***; ***Bayraktar and Doe, 2013***; ***Ren et al., 2018***; ***Viktorin et al., 2013***). To identify genes that regulate transitions of temporal patterning, we focused on genes with a dynamic expression pattern between INP populations. To this end, we focused on genes with a log2foldchange > 1 in either the D-to-Grh or Grh-to-Ey transition. From this list, we excluded genes with a log2foldchange < 0.5 in the remaining transition. We applied a cut-off of Rpm (reads per million mapped reads)>50 in one of the three temporal identity states due to the fact that all the other temporal identity factors, along with osa and ham, had high expression levels. With these criteria, we identified 71 genes (***Supplementary file 1*** and ***Supplementary file 2***), 49 of which displayed an expression pattern of high in D + INPs, low in Grh +INPs, and finally higher in Ey +INPs. Among these genes, odd-paired (opa) was ranked as the 5th hit that is most downregulated in Grh$^+$ INPs (***Figure 1G–I***, ***Supplementary file 1***). Since Osa binds to the TSS of opa in order to prime its expression (***Eroglu et al., 2014***), we investigated in detail the potential role of Opa in regulating INP temporal patterning.

Odd-paired (opa) is required for the progression of INP temporal patterning

Opa is a transcription factor containing five zinc finger domains and is essential for para-segmental subdivision of *Drosophila* embryos (***Benedyk et al., 1994***; ***Mizugishi et al., 2001***). During development, Opa ensures the timely activation of the transcription factors engrailed and wingless (***Benedyk et al., 1994***). To test if opa regulates INP temporal patterning, we depleted opa using RNAi expressed specifically in INPs with ermGal4. Opa knockdown slightly increased the total number of INPs (Dpn$^+$ cells), but drastically increased the number of D$^+$ INPs while decreasing the number of both Grh$^+$ and Ey$^+$ INPs (***Figure 2A–D***). We confirmed this result by performing mosaic

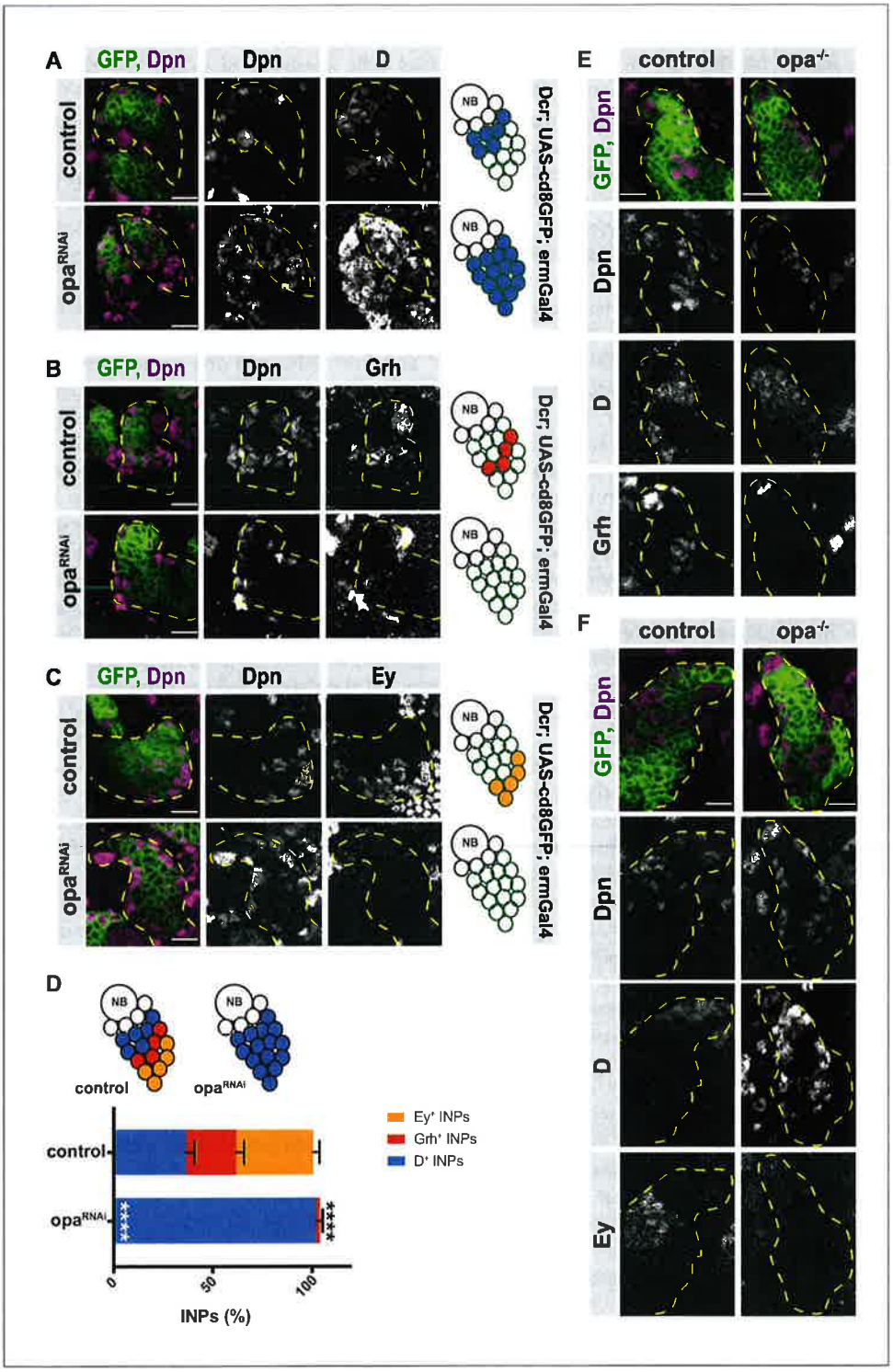

Figure 2. Opa is required for the progression of temporal patterning of INPs. (**A**) Close-up images of larval brains expressing RNAi against opa in INPs, stained for Dpn and D (induced with ermGal4, marked with membrane bound GFP). Lineages are outlined with yellow dashed line. (**B**) Close-up images of larval brains expressing RNAi against opa in INPs, stained for Dpn and Grh (induced with ermGal4, marked with membrane bound GFP). Lineages are outlined with yellow dashed line. (**C**) Close-up images of larval brains expressing RNAi against opa in INPs, stained for Dpn and Ey (induced with

Figure 2 continued on next page

Figure 2 continued

ermGal4, marked with membrane bound GFP). Lineages are outlined with yellow dashed line. (**D**) Quantification of INP numbers in different temporal stages identified by antibody staining of Dpn^+, D^+ cells, Dpn^+, Grh^+ cells, and Dpn^+, Ey^+ cells in control and opa knock-down brains, n = 10, total INP numbers in control were normalized to 100%. Data represent mean ± SD, ***p<=0.001, Student's t-test (D^+ INPs control 12.44 ± 1.42 [n = 10], opa RNAi 34.66 ± 1.02 [n = 12], p<0.001; Grh^+ INPs control 8.5 ± 1.32 [n = 10], opa RNAi 0.5 ± 0.65 [n = 12], p<0.001; Ey^+ INPs control 13.2 ± 0.98 [n = 10], opa RNAi 0.2 ± 0.4 [n = 10], p<0.001). (**E**) Control and opa mutant MARCM clones marked by membrane-bound GFP, stained for Dpn, Grh and D after 120 hr of induction. Control clone has D^+, Dpn^+ INPs followed by Grh^+ INPs while opa mutant clone has increased number of D^+ INPs and decreased number of Grh^+ INPs. (**F**) Control and opa mutant MARCM clones marked by membrane-bound GFP, stained for Dpn, D and Ey after 120 hr of induction. Opa mutant clone has higher number of D^+ INPs and lower number of Ey^+ INPs. Scale bar 10 μm in all images.

DOI: https://doi.org/10.7554/eLife.46566.013

The following source data and figure supplements are available for figure 2:

Source data 1. Quantification of number of INPs in three different temporal identities between control versus opa-depleted brains with INP-specific driver (***Figure 2D***).

DOI: https://doi.org/10.7554/eLife.46566.016

Figure supplement 1. Opa is required for D repression.

DOI: https://doi.org/10.7554/eLife.46566.014

Figure supplement 1—source data 1. Quantification of number of INPs in three different temporal identities between control versus opa-depleted brains with INP-specific driver in DM1 lineages (***Figure 2—figure supplement 1C***).

DOI: https://doi.org/10.7554/eLife.46566.017

Figure supplement 2. Opa regulates the transition from D-to-grh.

DOI: https://doi.org/10.7554/eLife.46566.015

Figure supplement 2—source data 2. Quantification of number of INPs in three different temporal identities between control versus opa-depleted brains with type II-specific driver (***Figure 2—figure supplement 2D***).

DOI: https://doi.org/10.7554/eLife.46566.018

analysis with a repressible cell marker (MARCM) to create mosaic opa (-/-) mutant or control opa (+/+) GFP^+ cell clones (***Lee and Luo, 1999***). Control clones were indistinguishable from WT, whereas opa mutant clones contained predominantly D^+ INPs, at the expense of the other two temporal states (***Figure 2E–F***). The RNAi and mosaic mutant analysis both indicate that loss of Opa causes a shift in INP temporal state identity such that the early generated D^+ INPs are increased while the later generated Grh^+ and Ey^+ INPs are decreased. These results suggest that opa is regulating the D-to-Grh transition by either repressing D or activating Grh. Since it has been previously shown that Grh is not sufficient for D repression (***Bayraktar and Doe, 2013***), we tested whether the main role of opa is to repress D. For this, we depleted opa in DM1 lineages, which undergo temporal patterning by expressing only D and then Ey (***Figure 2—figure supplement 1***). Opa knock-down in DM1 lineages caused a significant increase in the number of D^+ INPs at the expense of Ey^+ INPs, suggesting that opa is required for D repression (***Figure 2—figure supplement 1***).

Finally, we tested if opa regulates processes upstream of temporal patterning during the stages of initial INP maturation with a type II-specific driver line. When expressing opa RNAi specifically in type II NBs, we observed no effect on INP maturation (***Figure 2—figure supplement 2A***) as observed with sequential activation of Ase and Dpn, but immunofluorescent analysis of INPs for D, Grh and Ey expression showed the same phenotype as INPs depleted for opa (***Figure 2—figure supplement 2B-D***). Collectively, these data suggest that opa inhibits D expression. Furthermore, similar to hamlet, Opa appears to act as a temporal identity switch gene, controlling the transition from a D^+ to a Grh^+ state. To test if opa knock-down impairs INP asymmetric cell division leading to the disruption in temporal patterning, we analyzed the expression of Mira, a known scaffolding protein that localizes asymmetrically during cell division, and aPKC, which localizes to apical cortex (***Figure 2—figure supplement 2E***). Opa-depleted INPs can asymmetrically segregate Mira and aPKC, which suggests that asymmetric division is normal. Thus, opa is indeed a temporal switch factor required for the D-to-Grh state.

Opa regulates the transition from early to late born neurons and is required for motor function

INP temporal patterning results in the production of different neuronal subtypes at distinct periods of neurogenesis. For instance, 'young', D^+ INPs produce Brain-specific homeobox $(Bsh)^+$ neurons

and 'old', Ey$^+$ INPs produce Toy$^+$ neurons (***Bayraktar and Doe, 2013***). Since the progression of INP temporal identity is disrupted in opa-depleted INPs, we tested whether this disrupted identity affects the production of different types of neurons. INP-driven opa RNAi displayed a significant increase in Bsh$^+$ neurons, at the expense of Toy$^+$ neurons (***Figure 3A–C***). In addition, opa-depleted MARCM clones also contained increased numbers of Bsh$^+$ neurons compared to wild-type counterparts (***Figure 3D***). This result confirms that shifting the INP identity toward a D$^+$ identity leads to a concomitant increase in the Bsh$^+$ neurons produced by D$^+$ INPs. Thus, altering the temporal identity progression of neural progenitors can alter the proportions of neuronal subtypes in the brain.

We next investigated whether altering the proportions of neuronal subtypes leads to a defect on brain morphology and function. The adult central complex (CCX) brain region relies on type II NB neurogenesis (***Bayraktar et al., 2010***; ***Izergina et al., 2009***). Opa-depletion in INPs caused major alterations in the gross morphology of the adult CCX. The fan-shaped body (FB) was enlarged, the noduli (NO) and ellipsoid body (EB) only partially formed, and the protocerebral bridge (PB) appeared fragmented (***Figure 3E***). Since the CCX is required for adult motor functions (***Callaerts et al., 2001***; ***Young and Armstrong, 2010***), we tested whether altered CCX morphology affected motor behavior. Compared to control flies, INP-driven *opa* RNAi caused impaired negative geotaxis performance (***Figure 3F***). Thus, opa is a temporal switch gene required for neuronal subtype specification, which is required for the correct assembly and function of the adult central complex. Thus, the temporal identity specification of neural progenitors is crucial for proper neural cell complexity, and brain function.

Dichaete and Opa are sequentially expressed in INPs

If opa is required for the D-to-grh transition, what is the molecular mechanism of this transitional regulation? To answer this question, we first confirmed that opa is indeed a target of Osa in type II NB lineages by analyzing opa protein expression within the NB lineage, and whether this expression is regulated by Osa. We generated healthy, homozygous, endogenously C-terminally tagged opa::V5 knock-in flies (***Figure 4—figure supplement 1A***). Through immunofluorescent analysis of V5 tag expression, we observed that Opa is expressed throughout the type II lineage in INPs (marked with Dpn and Ase) and, GMCs (Pros$^+$ cells) and neurons, but not in NBs (Dpn$^+$) or immature INPs (Dpn$^-$/Ase$^-$ or Dpn$^-$/Ase$^+$ cells) (***Figure 4—figure supplement 1B-D***). Opa is also expressed in the DM1 lineage, even though DM1 lineages display a temporal patterning lacking Grh expression (***Figure 1—figure supplement 1E***). To check the specificity of the opa-V5 line, we depleted opa specifically in type II lineages using RNAi. As expected, opa-V5 expression decreased with opa-RNAi (***Figure 4—figure supplement 1E-F***). The proper expression of opa is dependent on Osa, since Osa-knockdown in type II NBs resulted in a loss of Opa (***Figure 4—figure supplement 2A and B***).

Since both D and opa are direct Osa targets, we next compared the expression pattern of D and opa (***Figure 4A***). Without exception, D$^+$/opa$^-$ INPs appeared before D$^+$/opa$^+$ cells in the lineage (***Figure 4A***). However, in later temporal states, all Grh$^+$ and Ey$^+$ INPs expressed opa (***Figure 4B***, and ***Figure 4—figure supplement 3A***). Our transcriptome data suggest that opa expression fluctuates throughout the three different INP populations. To confirm this hypothesis, we calculated the intensity of the opa-V5 signal among these three populations (***Figure 4C–D***, and ***Figure 4—figure supplement 3B***). Indeed, we found that D$^+$ INPs express the highest opa protein levels (***Figure 4C***), while Grh$^+$ INPs express the lowest (***Figure 4D*** and ***Figure 4—figure supplement 3B***). Since D expression precedes opa expression, it is possible that D activates opa. However, upon type II NB specific D knockdown, opa localization was unchanged (***Figure 4E***). Interestingly, D knockdown alone also did not prevent later temporal stages, Grh and Ey, to appear (***Bayraktar and Doe, 2013***), suggesting that other factor(s) are required to maintain temporal identities in INPs. Since Osa-depleted type II NB lineages fail to initiate temporal patterning (***Eroglu et al., 2014***), we hypothesized that one of these unidentified factors could be a target of Osa that remains expressed in D-depleted INPs, such as opa. To test this hypothesis, we examined the epistatic genetic interactions between D and Opa. Double knock down of D and opa by type II NB-specific RNAi produced type II lineages containing fewer Dpn$^+$/Ase$^+$ INPs compared to controls (***Figure 4F–G***). This result suggests that even though D and opa are Osa targets, two of them alone cannot fully account for Osa tumor suppressor role (***Figure 4F–G***). Importantly, all known temporal identity markers on the remaining cells were absent, suggesting a complete loss of temporal identity in these INPs (***Figure 4F–G***). However, since these cells also lost their INP identity due to lack of Dpn and Ase,

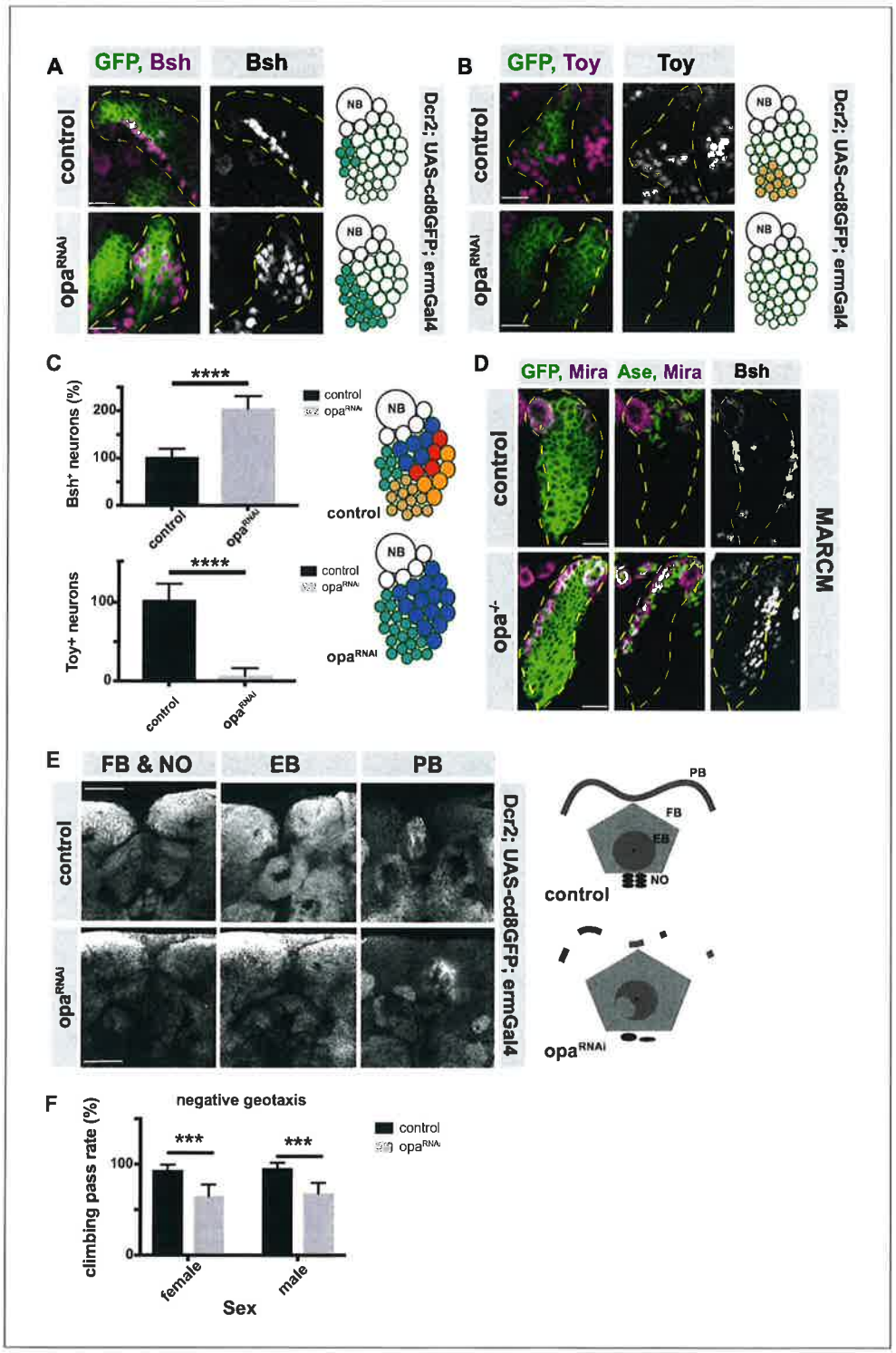

Figure 3. opa is an important factor for the generation of both early and late-born INP progeny and contributes to adult brain central complex. (**A–B**) Close-up images of larval brains expressing RNAi against opa in INPs, immunofluorescence for Bsh (**A**), and Toy (**B**) neuronal markers, scale bar 10 µm, lineages are outlined with yellow dashed line (induced with ermGal4, marked with membrane bound GFP). (**C**) Quantification of Bsh$^+$ and Toy$^+$ neurons in control and opa knock-down brains, n = 11, total Bsh$^+$ or Toy$^+$ neuron numbers in control were normalized to 100%. Data represent mean ± SD,

Figure 3 continued on next page

Figure 3 continued

***p<=0.001, Student's t-test. (D) Control and opa mutant MARCM clone marked by membrane-bound GFP, stained with Mira, Ase, and Bsh antibodies after 120 hr of induction. The clones are marked with yellow dashed line, scale bar 10 µm. (E) Close-up images of adult central complex, composed of fan-shaped body (FB), noduli (NO), ellipsoid body (EB), and protocerebral bridge (PB) of control and opa knock-down brains, stained with Bruchpilot antibody (gray) (induced with ermGal4) scale bar 50 µm. (F) Negative geotaxis assay with control and opa RNAi expressing flies (induced with ermGal4, marked with membrane bound GFP). For each genotype n = 10 replicates, each consisting of 10 adult female or male adults. Data are mean ± SD, ***p<0.001, Student's t-test.

DOI: https://doi.org/10.7554/eLife.46566.019

The following source data is available for figure 3:

Source data 1. Quantification of Bsh$^+$ or Toy$^+$ neuron numbers in control versus opa-depleted brains with INP-specific driver (***Figure 3C***).

DOI: https://doi.org/10.7554/eLife.46566.020

Source data 2. Quantification of the percentage pass rate of flies with control versus opa-depleted brains (***Figure 3F***).

DOI: https://doi.org/10.7554/eLife.46566.021

they exhibit a different phenotype than Osa knockdown. Therefore, our data suggest that opa is required for the repression of D, the activation of Grh, and thus the progression of temporal identities in INPs.

Opa is an expression level-dependent repressor of D

If Opa suppresses D, one puzzling aspect of our data is the presence of double-positive D$^+$/opa$^+$ INPs (***Figure 4A***). To better understand this paradox, we overexpressed opa in type II NBs during a period before D is normally expressed. Overexpression of opa resulted in shorter lineages (***Figure 5—figure supplement 1A-B***), decreased total INP numbers (***Figure 5—figure supplement 1A***), and a loss of type II NBs (marked by Dpn or Mira) (***Figure 5—figure supplement 1A-B***). Co-expressing the apoptosis inhibitor p35 did not prevent NB loss or shortened lineages, suggesting that opa overexpression does not induce cell death, but causes premature differentiation instead (***Figure 5—figure supplement 1C***). NBs and INPs overexpressing opa successfully segregated Mira and aPKC, excluding that asymmetric cell division was altered (***Figure 5—figure supplement 1D-E***, and ***Figure 2—figure supplement 2E***). Overexpressing opa in type II NB lineages caused complete loss of D$^+$ INPs, but the few remaining INPs could still activate Grh and Ey (***Figure 5A–C***), which is similar to D knockdown phenotype (***Bayraktar and Doe, 2013***).

To exclude that these could result from altered NB patterning, we next overexpressed opa in an INP-specific manner during a stage where D is normally expressed. Opa overexpression caused a decrease in D$^+$ INPs (***Figure 5D–F***), and a concomitant increase in both Grh$^+$ and Ey$^+$ INP populations (***Figure 5D–F***). This result further indicates that Opa represses the early D$^+$ temporal identity, but also activates later Grh$^+$ temporal identity. We also overexpressed opa in DM1 lineages in an INP-specific manner, which resulted in a decrease in D$^+$ INP numbers and an increase in Ey$^+$ INPs (***Figure 5—figure supplement 2A and C***). However, ectopic Grh expression was undetectable (***Figure 5—figure supplement 2B***), suggesting opa mis-expression does not cause ectopic Grh expression. Collectively, these results show that opa-mediated repression of D depends on Opa expression levels.

Opa and ham together control the correct representation of each temporal identity

Having established an interaction between opa and D, we next wondered if opa and ham, two temporal switch genes, can recapitulate the Osa loss-of-function phenotype, a more upstream regulator of lineage progression in type II NBs. Osa knock-down causes INPs to revert back to the NB-state due to a failure to initiate temporal patterning, while single depletion of opa or ham leads to either an increase in D$^+$ or Grh$^+$ cells, respectively (***Figure 2***; ***Eroglu et al., 2014***). Co-expressing opa RNAi with ham shmiR in an INP-specific manner caused supernumerary Dpn$^+$, Ase$^+$ INPs (***Figure 6—figure supplement 1A***). In addition, the number of D$^+$/Dpn$^+$ and Grh$^+$/Dpn$^+$ INPs were also increased, which is in contrast to single depletion of opa or ham (***Figure 6A–B***, ***Figure 2***; ***Eroglu et al., 2014***). Thus, opa and ham loss-of-function phenotypes are additive. Importantly, despite inducing over-proliferation of mature INPs (Ase$^+$/Dpn$^+$), depleting both opa and ham in type II NBs could not

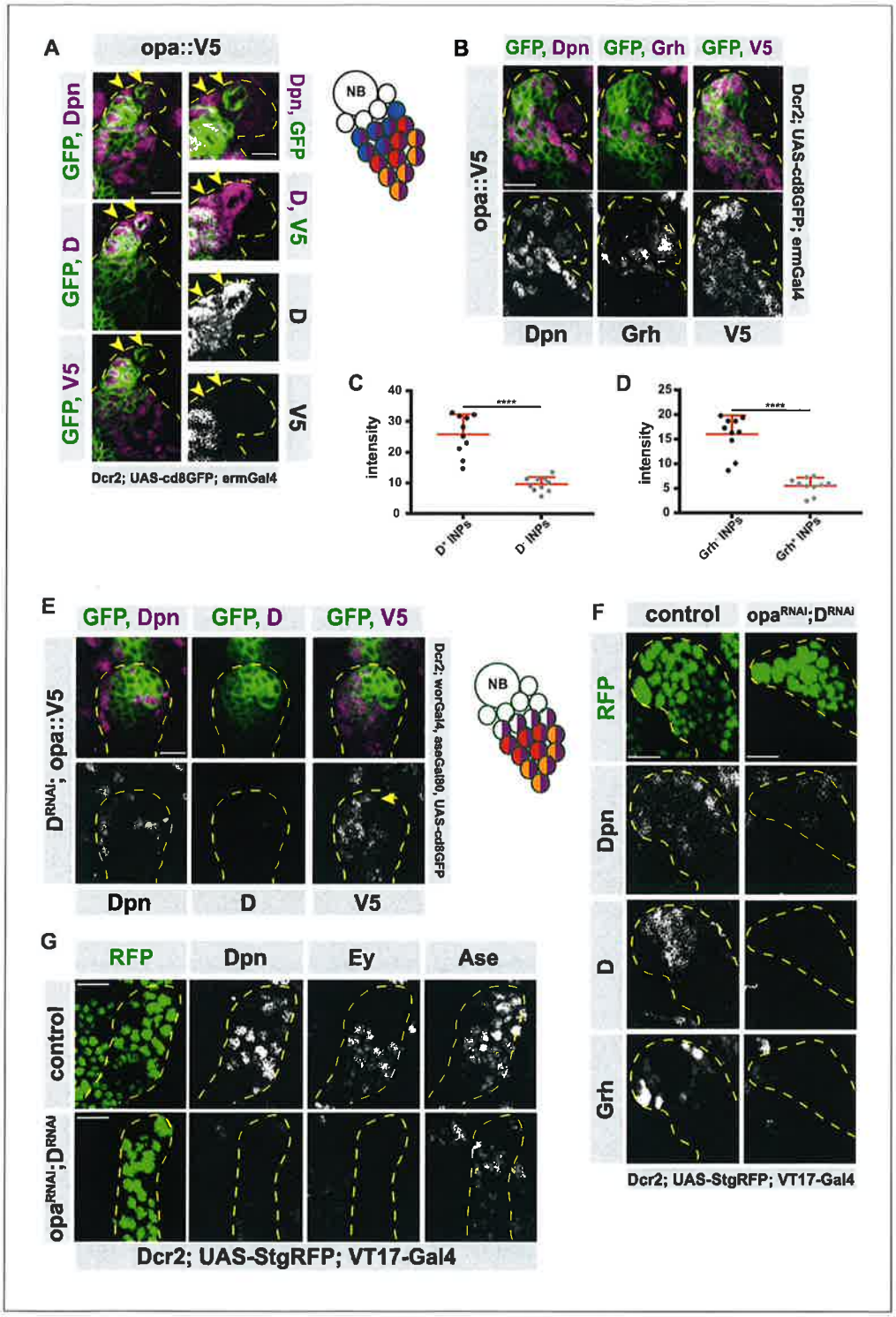

Figure 4. Osa initiates D expression before initiating Opa. (**A**) Close-up images of fly brains endogenously expressing V5-tagged opa in INPs, stained for V5, Dpn and D. D^+, $V5^-$ cell is marked with arrows, lineages are outlined with yellow dashed line, scale bar 10 µm and 5 µm, (induced with ermGal4, marked with membrane bound GFP). (**B**) Close-up images of fly brains endogenously expressing V5-tagged opa in INPs, stained for V5, Dpn and Grh, lineages are outlined with yellow dashed line, scale bar 10 µm, (induced with ermGal4, marked with membrane bound GFP). (**C**) Quantifications of opa::

Figure 4 continued on next page

Figure 4 continued

V5-signal intensity measurements of D^+ vs D^- INPs, n = 10, normalized to background intensity. Data represent mean ± SD, ***p<=0.001, Student's t-test. (**D**) Quantifications of opa::V5-signal intensity measurements of Grh^+ vs Grh^- INPs, n = 10, normalized to background intensity. Data represent mean ± SD, ***p<=0.001, Student's t-test. (**E**) Close-up images of fly brains endogenously expressing V5-tagged opa and RNAi for D in type II lineages, stained for V5, Dpn and D, lineages are outlined with yellow dashed line, scale bar 10 µm, (induced with worGal4, aseGal80, marked with membrane bound GFP). (**F–G**) Close up images of control versus opa and D double knock-down brains in type II lineages, stained with Dpn, D and Grh (**C**), or for Dpn, Ey and Ase (**C**) antibodies, lineages are outlined with yellow dashed lines, scale bar 10 µm, (induced with Dcr2; UAS-StgRFP; VT17-Gal4, marked with nuclear RFP).

DOI: https://doi.org/10.7554/eLife.46566.022

The following source data and figure supplements are available for figure 4:

Source data 1. Quantification of intensity measurements of opa::V5 signal in D^+ versus D^- INPs in wild-type brains (***Figure 4C***).

DOI: https://doi.org/10.7554/eLife.46566.026

Source data 2. Quantification of intensity measurements of opa::V5 signal in Grh^+ versus Grh^- INPs in wild-type brains (***Figure 4C***).

DOI: https://doi.org/10.7554/eLife.46566.027

Figure supplement 1. Opa is expressed in type II lineages.

DOI: https://doi.org/10.7554/eLife.46566.023

Figure supplement 2. Osa initiates the expression of opa in INPs.

DOI: https://doi.org/10.7554/eLife.46566.024

Figure supplement 3. Different temporal states have different opa levels.

DOI: https://doi.org/10.7554/eLife.46566.025

Figure supplement 3—source data 1. Quantification of intensity measurements of opa::V5 signal in Ey^+ versus Ey^- INPs in wild-type brains (***Figure 4—figure supplement 3B***).

DOI: https://doi.org/10.7554/eLife.46566.028

recapitulate the Osa loss-of-function phenotype because imINPs could mature and express Ase, and therefore did not revert into ectopic NBs (***Figure 6—figure supplement 1B***). This suggests that Osa regulates temporal patterning in two levels: initiation by D activation, and progression by opa and ham.

Discussion

Temporal patterning is a phenomenon where NSCs alter the fate of their progeny chronologically. Understanding how temporal patterning is regulated is crucial to understanding how the cellular complexity of the brain develops. Here, we present a novel, FACS-based approach that enabled us to isolate distinct temporal states of neural progenitors with very high purity from Drosophila larvae. This allowed us to study the transitions between different temporal identity states. We identified odd-paired (opa), a transcription factor that is required for INP temporal patterning. By studying the role of this factor in temporal patterning, we propose a novel model for the regulation of temporal patterning in *Drosophila* neural stem cells.

We establish two different roles of the SWI/SNF complex subunit, Osa, in regulating INP temporal patterning. Initially, Osa initiates temporal patterning by activating the transcription factor D. Subsequently, Osa regulates the progression of temporal patterning by activating opa and ham, which in turn downregulate D and Grh, respectively (***Figure 6C***). The concerted, but complementary action of opa and ham ensures temporal identity progression by promoting the transition between temporal stages. For instance, opa regulates the transition from D to Grh, while ham regulates the transition from Grh to Ey. We propose that opa achieves this by repressing D and activating grh, as indicated by the lack of temporal patterning in D and opa-depleted INPs (***Figure 4C–D***, ***Figure 6C***). Loss of opa or ham causes INPs to lose their temporal identity and overproliferate. Moreover, we propose that D and opa activate Grh expression against the presence of ham, which represses Grh expression. As D and opa levels decrease as INPs age and become Grh positive, ham is capable of repressing Grh later on in temporal patterning (***Figure 6C***). This explains how opa and ham act only during specific stages even though they are expressed throughout the entire lineage.

An open question pertains to the fact that the double knock-down of opa and ham, as well as that of D and opa, failed to recapitulate the Osa phenotype. Even though opa and ham RNAi caused massive overproliferation in type II lineages, we could not detect any Dpn^+ Ase^- ectopic NB-like cells

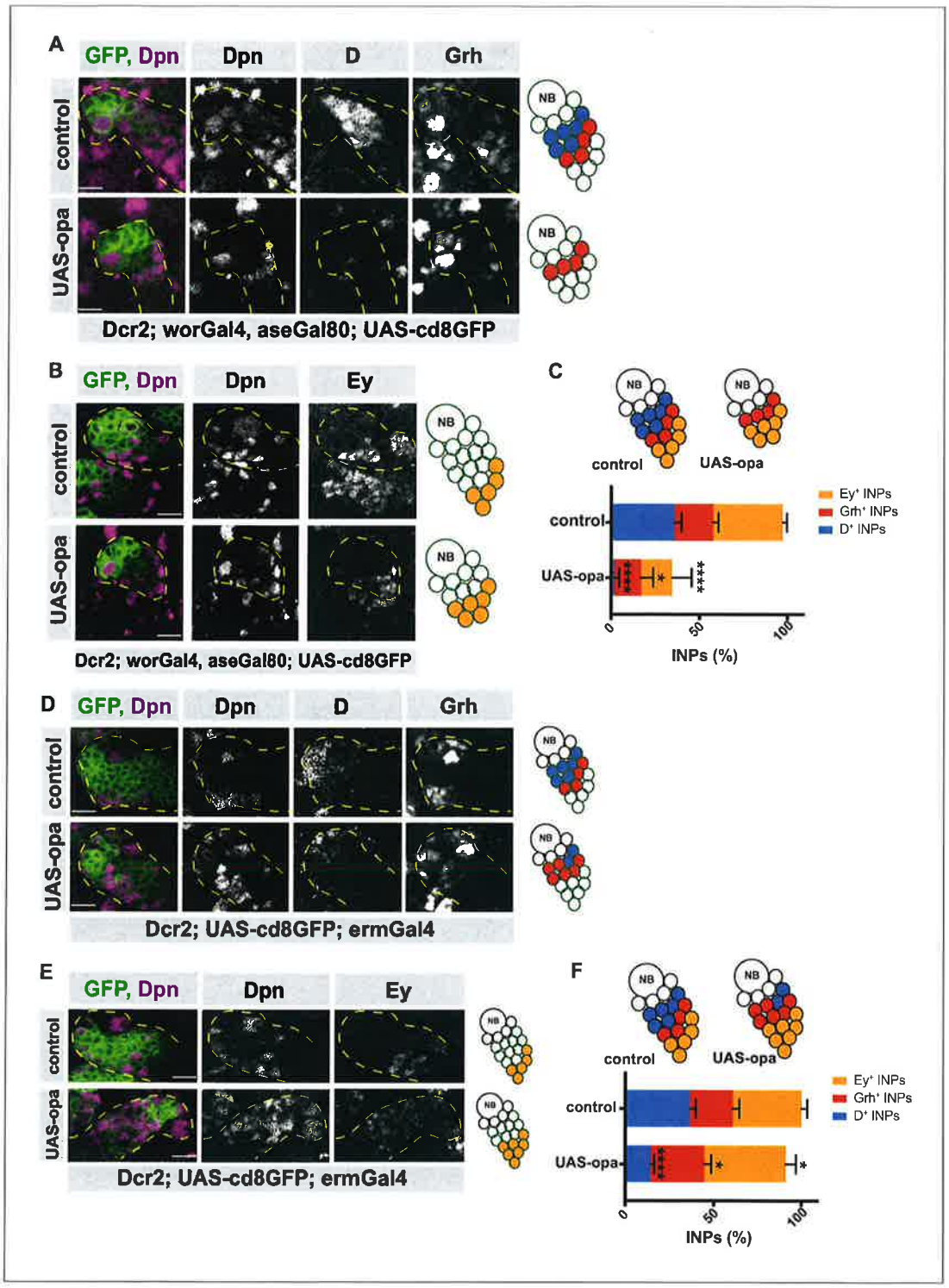

Figure 5. Opa overexpression results in the loss of D^+INPs. **(A)** Close-up images of control and opa overexpressing brains in type II lineages, stained for Dpn, D and Grh antibodies, lineages are outlined with yellow dashed lines, scale bar 10 µm, (induced with worGal4, aseGal80, marked with membrane bound GFP). Overexpression of opa in type II lineages causes the loss of D^+ INPs. **(B)** Close-up images of control and opa overexpressing brains in type II lineages, stained for Dpn, and Ey antibodies, lineages are outlined with yellow dashed lines, scale bar 10 µm, (induced with worGal4,

Figure 5 continued on next page

Figure 5 continued

aseGal80, marked with membrane bound GFP). (**C**) Quantification of D^+, Grh^+ and Ey^+ INPs in control and opa overexpressing brains, n = 10, total INP numbers in control were normalized to 100%. Data represent mean ± SD, p<=0.05, ***p<=0.001, Student's t-test (D^+ INPs control 12.18 ± 1.33 [n = 10], opa GOF 0.4 ± 0.6 [n = 10], p<0.001; Grh^+ INPs control 7.38 ± 1 [n = 10], opa GOF 5.12 ± 2.20 [n = 10], p<0.05; Ey^+ INPs control 13.5 ± 0.76 [n = 10], opa GOF 6 ± 3.5 [n = 10], p<0.001). (**D**) Close-up images of control and opa overexpressing brains in INPs, stained for Dpn, and Ey, lineages are outlined with yellow dashed lines, scale bar 10 µm, (induced with ermGal4, marked with membrane bound GFP). (**E**) Close-up images of control and opa overexpressing brains in INPs, stained for Dpn, D and Grh, lineages are outlined with yellow dashed lines, scale bar 10 µm, (induced with ermGal4, marked with membrane bound GFP). (**F**) Quantification of D^+, Grh^+ and Ey^+ INPs in control and opa overexpressing brains, n = 5, total INP numbers in control were normalized to 100%. Data represent mean ± SD, *p<=0.05, ***p<0.001, Student's t-test (D^+ INPs control 12.4 ± 1.01 [n = 5], opa GOF 4.83 ± 0.68 [n = 5], p<0.0001; Grh^+ INPs control 8.2 ± 1.16 [n = 5], opa GOF 10.33 ± 1.24 [n = 5], p<0.05; Ey^+ INPs control 13.4 ± 1.01 [n = 5], opa GOF 15.71 ± 1.9 [n = 5], p<0.05).

DOI: https://doi.org/10.7554/eLife.46566.029

The following source data and figure supplements are available for figure 5:

Source data 1. Quantification of number of INPs in three different temporal identities between control versus opa-overexpressed brains with type II-specific driver (***Figure 5C***).

DOI: https://doi.org/10.7554/eLife.46566.032

Source data 2. Quantification of number of INPs in three different temporal identities between control versus opa-overexpressed brains with INP-specific driver (***Figure 5F***).

DOI: https://doi.org/10.7554/eLife.46566.033

Figure supplement 1. Opa overexpression causes shorter type II lineages.

DOI: https://doi.org/10.7554/eLife.46566.030

Figure supplement 2. Opa overexpression causes loss of D^+INPs in DM1 lineages.

DOI: https://doi.org/10.7554/eLife.46566.031

Figure supplement 2—source data 1. Quantification of number of INPs in three different temporal identities between control versus opa-overexpressed brains with INP-specific driver in DM1 lineages (***Figure 5—figure supplement 2C***).

DOI: https://doi.org/10.7554/eLife.46566.034

(as occurs in Osa mutant clones, ***Eroglu et al., 2014***). We propose that this is caused by D expression which is still induced even upon opa/ham double knockdown, but not upon Osa knock-down where D expression fails to be initiated. Thus, the initiation of the first temporal identity state may block the reversion of INPs to a NB-state. In the future, it will be important to understand the exact mechanisms of how opa regulates temporal patterning.

We further demonstrate that Osa initiates D expression earlier than opa expression. Osa is a subunit of SWI/SNF chromatin remodeling complex, and it guides the complex to specific loci throughout the genome, such as the TSS of both D and opa. The differences in timing of D and opa expression may be explained by separate factors involved in their activation. Previous work suggests that the transcription factor earmuff may activate (***Janssens et al., 2014***; ***Janssens et al., 2017***). However, it remains unknown which factor activates opa expression. One possibility is that the cell cycle activates opa, since its expression begins in mINPs, a dividing cell unlike imINPs, which are in cell cycle arrest.

We propose that balanced expression levels of D and opa regulates the timing of transitions between temporal identity states. Indeed, Osa initiates D and opa, the repressor of D, at slightly different times, which could allow a time window for D to be expressed, perform its function, then become repressed again by opa. Deregulating this pattern, for example by overexpressing opa in the earliest INP stage, results in a false start of temporal patterning and premature differentiation. This elegant set of genetic interactions resembles that of an incoherent feedforward loop (FFL) (***Kim et al., 2008***; ***Mangan and Alon, 2003***). In such a network, pathways have opposing roles. For instance, Osa promotes both the expression and repression of D. Similar examples can be observed in other organisms, such as in the galactose network of *E. coli*, where the transcriptional activator CRP activates galS and galE, while galS also represses galE (***Shen-Orr et al., 2002***). In Drosophila SOP determination, miR-7, together with Atonal also forms an incoherent FFL (***Li et al., 2009***). Furthermore, mammals apply a similar mechanism in the c-Myc/E2F1 regulatory system (***O'Donnell et al., 2005***).

The vertebrate homologues of opa consist of the Zinc-finger protein of the cerebellum (ZIC) family, which are suggested to regulate the transcriptional activity of target genes, and to have a role in CNS development (***Elms et al., 2004***; ***Elms et al., 2003***; ***Gaston-Massuet et al., 2005***; ***Inoue et al.,***

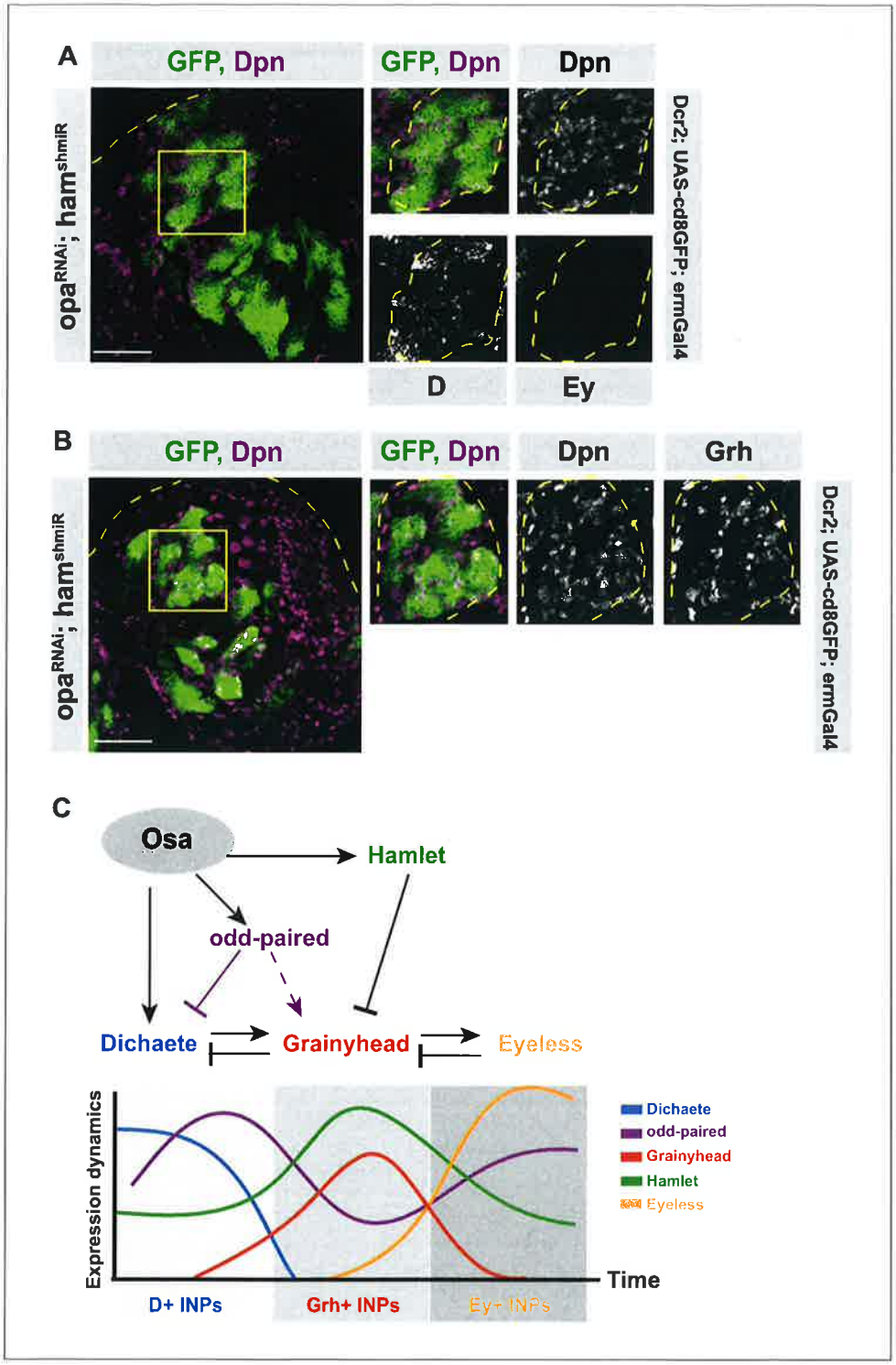

Figure 6. Opa and hamlet are required for INP temporal patterning and correct lineage progression. (**A–B**) Overview images of brain lobes expressing RNAi against opa and ham in INPs and their close-up images (marked with yellow squares), stained for Dpn, D and Ey (**A**), or Dpn and Grh (**B**) antibodies, lineages and lobes are outlined with yellow dashed lines, scale bar 50 µm for brain lobes, 10 µm for zoomed images, (induced with

Figure 6 continued on next page

Figure 6 continued

ermGal4, marked with membrane bound GFP). (**C**) Model depicting the genetic interactions between temporal switch genes (opa and hamlet), and temporal identity genes (D, Grh, and Ey).

DOI: https://doi.org/10.7554/eLife.46566.035

The following figure supplement is available for figure 6:

Figure supplement 1. Opa and hamlet cannot recapitulate Osa knock-down phenotype.

DOI: https://doi.org/10.7554/eLife.46566.036

2004; ***Inoue et al., 2007***). In mice, during embryonic cortical development, ZIC family proteins regulate the proliferation of meningeal cells, which are required for normal cortical development (***Inoue et al., 2008***). In addition, another member of the ZIC family, Zic1, is a Brn2 target, which itself controls the transition from early-to-mid neurogenesis in the mouse cortex (***Urban et al., 2015***). Along with these lines, it has been shown that ZIC family is important in brain development in zebrafish (***Maurus and Harris, 2009***; ***Sanek and Grinblat, 2008***). Furthermore, the role of ZIC has been implicated in variety of brain malformations and/or diseases (***Aruga et al., 2010***; ***Blank et al., 2011***; ***Hatayama et al., 2011***). These data provide mere glimpses into the roles of ZIC family proteins in neuronal fate decisions in mammals, and our study offers an important entry point to start understanding these remarkable proteins.

Our findings provide a novel regulatory network model controlling temporal patterning, which may occur in all metazoans, including humans. In contrast to existing cascade models, we instead show that temporal patterning is a highly coordinated ensemble that allows regulation on additional levels than was previously appreciated to ensure a perfectly balanced generation of different neuron/glial cell types. Together, our results demonstrate that *Drosophila* is a powerful system to dissect the genetic mechanisms underlying the temporal patterning of neural stem cells and how the disruption of such mechanisms impacts brain development and behavior.

Materials and methods

Key resources table

Reagent type (species) or resource	Designation	Source or reference	Identifiers	Additional information
Gene (*Drosophila melanogaster*)	osa	NA	FBgn0261885	
Gene (*D. melanogaster*)	Dichaete	NA	FBgn0000411	
Gene (*D. melanogaster*)	Grainyhead	NA	FBgn0259211	
Gene (*D. melanogaster*)	Eyeless	NA	FBgn0259211	
Gene (*D. melanogaster*)	Hamlet	NA	FBgn0045852	
Gene (*D. melanogaster*)	Odd-paired	NA	FBgn0003002	
Genetic reagent (*D. melanogaster*)	UAS-CD8::GFP; *erm*GAL4	PMID:18621688 and 20152183		
Genetic reagent (*D. melanogaster*)	UAS-CD8::td Tomato; *erm*GAL4	PMID:18621688 and 20152183		
Genetic reagent (*D. melanogaster*)	UAS-*dcr2; wor*-GAL4, *ase*GAL80; UAS-CD8::GFP	PMID:21549331		
Genetic reagent (*D. melanogaster*)	*VT17*-GAL4	Vienna Drosophila RNAi Center	212057, discarded	
Genetic reagent (*D. melanogaster*)	UAS-*stinger*::RFP	PMID:11056799		

Continued on next page

Continued

Reagent type (species) or resource	Designation	Source or reference	Identifiers	Additional information
Genetic reagent (*D. melanogaster*)	UAS-*opa*^{RNAi}	Vienna Drosophila RNAi Center	101531	
Genetic reagent (*D. melanogaster*)	UAS-D^{RNAi}	Vienna Drosophila RNAi Center	49549 and 107194	
Genetic reagent (*D. melanogaster*)	UAS-mcherry^{shmiR}	Bloomington Drosophila Stock Center	35785	
Genetic reagent (*D. melanogaster*)	UAS-osa^{RNAi}	Vienna Drosophila RNAi Center	7810	
Genetic reagent (*D. melanogaster*)	UAS-ham^{shmiR}	Bloomington Drosophila Stock Center	32470	
Genetic reagent (*D. melanogaster*)	UAS-osa^{shmiR}	PMID:2460726		
Genetic reagent (*D. melanogaster*)	UAS-p35	PMID:7925015		
Genetic reagent (*D. melanogaster*)	UAS-opa	PMID:17329368		
Genetic reagent (*D. melanogaster*)	D::GFP	this paper		endogenously GFP-tagged D in C-terminus
Genetic reagent (*D. melanogaster*)	Grh-GFP	Bloomington Drosophila Stock Center	42272	
Genetic reagent (*D. melanogaster*)	Ey-GFP	Bloomington Drosophila Stock Center	42271	
Genetic reagent (*D. melanogaster*)	opa::V5	this paper		endogenously V5-tagged opa in C-terminus
Genetic reagent (*D. melanogaster*)	FRT82B, *opa*^{7}	PMID:17329368		
Genetic reagent (*D. melanogaster*)	*elav*Gal4 (C155)	PMID:10197526		
Genetic reagent (*D. melanogaster*)	actCas9	Bloomington Drosophila Stock Center	54590	
Genetic reagent (*D. melanogaster*)	hsCre	Bloomington Drosophila Stock Center	851	
Antibody	anti-Deadpan (guinea pig, polyclonal)	PMID:2460726		(1:1000)
Antibody	anti-Asense (rat, polyclonal)	PMID:2460726		(1:500)
Antibody	anti-Miranda (guinea pig, polyclonal)	PMID:2460726		(1:500)
Antibody	anti-Grainyhead (rat, polyclonal)	PMID:19945380		(1:1000)
Antibody	anti-Dichaete (rabbit, polyclonal)	gift from Steve Russell		(1:1000)
Antibody	anti-Eyeless (mouse, monoclonal)	Developmental Studies Hybridoma Bank	anti-eyeless	(1:50), RRID:AB_2253542
Antibody	anti-Toy (guinea pig, polyclonal)	gift from Uwe Walldorf		(1:500)

Continued on next page

Continued

Reagent type (species) or resource	Designation	Source or reference	Identifiers	Additional information
Antibody	anti-Bsh (guinea pig, polyclonal)	gift from Makoto Sato, PMID:21303851		(1:500), RRID:AB_2567934
Antibody	anti-V5 (mouse, monoclonal)	Sigma Aldrich	V8012	(1:500 IF, 1:1000 WB), RRID:AB_261888
Antibody	anti-Bruchpilot nc82 (mouse, monoclonal)	Developmental Studies Hybridoma Bank	nc82	(1:10), RRID:AB_2314866
Antibody	anti-V5 IgG2a (mouse, monoclonal)	Thermo Fisher Scientific	R960-25	(1:500), RRID:AB_2556564
Antibody	anti-V5 (rabbit, polyclonal)	Abcam	ab9116	(1:500), RRID:AB_307024
Antibody	anti-Prospero (mouse, monoclonal)	Developmental Studies Hybridoma Bank	MR1A	(1:20), RRID:AB_528440
Antibody	anti-pH3(Ser10) (mouse, monoclonal)	Cell Signaling Technologies	9706S	(1:1000), RRID:AB_331748
Antibody	anti-aPKC (rabbit, polyclonal)	Santa Cruz Biotechnologies	sc-216	(1:500), RRID:AB_2300359
Antibody	anti-alpha tubulin (mouse, monoclonal)	Sigma Aldrich	T6199	(1:10000), RRID:AB_477583
Antibody	Alexa 405, 568, 647	Invitrogen	Alexa Fluor dyes	(1:500)
Antibody	IRDye 700, 800	LI-COR	IRDye	(1:15000)
Software, algorithm	Prism 7	GraphPad Software		
Software, algorithm	BWA	PMID:19451168		RRID:SCR_010910
Software, algorithm	TopHat	PMID:19289445		RRID:SCR_013035
Software, algorithm	HTSeq	PMID:25260700		RRID:SCR_005514
Software, algorithm	DESeq2 (v1.12.4)	PMID:25516281		RRID:SCR_016533
Software, algorithm	bedtools (v2.26.0)	PMID:20110278		RRID:SCR_006646
Commercial assay	TRIzol LS	Ambion	10296010	
Commercial assay	Agencourt AMPure XP beads	Beckman Coulter	A63880	
Commercial assay	Nextera DNA Library Prep Kit	Illumina	FC-121–1031	
Recombinant DNA reagent	pU6-BbsI-chiRNA	PMID:23709638		
Other	Rinaldini solution	PMID:22884370		

Fly strains, RNAi, and clonal analysis

The following *Drosophila* stocks were used: UAS-*opa*^{RNAi} (VDRC, TID: 101531), UAS-mcherry^{shmiR} (BL35785), UAS-D^{RNAi} (VDRC, TID: 49549, 107194), UAS-osa^{RNAi} (VDRC, TID: 7810), UAS-ham^{shmiR} (BL32470), UAS-osa^{shmiR} (***Eroglu et al., 2014***), UAS-p35, UAS-opa (***Lee et al., 2007***), PBac{grh-GFP.FPTB}VK00033 (BL42272), PBac{EyGFP.FPTB}VK00033 (BL42271) (***Spokony and White, 2012***), D::GFP (generated in this study), opa::V5 (generated in this study). GAL4 driver lines used: UAS-cd8::tdTomato; *erm*Gal4, UAS-cd8::GFP; *erm*Gal4 (***Pfeiffer et al., 2008***; ***Weng et al., 2010***), UAS-*dcr2; wor*Gal4, *ase*Gal80; UAS-cd8::GFP (***Neumüller et al., 2011***), UAS-*dcr2*; UAS-cd8::GFP; VT17-Gal4

(VDRC, TID: 212057, discarded). Mutant fly strains used for clonal analysis were FRT82B, *opa*^{7} (**Lee et al., 2007**). Clones were generated by Flippase (FLP)/FLP recombination target (FRT)-mediated mitotic recombination, using the *elav*Gal4 (C155) (**Lee and Luo, 1999**). Larvae were heat shocked for 90 min at 37˚C and dissected as third-instar wandering larvae (120 hr). RNAi crosses were set up and reared at 29˚C, and five days later, third-instar wandering larvae were dissected. w^{118} was used as control for comparison with RNAi lines, whereas UAS-mcherry^{shmiR} was used as control for comparison with shmiR lines, and experiments involving UAS-transgenes.

Generation of opa::V5 and D::GFP flies

For both genes, the guides were cloned as overlapping oligos into linearized pU6-BbsI-chiRNA (Addgene 45946, **Gratz et al., 2013**) and injected at 100 ng/µl into actCas9 flies (BL 54590, **Port et al., 2014**). Donors (either oligos or plasmid) were co-injected at 250 ng/µl. For opa, donors were Ultramer Oligos from IDT with around 60nt homology arms on either side. For D, homology arms were 800 bp and 900 bp long. Donor plasmid contained GFP, V5, 3xFlag, and dsRed. They were screened for dsRed eyes and then, the selection cassette was removed with hsCre (BL 851).
opa gRNA GATGCATCCCGGCGCAGCGA *opa* donor GAACCCGCTGAACCATTTCGGACACCA
TCACCACCACCACCACCTGATGCATCCCGGCGCgGCaACcGCGTATggtaagcctatacc-
taaccctcttcttggTCTAGAtagcacgTGAGAGTGGGAGAACTGG
TGGCCCGAGGAGGCGCCACCGCCGGCCGCCCAACCGA
D gRNA GTGCTCTATTAGAGTGGAGT

Negative geotaxis assay

Negative geotaxis assay was used as described before (**Ali et al., 2011**), where the percentage of flies passing the 8.5 cm mark in 10 s was assessed. For each genotype and gender, 10 two-day old adult flies in 10 biological replicates were measured and for each replicate, 10 measurements were performed with 1 min rest period in between.

Immunohistochemistry and antibodies

Larval or adult brains were dissected in 1X PBS, and then fixed for 20 min at room temperature (RT) in 5% paraformaldehyde in PBS and washed once with 0.1% TritonX in PBS (PBST). The brains were incubated for 1 hr at RT with blocking solution (5% normal goat serum or 1% BSA in PBST). Blocking was followed by overnight incubation at 4˚C with primary antibodies in blocking solution. Then, the brains were washed three times with PBST, and incubated for 1 hr at RT with secondary antibodies (1:500, goat Alexa Fluor, Invitrogen) in blocking solution. After secondary antibody, brains were washed three times with PBST, and mounted in Vectashield Antifade Mounting Medium (Vector Labs).

Antibodies used in this study were: guinea pig anti-Deadpan (1:1000, **Eroglu et al., 2014**), rat anti-Asense (1:500, **Eroglu et al., 2014**), guinea pig anti-Miranda (1:500, **Eroglu et al., 2014**), rat anti-Grh (1:1,000; **Baumgardt et al., 2009**); rabbit anti-D (1:1,000; gift from Steve Russell); mouse anti-Ey (1:10; DSHB); guinea pig anti-Toy (gift from Uwe Walldorf), guinea pig anti-Bsh (gift from Makoto Sato), mouse anti-Bruchpilot nc82 (1:10, DSHB), mouse anti-V5 (1:500, Sigma Aldrich, V8012), mouse antiV5 IgG2a (Thermo Fisher Scientific, R960-25, used in ***Figure 4—figure supplement 1D***), rabbit anti-V5 (Abcam, ab9116, used in ***Figure 4—figure supplement 3A***), mouse anti-Pros (1:100, Developmental Studies Hybridoma Bank), mouse anti-pH3(Ser10) (1:500, Cell Signaling Technologies, 9701S), rabbit anti-aPKC (1:500, Santa Cruz Biotechnology, sc-216). Throughout the paper, for every quantification, dorsomedial 2 and 3 type II NB lineages (DM2 and 3) were considered, if not stated otherwise.

In vitro immunofluorescence

FACS-sorted cells from ~300 larval brains (UAS-cd8::tdTomato, *erm*Gal4) or their unsorted control matches were plated on cover glass (Labtek II Chambered Coverglass, 8-well, 155409, Thermo Fisher Scientific) into Schneider's medium (**Homem et al., 2013**). The dishes were placed onto ice and cells were incubated for 1 hr to settle down. Cells were then fixed with 5% PFA in PBS at RT and washed three times with 0.1% PBST. After washes, cells were incubated for 1 hr at RT with blocking solution (5% normal goat serum in 0.1% PBST). The cells were then incubated overnight at

4°C with primary antibodies in blocking solution, which was followed by three washes with 0.1% PBST, and secondary antibody (1:500, goat Alexa Fluor, Invitrogen) incubation for 1 hr at RT. Cells were again washed three times with 0.1% PBST, and then mounted in in Vectashield Antifade Mounting Medium with Dapi (Vector Labs).

Microscopy

Confocal images were acquired with Zeiss LSM 780 confocal microscopes.

Western blot

Embryos were collected and dechorionated, then boiled in 2x Laemmli buffer and loaded on 4–12% gradient Bis-Tris gels (NuPAGE, Invitrogen). After SDS-PAGE according to Invitrogen's protocol, proteins were transferred to a Nitrocellulose membrane (0.22 µm, Odyssey LI-COR) for 2 hr at 100V, blocked with 5% milk powder in blocking solution (PBS with 0.2% Tween) for 1 hr, overnight incubation with primary antibody in blocking solution at 4°C, 3x washed with washing solution (PBS with 0.1% Tween) and followed by 1 hr incubation with secondary antibody (1:15000, goat IRDye, LI-COR)in blocking solution. After three washes with washing solution, the membranes were air-dried, and fluorescent signal were detected with Odyssey CLx imaging system (Odyssey CLx LI-COR). Antibodies used were: mouse anti-V5 (1:1000, Sigma Aldrich, V8012), anti-alpha tubulin (1:10000, Sigma Aldrich, T6199).

Intensity measurements

For intensity measurements of opa-V5 signal, cells expressing Dpn and temporal identity markers (D, Grh or Ey) were circled with selection tools. Raw integrity density (sum of gray values of all selected pixels) was measured using FIJI. In each image, five temporal identity positive INP and five temporal identity negative INP were measured for raw integrity density along with three background circles with no opa-V5 signal, (eg. D^+ vs D^- INPs). Then, corrected total cell fluorescent (CTCF) were calculated with 'Integrated density – (Area of selected cells X Mean fluorescence of background readings)' (***McCloy et al., 2014***). Then, the mean of temporal identity positive versus negative cells were calculated and the values were normalized to means of background for each brain.

Statistics

Statistical analyses were performed with GraphPad Prism 7. Unpaired two-tailed Student's *t*-test was used to assess statistical significance between two genotypes. Experiments were not randomized, and investigator was not blinded. Sample sizes for experiments were estimated on previous experience with similar setup which showed significance, thus, no statistical method was used to determine sample size.

Cell dissociation and FACS

Cell dissociation and FACS were performed as previously described with minor changes (***Berger et al., 2012***; ***Harzer et al., 2013***). UAS-cd8::tdTomato; *erm*Gal4 driver line was used to induce expression of membrane bound tdTomato in INPs. In addition to the driver lines, temporal identity factors were tagged with GFP. Flies expressing both fluorophores were dissected at L3 stage, and then dissociated into single cell suspension. Decreasing levels of tdTomato were observed in differentiated cells due to lack of driver line expression. Thus, biggest cells with highest tdTomato expression and highest GFP expression were sorted.

For RNA isolation, cells were sorted directly in TRIzol LS (10296010, Invitrogen), while for cell staining, they were sorted on coated glass-bottomed dishes and stained as previously described (***Berger et al., 2012***).

RNA isolation, cDNA synthesis and qPCR

RNA was isolated using TRIzol LS reagent (10296010, Invitrogen) from FACS sorted cells. Then RNA samples were used as template for first-strand cDNA synthesis with random hexamer primers (SuperScriptIII, Invitrogen). qPCR was done using Bio-Rad IQ SYBR Greeen Supermix on a Bio-Rad CFX96 cycler. Expression of each gene was normalized to Act5c, and relative levels were calculated using the $2^{-\Delta\Delta CT}$ method (***Livak and Schmittgen, 2001***). Primer used were:

act5c AGTGGTGGAAGTTTGGAGTG, GATAATGATGATGGTGTGCAGG
D ATGGGTCAACAGAAGTTGGGAG, GTATGGCGGTAGTTGATGGAATG
grh TCCCCTGCTTATGCTATGACCT, TACGGCTAGAGTTCGTGCAGA
ey TCGTCCGCTAACACCATGA, TGCTCAAATCGCCAGTCTGT
ham ATAGATCCTTTGGCCAGCAGAC, AGTACTCCTCCCTTTCGGCAAT
opa CTGAACCATTTCGGACACCATC, CCAGTTCTCCCACTCTCAATAC

RNA sequencing – DigiTAG

For each experiment 6000–7000 FACS-sorted D^+, Grh^+ or Ey^+ INPs were isolated by TRIzol purification. Three replicates from each temporal state were analyzed. RNA samples were reverse transcribe into first-strand cDNA using SuperScriptIII Reverse Transcriptase (Invitrogen) with oligo-(dT)2- primers. Then the second-strand cDNA were generated. It was followed by library preparation with Nextera DNA Library Preparation Kit (Illumina) as previously described (***Landskron et al., 2018***; ***Wissel et al., 2018***). Libraries were purified with Agencourt AMPure XP beads. Purified libraries were then subjected to 50 base pair Illumina single-end sequencing on a Hiseq2000 platform.

Transcriptome data analysis

Alignment

Unstranded reads were screened for ribosomal RNA by aligning with BWA (v0.7.12; ***Li and Durbin, 2009***) against known rRNA sequences (RefSeq). The rRNA subtracted reads were aligned with TopHat (v2.1.1; ***Kim et al., 2013***) against the Drosophila genome (FlyBase r6.12). Introns between 20 and 150,000 bp are allowed, which is based on FlyBase statistics. Microexon-search was enabled. Additionally, a gene model was provided as GTF (FlyBase r6.12).

Deduplication

Reads arising from duplication events are marked as such in the alignment (SAM/BAM files) as follows. The different tags are counted at each genomic position. Thereafter, the diversity of tags at each position is examined. First, tags are sorted descending by their count. If several tags have the same occurrence, they are further sorted alphanumerically. Reads sharing the same tag are sorted by the mean PHRED quality. Again, if several reads have the same quality, they are further sorted alphanumerically. Now the tags are cycled through by their counts. Within one tag, the read with the highest mean PHRED quality is the unique cor- rect read and all subsequent reads with the same tag are marked as duplicates. Furthermore, all reads that have tags with one mis- match difference compared the pool of valid read tags are also marked as duplicates.

Summarization

Small nuclear RNA, rRNA, tRNA, small nucleolar RNA, and pseudogenes are masked from the GTF (FlyBase r6.12) with subtractBed from bedtools (v2.26.0; ***Quinlan and Hall, 2010***). The aligned reads were counted with HTSeq (v0.6.1; intersec- tion-nonempty), and genes were subjected to differential expres- sion analysis with DESeq2 (v1.12.4; ***Love et al., 2014***).

Hierarchical clustering analysis

Genes are filtered by the indicated log2fc and an adjusted P value < 0.05 in at least one pairwise comparison. In addition, a minimal expression of 10 RPM in at least one condition was required. The tree cut into four clusters (different cluster numbers were tested; ***Kolde and Package, 2015***, 202AD). GO analysis was performed with FlyMine (***Lyne et al., 2007***), Holm-Bonferroni correction with max p-value 0.05 was used. Biological process and molecular function were the ontologies.

Accession numbers

The Gene Expression Omnibus accession number for the RNA-sequencing data reported in this paper is GSE127516.

GO-term analysis

Gene Ontology (GO) enrichment analysis were performed on www.flymine.org/with Holm-Bonferroni correction with max p-value 0.05. Biological process and molecular function were the ontologies.

Acknowledgements

We thank all Knoblich lab members for support and discussions, Francois Bonnay, Tom Kruitwagen and Joshua A Bagley for comments on the manuscript, Peter Duchek, Joseph Gokcezade, Elke Kleiner, the IMP/IMBA Biooptics Facility and the Next Generation Sequencing Unit of the Vienna Biocenter Core Facilities (VBCF) for assistance and Makoto Sato, Uwe Walldorf, Stefan Thor and Steve Russel for sharing reagents, and the Harvard TRiP collection, the Bloomington Drosophila stock center and the Vienna Drosophila Resource Center (VDRC) for reagents.

Additional information

Funding

Funder	Grant reference number	Author
Austrian Academy of Sciences		Jürgen A Knoblich
Austrian Science Fund	Z_153_B09	Jürgen A Knoblich
European Commission		Jürgen A Knoblich

The funders had no role in study design, data collection and interpretation, or the decision to submit the work for publication.

Author contributions

Merve Deniz Abdusselamoglu, Conceptualization, Formal analysis, Investigation, Visualization, Writing—original draft, Project administration; Elif Eroglu, Conceptualization, Data curation, Formal analysis; Thomas R Burkard, Formal analysis, Conducted all bioinformatic analyses; Jürgen A Knoblich, Conceptualization, Supervision, Funding acquisition, Writing—original draft, Project administration, Writing—review and editing

Author ORCIDs

Merve Deniz Abdusselamoglu https://orcid.org/0000-0001-8467-3947
Jürgen A Knoblich https://orcid.org/0000-0002-6751-3404

Decision letter and Author response

Decision letter https://doi.org/10.7554/eLife.46566.041
Author response https://doi.org/10.7554/eLife.46566.042

Additional files

Supplementary files

- Supplementary file 1. List of genes that are dynamically changing between INP populations with higher expression in D^+ and Ey^+ INPs.

DOI: https://doi.org/10.7554/eLife.46566.037

- Supplementary file 2. List of genes that are dynamically changing between INP populations with highest expression in Grh^+ INPs.

DOI: https://doi.org/10.7554/eLife.46566.038

- Transparent reporting form

DOI: https://doi.org/10.7554/eLife.46566.039

Data availability

Sequencing data have been deposited in GEO under accession code GSE127516. All data generated or analyzed during this study are included in the manuscript and supporting files. Source data files have been provided for Fig1, Fig1supp1, Fig2, Fig2supp1, Fig2supp2, Fig3, Fig4, Fig4supp3, Fig5 and Fig5supp2.

References

Ali YO, Escala W, Ruan K, Zhai RG. 2011. Assaying locomotor, learning, and memory deficits in *Drosophila* models of neurodegeneration. *Journal of Visualized Experiments*. DOI: https://doi.org/10.3791/2504, PMID: 21445036

Alon U. 2007. Network motifs: theory and experimental approaches. *Nature Reviews Genetics* **8**:450–461. DOI: https://doi.org/10.1038/nrg2102, PMID: 17510665

Alsiö JM, Tarchini B, Cayouette M, Livesey FJ. 2013. Ikaros promotes early-born neuronal fates in the cerebral cortex. *PNAS* **110**:E716–E725. DOI: https://doi.org/10.1073/pnas.1215707110, PMID: 23382203

Aruga J, Nozaki Y, Hatayama M, Odaka YS, Yokota N. 2010. Expression of ZIC family genes in meningiomas and other brain tumors. *BMC Cancer* **10**:79. DOI: https://doi.org/10.1186/1471-2407-10-79, PMID: 20199689

Baumgardt M, Karlsson D, Terriente J, Díaz-Benjumea FJ, Thor S. 2009. Neuronal subtype specification within a lineage by opposing temporal feed-forward loops. *Cell* **139**:969–982. DOI: https://doi.org/10.1016/j.cell.2009.10.032, PMID: 19945380

Baumgardt M, Karlsson D, Salmani BY, Bivik C, MacDonald RB, Gunnar E, Thor S. 2014. Global programmed switch in neural daughter cell proliferation mode triggered by a temporal gene cascade. *Developmental Cell* **30**:192–208. DOI: https://doi.org/10.1016/j.devcel.2014.06.021, PMID: 25073156

Bayraktar OA, Boone JQ, Drummond ML, Doe CQ. 2010. *Drosophila* type II neuroblast lineages keep prospero levels low to generate large clones that contribute to the adult brain central complex. *Neural Development* **5**:26. DOI: https://doi.org/10.1186/1749-8104-5-26, PMID: 20920301

Bayraktar OA, Doe CQ. 2013. Combinatorial temporal patterning in progenitors expands neural diversity. *Nature* **498**:449–455. DOI: https://doi.org/10.1038/nature12266, PMID: 23783519

Bello BC, Izergina N, Caussinus E, Reichert H. 2008. Amplification of neural stem cell proliferation by intermediate progenitor cells in *Drosophila* brain development. *Neural Development* **3**:5. DOI: https://doi.org/10.1186/1749-8104-3-5, PMID: 18284664

Benedyk MJ, Mullen JR, DiNardo S. 1994. odd-paired: a zinc finger pair-rule protein required for the timely activation of engrailed and wingless in *Drosophila* embryos. *Genes & Development* **8**:105–117. DOI: https://doi.org/10.1101/gad.8.1.105, PMID: 8288124

Berger C, Harzer H, Burkard TR, Steinmann J, van der Horst S, Laurenson AS, Novatchkova M, Reichert H, Knoblich JA. 2012. FACS purification and transcriptome analysis of *Drosophila* neural stem cells reveals a role for klumpfuss in self-renewal. *Cell Reports* **2**:407–418. DOI: https://doi.org/10.1016/j.celrep.2012.07.008, PMID: 22884370

Blank MC, Grinberg I, Aryee E, Laliberte C, Chizhikov VV, Henkelman RM, Millen KJ. 2011. Multiple developmental programs are altered by loss of Zic1 and Zic4 to cause Dandy-Walker malformation cerebellar pathogenesis. *Development* **138**:1207–1216. DOI: https://doi.org/10.1242/dev.054114, PMID: 21307096

Boone JQ, Doe CQ. 2008. Identification of *Drosophila* type II neuroblast lineages containing transit amplifying ganglion mother cells. *Developmental Neurobiology* **68**:1185–1195. DOI: https://doi.org/10.1002/dneu.20648, PMID: 18548484

Bowman SK, Rolland V, Betschinger J, Kinsey KA, Emery G, Knoblich JA. 2008. The tumor suppressors brat and numb regulate transit-amplifying neuroblast lineages in *Drosophila*. *Developmental Cell* **14**:535–546. DOI: https://doi.org/10.1016/j.devcel.2008.03.004, PMID: 18342578

Callaerts P, Leng S, Clements J, Benassayag C, Cribbs D, Kang YY, Walldorf U, Fischbach KF, Strauss R. 2001. *Drosophila* Pax-6/eyeless is essential for normal adult brain structure and function. *Journal of Neurobiology* **46**:73–88. DOI: https://doi.org/10.1002/1097-4695(20010205)46:2<73::AID-NEU10>3.0.CO;2-N, PMID: 11153010

Cepko CL, Austin CP, Yang X, Alexiades M, Ezzeddine D. 1996. Cell fate determination in the vertebrate retina. *PNAS* **93**:589–595. DOI: https://doi.org/10.1073/pnas.93.2.589, PMID: 8570600

Doe CQ. 2017. Temporal patterning in the *Drosophila* CNS. *Annual Review of Cell and Developmental Biology* **33**:219–240. DOI: https://doi.org/10.1146/annurev-cellbio-111315-125210, PMID: 28992439

Elms P, Siggers P, Napper D, Greenfield A, Arkell R. 2003. Zic2 is required for neural crest formation and hindbrain patterning during mouse development. *Developmental Biology* **264**:391–406. DOI: https://doi.org/10.1016/j.ydbio.2003.09.005, PMID: 14651926

Elms P, Scurry A, Davies J, Willoughby C, Hacker T, Bogani D, Arkell R. 2004. Overlapping and distinct expression domains of Zic2 and Zic3 during mouse gastrulation. *Gene Expression Patterns* **4**:505–511. DOI: https://doi.org/10.1016/j.modgep.2004.03.003, PMID: 15261827

Eroglu E, Burkard TR, Jiang Y, Saini N, Homem CCF, Reichert H, Knoblich JA. 2014. SWI/SNF complex prevents lineage reversion and induces temporal patterning in neural stem cells. *Cell* **156**:1259–1273. DOI: https://doi.org/10.1016/j.cell.2014.01.053, PMID: 24630726

Gao P, Postiglione MP, Krieger TG, Hernandez L, Wang C, Han Z, Streicher C, Papusheva E, Insolera R, Chugh K, Kodish O, Huang K, Simons BD, Luo L, Hippenmeyer S, Shi SH. 2014. Deterministic progenitor behavior and unitary production of neurons in the neocortex. *Cell* **159**:775–788. DOI: https://doi.org/10.1016/j.cell.2014.10.027, PMID: 25417155

Gaston-Massuet C, Henderson DJ, Greene ND, Copp AJ. 2005. Zic4, a zinc-finger transcription factor, is expressed in the developing mouse nervous system. *Developmental Dynamics* **233**:1110–1115. DOI: https://doi.org/10.1002/dvdy.20417, PMID: 15895369

Gratz SJ, Cummings AM, Nguyen JN, Hamm DC, Donohue LK, Harrison MM, Wildonger J, O'Connor-Giles KM. 2013. Genome engineering of *Drosophila* with the CRISPR RNA-guided Cas9 nuclease. *Genetics* **194**:1029–1035. DOI: https://doi.org/10.1534/genetics.113.152710, PMID: 23709638

Greig LC, Woodworth MB, Galazo MJ, Padmanabhan H, Macklis JD. 2013. Molecular logic of neocortical projection neuron specification, development and diversity. *Nature Reviews Neuroscience* **14**:755–769. DOI: https://doi.org/10.1038/nrn3586, PMID: 24105342

Harzer H, Berger C, Conder R, Schmauss G, Knoblich JA. 2013. FACS purification of *Drosophila* larval neuroblasts for next-generation sequencing. *Nature Protocols* **8**:1088–1099. DOI: https://doi.org/10.1038/nprot.2013.062, PMID: 23660757

Hatayama M, Ishiguro A, Iwayama Y, Takashima N, Sakoori K, Toyota T, Nozaki Y, Odaka YS, Yamada K, Yoshikawa T, Aruga J. 2011. Zic2 hypomorphic mutant mice as a schizophrenia model and ZIC2 mutations identified in schizophrenia patients. *Scientific Reports* **1**:16. DOI: https://doi.org/10.1038/srep00016, PMID: 22355535

Holguera I, Desplan C. 2018. Neuronal specification in space and time. *Science* **362**:176–180. DOI: https://doi.org/10.1126/science.aas9435, PMID: 30309944

Homem CC, Reichardt I, Berger C, Lendl T, Knoblich JA. 2013. Long-term live cell imaging and automated 4D analysis of *Drosophila* neuroblast lineages. *PLOS ONE* **8**:e79588. DOI: https://doi.org/10.1371/journal.pone.0079588, PMID: 24260257

Homem CC, Knoblich JA. 2012. *Drosophila* neuroblasts: a model for stem cell biology. *Development* **139**:4297–4310. DOI: https://doi.org/10.1242/dev.080515, PMID: 23132240

Inoue T, Hatayama M, Tohmonda T, Itohara S, Aruga J, Mikoshiba K. 2004. Mouse Zic5 deficiency results in neural tube defects and hypoplasia of cephalic neural crest derivatives. *Developmental Biology* **270**:146–162. DOI: https://doi.org/10.1016/j.ydbio.2004.02.017, PMID: 15136147

Inoue T, Ota M, Ogawa M, Mikoshiba K, Aruga J. 2007. Zic1 and Zic3 regulate medial forebrain development through expansion of neuronal progenitors. *Journal of Neuroscience* **27**:5461–5473. DOI: https://doi.org/10.1523/JNEUROSCI.4046-06.2007, PMID: 17507568

Inoue T, Ogawa M, Mikoshiba K, Aruga J. 2008. Zic deficiency in the cortical marginal zone and meninges results in cortical lamination defects resembling those in type II lissencephaly. *Journal of Neuroscience* **28**:4712–4725. DOI: https://doi.org/10.1523/JNEUROSCI.5735-07.2008, PMID: 18448648

Isshiki T, Pearson B, Holbrook S, Doe CQ. 2001. *Drosophila* neuroblasts sequentially express transcription factors which specify the temporal identity of their neuronal progeny. *Cell* **106**:511–521. DOI: https://doi.org/10.1016/S0092-8674(01)00465-2, PMID: 11525736

Izergina N, Balmer J, Bello B, Reichert H. 2009. Postembryonic development of transit amplifying neuroblast lineages in the *Drosophila* brain. *Neural Development* **4**:44. DOI: https://doi.org/10.1186/1749-8104-4-44, PMID: 20003348

Janssens DH, Komori H, Grbac D, Chen K, Koe CT, Wang H, Lee CY. 2014. Earmuff restricts progenitor cell potential by attenuating the competence to respond to self-renewal factors. *Development* **141**:1036–1046. DOI: https://doi.org/10.1242/dev.106534, PMID: 24550111

Janssens DH, Hamm DC, Anhezini L, Xiao Q, Siller KH, Siegrist SE, Harrison MM, Lee CY. 2017. An Hdac1/Rpd3-Poised circuit balances continual Self-Renewal and rapid restriction of developmental potential during asymmetric stem cell division. *Developmental Cell* **40**:367–380. DOI: https://doi.org/10.1016/j.devcel.2017.01.014, PMID: 28245922

Kim D, Kwon YK, Cho KH. 2008. The biphasic behavior of incoherent feed-forward loops in biomolecular regulatory networks. *BioEssays* **30**:1204–1211. DOI: https://doi.org/10.1002/bies.20839, PMID: 18937374

Kim D, Pertea G, Trapnell C, Pimentel H, Kelley R, Salzberg SL. 2013. TopHat2: accurate alignment of transcriptomes in the presence of insertions, deletions and gene fusions. *Genome Biology* **14**:R36. DOI: https://doi.org/10.1186/gb-2013-14-4-r36, PMID: 23618408

Kohwi M, Lupton JR, Lai SL, Miller MR, Doe CQ. 2013. Developmentally regulated subnuclear genome reorganization restricts neural progenitor competence in *Drosophila*. *Cell* **152**:97–108. DOI: https://doi.org/10.1016/j.cell.2012.11.049, PMID: 23332748

Kolde R, Package MKR. 2015. *Package Pheatmap*.

Landskron L, Steinmann V, Bonnay F, Burkard TR, Steinmann J, Reichardt I, Harzer H, Laurenson AS, Reichert H, Knoblich JA. 2018. The asymmetrically segregating lncRNA cherub is required for transforming stem cells into malignant cells. *eLife* **7**:e31347. DOI: https://doi.org/10.7554/eLife.31347, PMID: 29580384

Lee H, Stultz BG, Hursh DA. 2007. The zic family member, odd-paired, regulates the *Drosophila* BMP, decapentaplegic, during adult head development. *Development* **134**:1301–1310. DOI: https://doi.org/10.1242/dev.02807, PMID: 17329368

Lee T, Luo L. 1999. Mosaic analysis with a repressible cell marker for studies of gene function in neuronal morphogenesis. *Neuron* **22**:451–461. DOI: https://doi.org/10.1016/S0896-6273(00)80701-1, PMID: 10197526

Li X, Cassidy JJ, Reinke CA, Fischboeck S, Carthew RW. 2009. A microRNA imparts robustness against environmental fluctuation during development. *Cell* **137**:273–282. DOI: https://doi.org/10.1016/j.cell.2009.01.058, PMID: 19379693

Li H, Durbin R. 2009. Fast and accurate short read alignment with Burrows-Wheeler transform. *Bioinformatics* **25**:1754–1760. DOI: https://doi.org/10.1093/bioinformatics/btp324, PMID: 19451168

Liu Z, Yang CP, Sugino K, Fu CC, Liu LY, Yao X, Lee LP, Lee T. 2015. Opposing intrinsic temporal gradients guide neural stem cell production of varied neuronal fates. *Science* **350**:317–320. DOI: https://doi.org/10.1126/science.aad1886, PMID: 26472907

Livak KJ, Schmittgen TD. 2001. Analysis of relative gene expression data using real-time quantitative PCR and the 2(-Delta delta C(T)) Method. *Methods* **25**:402–408. DOI: https://doi.org/10.1006/meth.2001.1262, PMID: 11846609

Livesey FJ, Cepko CL. 2001. Vertebrate neural cell-fate determination: lessons from the retina. *Nature Reviews Neuroscience* **2**:109–118. DOI: https://doi.org/10.1038/35053522, PMID: 11252990

Love MI, Huber W, Anders S. 2014. Moderated estimation of fold change and dispersion for RNA-seq data with DESeq2. *Genome Biology* **15**:550. DOI: https://doi.org/10.1186/s13059-014-0550-8, PMID: 25516281

Lyne R, Smith R, Rutherford K, Wakeling M, Varley A, Guillier F, Janssens H, Ji W, Mclaren P, North P, Rana D, Riley T, Sullivan J, Watkins X, Woodbridge M, Lilley K, Russell S, Ashburner M, Mizuguchi K, Micklem G. 2007. FlyMine: an integrated database for *Drosophila* and anopheles genomics. *Genome Biology* **8**:R129. DOI: https://doi.org/10.1186/gb-2007-8-7-r129, PMID: 17615057

Mangan S, Alon U. 2003. Structure and function of the feed-forward loop network motif. *PNAS* **100**:11980–11985. DOI: https://doi.org/10.1073/pnas.2133841100, PMID: 14530388

Mattar P, Ericson J, Blackshaw S, Cayouette M. 2015. A conserved regulatory logic controls temporal identity in mouse neural progenitors. *Neuron* **85**:497–504. DOI: https://doi.org/10.1016/j.neuron.2014.12.052, PMID: 25654255

Maurus D, Harris WA. 2009. Zic-associated holoprosencephaly: zebrafish Zic1 controls midline formation and forebrain patterning by regulating nodal, hedgehog, and retinoic acid signaling. *Genes & Development* **23**:1461–1473. DOI: https://doi.org/10.1101/gad.517009, PMID: 19528322

McCloy RA, Rogers S, Caldon CE, Lorca T, Castro A, Burgess A. 2014. Partial inhibition of Cdk1 in G 2 phase overrides the SAC and decouples mitotic events. *Cell Cycle* **13**:1400–1412. DOI: https://doi.org/10.4161/cc.28401, PMID: 24626186

Mizugishi K, Aruga J, Nakata K, Mikoshiba K. 2001. Molecular properties of zic proteins as transcriptional regulators and their relationship to GLI proteins. *Journal of Biological Chemistry* **276**:2180–2188. DOI: https://doi.org/10.1074/jbc.M004430200, PMID: 11053430

Naka H, Nakamura S, Shimazaki T, Okano H. 2008. Requirement for COUP-TFI and II in the temporal specification of neural stem cells in CNS development. *Nature Neuroscience* **11**:1014–1023. DOI: https://doi.org/10.1038/nn.2168, PMID: 19160499

Neumüller RA, Richter C, Fischer A, Novatchkova M, Neumüller KG, Knoblich JA. 2011. Genome-wide analysis of self-renewal in *Drosophila* neural stem cells by transgenic RNAi. *Cell Stem Cell* **8**:580–593. DOI: https://doi.org/10.1016/j.stem.2011.02.022, PMID: 21549331

O'Donnell KA, Wentzel EA, Zeller KI, Dang CV, Mendell JT. 2005. c-Myc-regulated microRNAs modulate E2F1 expression. *Nature* **435**:839–843. DOI: https://doi.org/10.1038/nature03677, PMID: 15944709

Okamoto M, Miyata T, Konno D, Ueda HR, Kasukawa T, Hashimoto M, Matsuzaki F, Kawaguchi A. 2016. Cell-cycle-independent transitions in temporal identity of mammalian neural progenitor cells. *Nature Communications* **7**:11349. DOI: https://doi.org/10.1038/ncomms11349, PMID: 27094546

Pfeiffer BD, Jenett A, Hammonds AS, Ngo T-TB, Misra S, Murphy C, Scully A, Carlson JW, Wan KH, Laverty TR, Mungall C, Svirskas R, Kadonaga JT, Doe CQ, Eisen MB, Celniker SE, Rubin GM. 2008. Tools for neuroanatomy and neurogenetics in *Drosophila*. *PNAS* **105**:9715–9720. DOI: https://doi.org/10.1073/pnas.0803697105

Port F, Chen HM, Lee T, Bullock SL. 2014. Optimized CRISPR/Cas tools for efficient germline and somatic genome engineering in *Drosophila*. *PNAS* **111**:E2967–E2976. DOI: https://doi.org/10.1073/pnas.1405500111, PMID: 25002478

Quinlan AR, Hall IM. 2010. BEDTools: a flexible suite of utilities for comparing genomic features. *Bioinformatics* **26**:841–842. DOI: https://doi.org/10.1093/bioinformatics/btq033, PMID: 20110278

Ren Q, Yang CP, Liu Z, Sugino K, Mok K, He Y, Ito M, Nern A, Otsuna H, Lee T. 2017. Stem Cell-Intrinsic, Seven-up-Triggered temporal factor gradients diversify intermediate neural progenitors. *Current Biology* **27**:1303–1313. DOI: https://doi.org/10.1016/j.cub.2017.03.047, PMID: 28434858

Ren Q, Awasaki T, Wang YC, Huang YF, Lee T. 2018. Lineage-guided Notch-dependent gliogenesis by *Drosophila* multi-potent progenitors. *Development* **145**:dev160127. DOI: https://doi.org/10.1242/dev.160127, PMID: 29764857

Sanek NA, Grinblat Y. 2008. A novel role for zebrafish zic2a during forebrain development. *Developmental Biology* **317**:325–335. DOI: https://doi.org/10.1016/j.ydbio.2008.02.029, PMID: 18358464

Shen-Orr SS, Milo R, Mangan S, Alon U. 2002. Network motifs in the transcriptional regulation network of *Escherichia coli*. *Nature Genetics* **31**:64–68. DOI: https://doi.org/10.1038/ng881

Spokony R, White K. 2012. *Spokony Insertions*: Personal communication to FlyBase.

Syed MH, Mark B, Doe CQ. 2017. Steroid hormone induction of temporal gene expression in *Drosophila* brain neuroblasts generates neuronal and glial diversity. *eLife* **6**:e26287. DOI: https://doi.org/10.7554/eLife.26287, PMID: 28394252

Toma K, Kumamoto T, Hanashima C. 2014. The timing of upper-layer neurogenesis is conferred by sequential derepression and negative feedback from deep-layer neurons. *Journal of Neuroscience* **34**:13259–13276. DOI: https://doi.org/10.1523/JNEUROSCI.2334-14.2014, PMID: 25253869

Urban S, Kobi D, Ennen M, Langer D, Le Gras S, Ye T, Davidson I. 2015. A Brn2-Zic1 axis specifies the neuronal fate of retinoic-acid-treated embryonic stem cells. *Journal of Cell Science* **128**:2303–2318. DOI: https://doi.org/10.1242/jcs.168849, PMID: 25991548

Viktorin G, Riebli N, Reichert H. 2013. A multipotent transit-amplifying neuroblast lineage in the central brain gives rise to optic lobe glial cells in *Drosophila*. *Developmental Biology* **379**:182–194. DOI: https://doi.org/10.1016/j.ydbio.2013.04.020, PMID: 23628691

Walsh KT, Doe CQ. 2017. *Drosophila* embryonic type II neuroblasts: origin, temporal patterning, and contribution to the adult central complex. *Development* **144**:4552–4562. DOI: https://doi.org/10.1242/dev.157826, PMID: 29158446

Wang W, Jossin Y, Chai G, Lien WH, Tissir F, Goffinet AM. 2016. Feedback regulation of apical progenitor fate by immature neurons through Wnt7-Celsr3-Fzd3 signalling. *Nature Communications* **7**:10936. DOI: https://doi.org/10.1038/ncomms10936, PMID: 26939553

Weng M, Golden KL, Lee CY. 2010. dFezf/Earmuff maintains the restricted developmental potential of intermediate neural progenitors in *Drosophila*. *Developmental Cell* **18**:126–135. DOI: https://doi.org/10.1016/j.devcel.2009.12.007, PMID: 20152183

Wissel S, Harzer H, Bonnay F, Burkard TR, Neumüller RA, Knoblich JA. 2018. Time-resolved transcriptomics in neural stem cells identifies a v-ATPase/Notch regulatory loop. *The Journal of Cell Biology* **217**:3285–3300. DOI: https://doi.org/10.1083/jcb.201711167, PMID: 29959232

Young JM, Armstrong JD. 2010. Structure of the adult central complex in *Drosophila*: organization of distinct neuronal subsets. *The Journal of Comparative Neurology* **518**:1500–1524 . DOI: https://doi.org/10.1002/cne.22284, PMID: 20187142

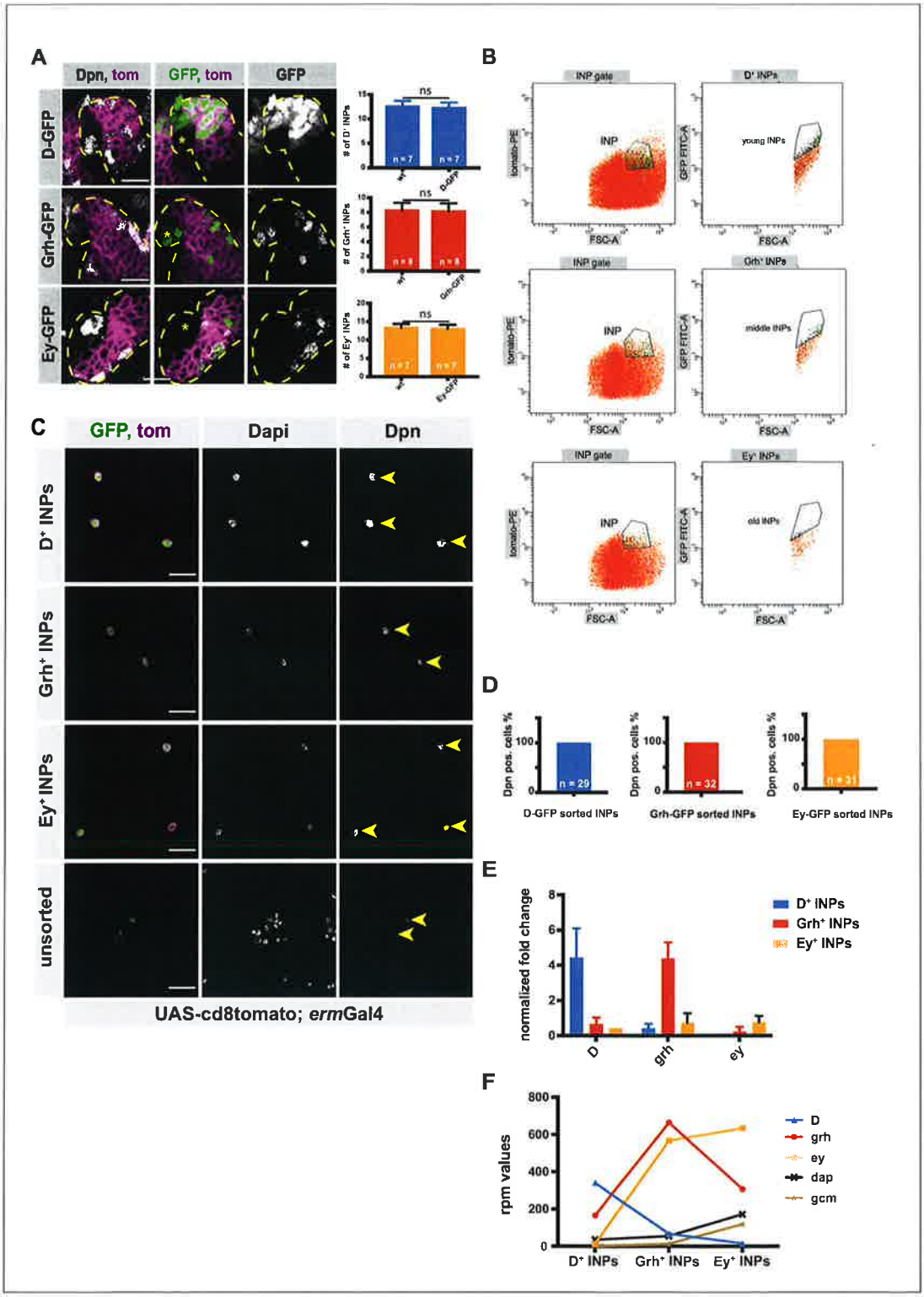

Figure 1—figure supplement 1. INPs can be FACS-sorted depending on their temporal identity. (**A**) Close-up images of larval brains expressing tdtomato in INP-specific manner (UAS-cd8tomato; ermGal4, shown in magenta) and temporal identity markers, Dichaete, Grainyhead and Eyeless

Figure 1—figure supplement 1 continued on next page

Figure 1—figure supplement 1 continued

tagged with GFP, stained for Dpn (gray). Type II lineages are outlined with yellow dashed lines, NBs are marked with *, scale bar 10 µm, (induced with ermGal4, marked with membrane bound tdTomato). Graphs showing the numbers of each temporal identity markers in control vs GFP-tagged brains. (**B**) Representative FACS plots of sorted INP temporal stages. The population with highest tomato and GFP expression (vertical axis) versus biggest cell size (horizontal axis) was sorted to obtain D^+, Grh^+, and Ey^+ INPs. (**C**) D-, Grh- and Ey-GFP FACS-sorted cells and their unsorted control are stained for Dpn (gray), GFP-tagging temporal identity factors (in green, D or, Grh or Ey), tdTomato tagging the membrane of INPs (magenta), Dapi (gray), scale bar 20 µm, yellow arrowheads mark Dpn positive cells, (induced with ermGal4, marked with membrane bound tdTomato). (**D**) Graph showing the percentages of Dpn positive cells, n is the number of the cells analyzed. (**E**) qPCR analysis of temporal identity expression levels in FACS-sorted D^+, Grh^+ and Ey^+ INPs. Data are mean ± SD, n = 3, genes were normalized to Act5c, and then the average expression levels, Delta-Delta Ct method is used. (**F**) Graph showing the rpm levels of marker genes between different INP temporal stages.

DOI: https://doi.org/10.7554/eLife.46566.004

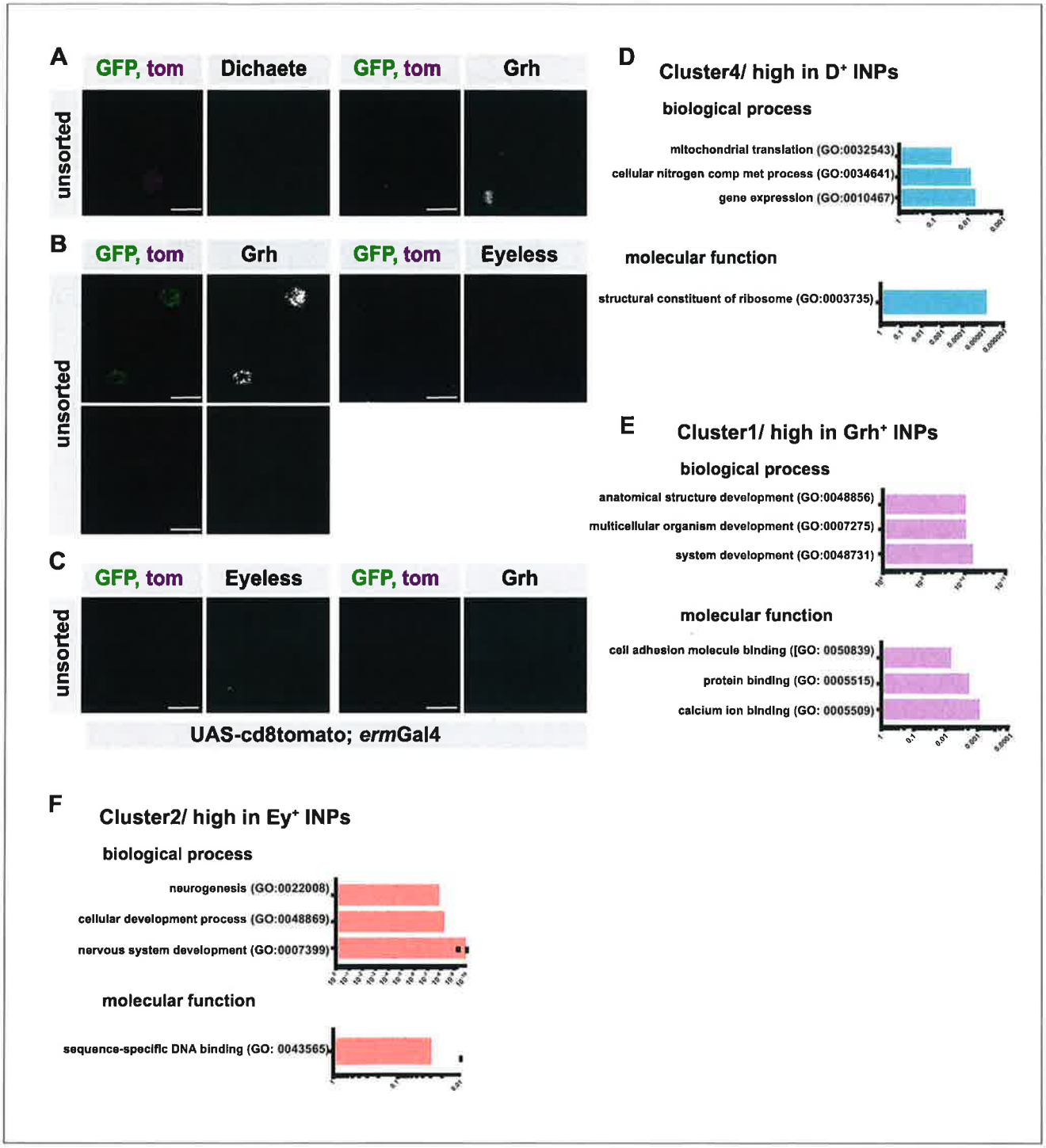

Figure 1—figure supplement 2. Temporally sorted INPs are pure populations. (**A–C**) Immunofluorescence of unsorted controls for ***Figure 1C–E***, scale bar 10 μm, (induced with ermGal4, marked with membrane bound tdTomato). (D–F) GO-term analysis of each cluster found in hierarchical clustering analysis for biological process, and molecular function. The graphs are color-coded with their respective clusters, the top three hits were shown if applicable. Cluster two doesn't have any GO-term enrichment.

DOI: https://doi.org/10.7554/eLife.46566.005

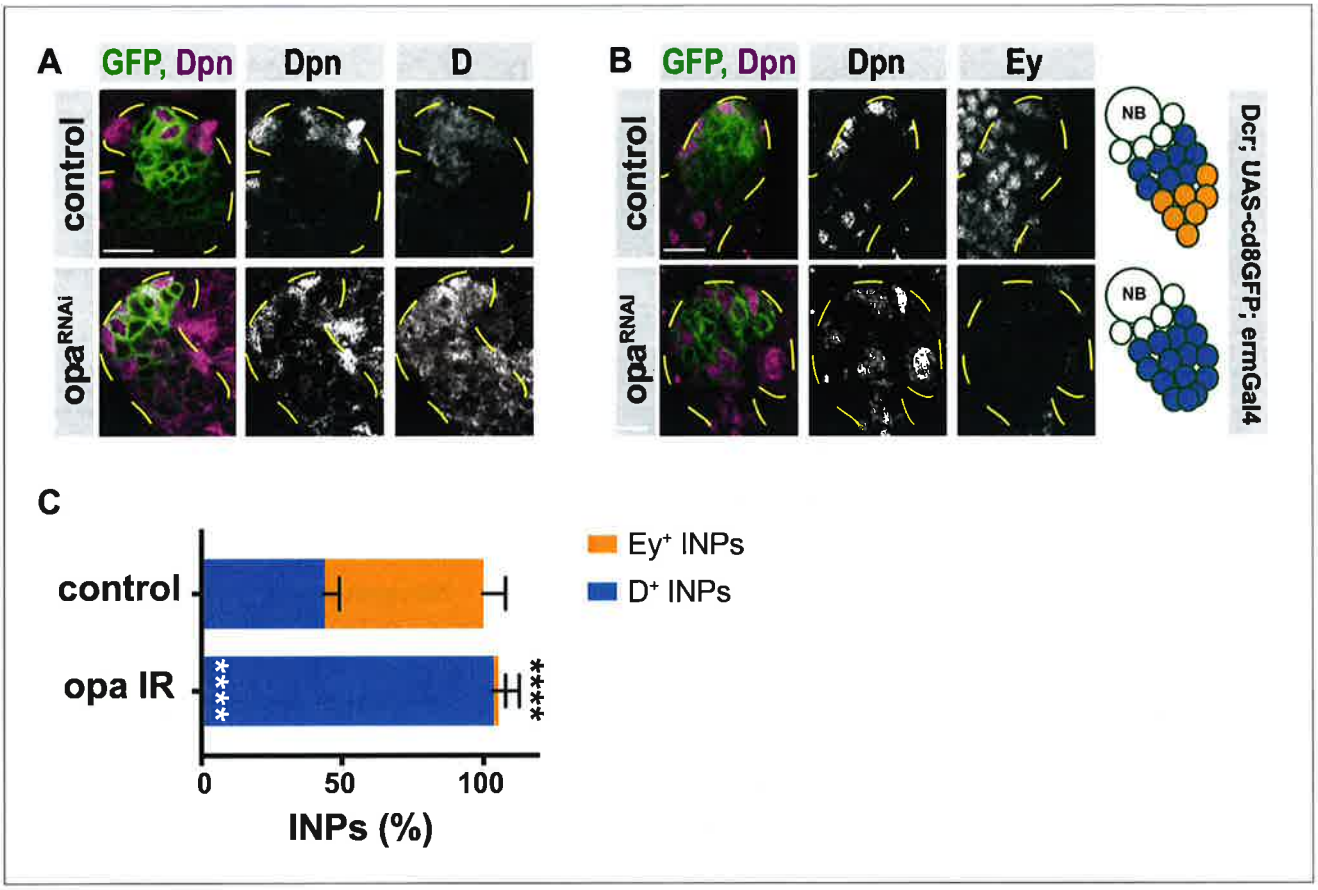

Figure 2—figure supplement 1. Opa is required for D repression. (**A–B**) Close-up images of larval brains expressing RNAi against opa in type II DM1 lineages, stained for Dpn, D (**A**), Dpn and Ey (**B**), lineages are outlined with yellow dashed line, scale bar 10 μm (induced with ermGal4, marked with membrane bound GFP). (**C**) Quantification of Dpn^+, D^+, and Dpn^+, Ey^+ INPs in control and opa knock-down brains, n = 5, total INP numbers in control were normalized to 100%. Data represent mean ± SD, ***p<=0.001, Student's t-test. (D^+ INPs control 11.14 ± 0.55 [n = 7], opa RNAi 26.43 ± 0.92 [n = 7], p<0.001; Ey^+ INPs control 14.4 ± 0.92 [n = 5], opa RNAi 0.43 ± 0.29 [n = 7], p<0.001).

DOI: https://doi.org/10.7554/eLife.46566.014

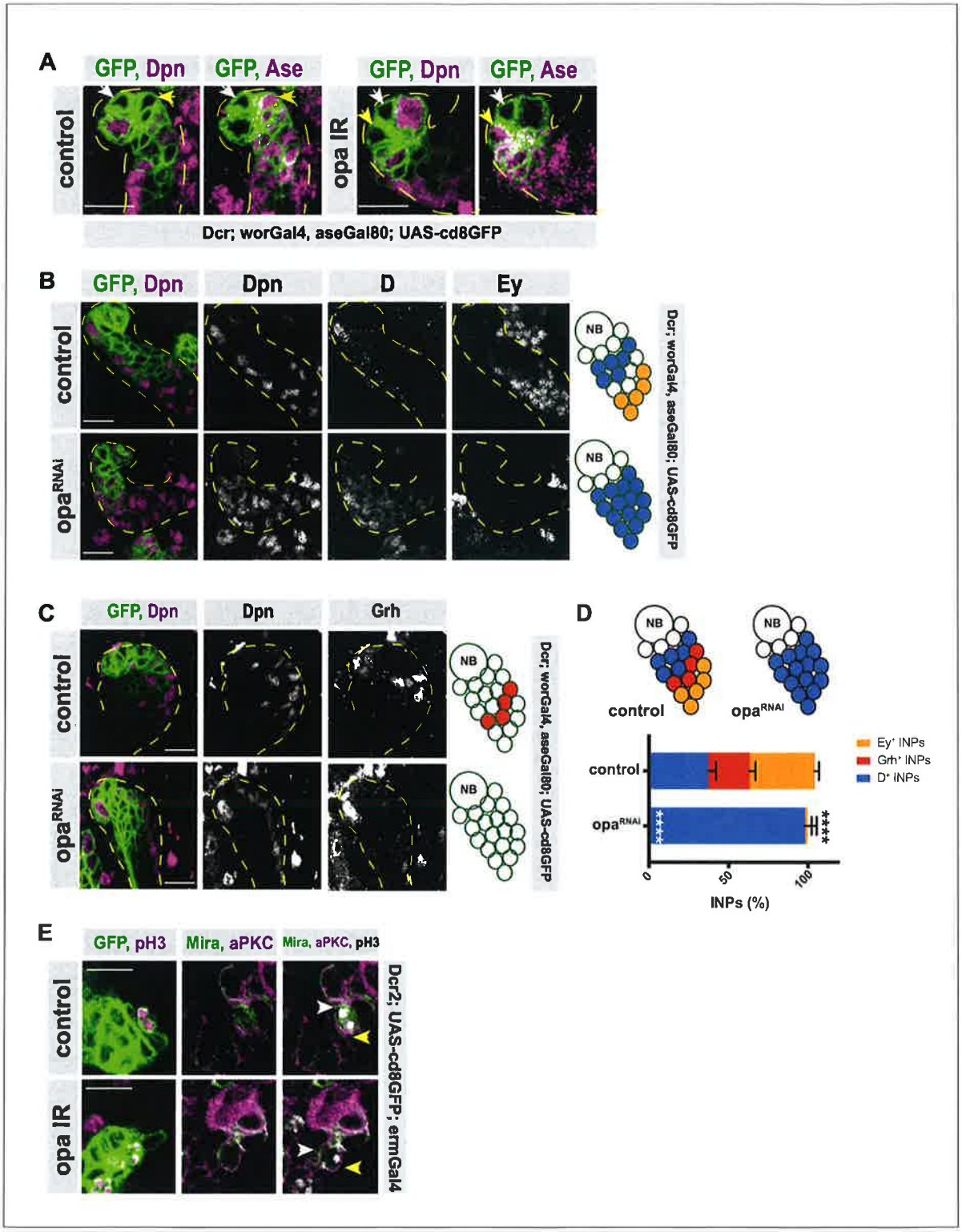

Figure 2—figure supplement 2. Opa regulates the transition from D-to-grh. (A) Close-up images of larval brains expressing RNAi against opa in type II lineages, stained for Dpn and Ase, lineages outlined with yellow dashed lines, Dpn^-/Ase^- INPs are marked with white arrowhead, Dpn^-/Ase^+ INPs are

Figure 2—figure supplement 2 continued on next page

Figure 2—figure supplement 2 continued

marked with yellow arrowhead, scale bar 10 µm (induced with worGal4, aseGal80, marked with membrane bound GFP). (**B–C**) Close-up images of larval brains expressing RNAi against opa in type II lineages, stained for Dpn, D and Ey (**B**), and Grh (**C**), lineages are outlined with yellow dashed line, scale bar 10 µm (induced with worGal4, aseGal80, marked with membrane bound GFP). (**D**) Quantification of Dpn^+, D^+, and Dpn^+, Grh^+, and Dpn^+, Ey^+ INPs in control and opa knock-down brains, n = 5, total INP numbers in control were normalized to 100%. Data represent mean ± SD, ***p<=0.001, Student's t-test. (D^+ INPs control 12.6 ± 1.5 [n = 5], opa RNAi 33.3 ± 2.35 [n = 6], p<0.001; Grh^+ INPs control 8.8 ± 1.6 [n = 5], opa RNAi 0 [n = 6], p<0.001; Ey^+ INPs control 14 ± 0.89 [n = 5], opa RNAi 0.5 ± 0.86 [n = 5], p<0.001). (**E**) Close-up images of larval brains expressing opa RNAi in INPs, stained for pH3, Mira and aPKC, the crescents of Mira staining are marked with white arrowhead, and the crescents of aPKC staining are marked with yellow arrowhead, scale bar 10 µm, (induced with ermGal4, marked with membrane bound GFP).

DOI: https://doi.org/10.7554/eLife.46566.015

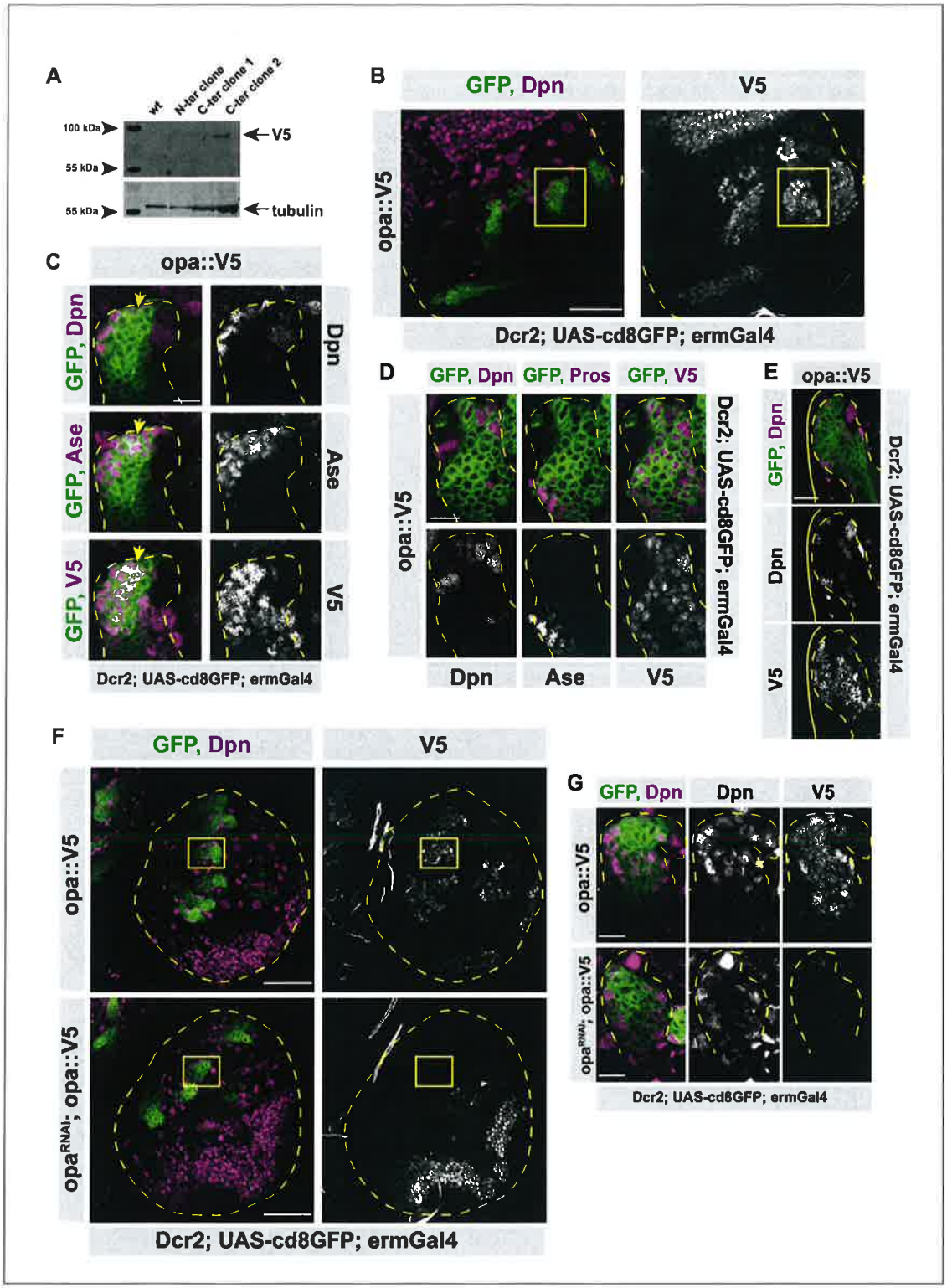

Figure 4—figure supplement 1. Opa is expressed in type II lineages. (**A**) Western blot confirmation of opa::V5 expressing flies. Wild-type embryos were used as control, three different clones were tested: two C-terminus tagged embryos and one N-terminus tagged embryos were used. Alpha-

Figure 4—figure supplement 1 continued on next page

Figure 4—figure supplement 1 continued

tubulin is used as loading control while V5 antibody was used for opa::V5 tag. (**B**) Opa is expressed in type II lineages. Overview image of brain lobe expressing endogenously V5-tagged opa, stained for Dpn and V5 antibodies, lobes are outlined with yellow dashed lines, scale bar 50 µm, (induced with ermGal4, marked with membrane bound GFP). (**C**) Close-up images of (**B**) marked with yellow square, stained for Dpn, Ase, and V5 antibodies. Type II lineage is outlined with yellow dashed lines, scale bar 10 µm, (induced with ermGal4, marked with membrane bound GFP). Yellow arrow is marking the start of opa expression. (**D**) Close-up images of brain lobes expressing endogenously V5-tagged opa, stained for Dpn, Prospero and V5 antibodies, lineages are outlined with yellow dashed lines, scale bar 10 µm, (induced with ermGal4, marked with membrane bound GFP). (**E**) Close-up images of DM1 lineage expressing endogenously V5-tagged opa, stained for Dpn and V5 antibodies, lineage is outlined with yellow dashed lines, while the brain lobe is outlined with yellow line (DM1 lineages can be deduced from their localization in the brain lobe), scale bar 10 µm, (induced with ermGal4, marked with membrane bound GFP). (**F**) Overview images of brain lobes expressing opa-V5 alone or along with opa RNAi in type II lineages, stained for Dpn and V5 antibodies, lobes are outlined with yellow dashed lines, scale bar 50 µm, (induced with worGal4, aseGal80, marked with membrane bound GFP). (**G**) Close up images of (**F**) marked with yellow square, stained with Dpn and V5 antibodies. Type II lineages are outlined with yellow dashed lines, scale bar 10 µm, (induced with worGal4, aseGal80, marked with membrane bound GFP).

DOI: https://doi.org/10.7554/eLife.46566.023

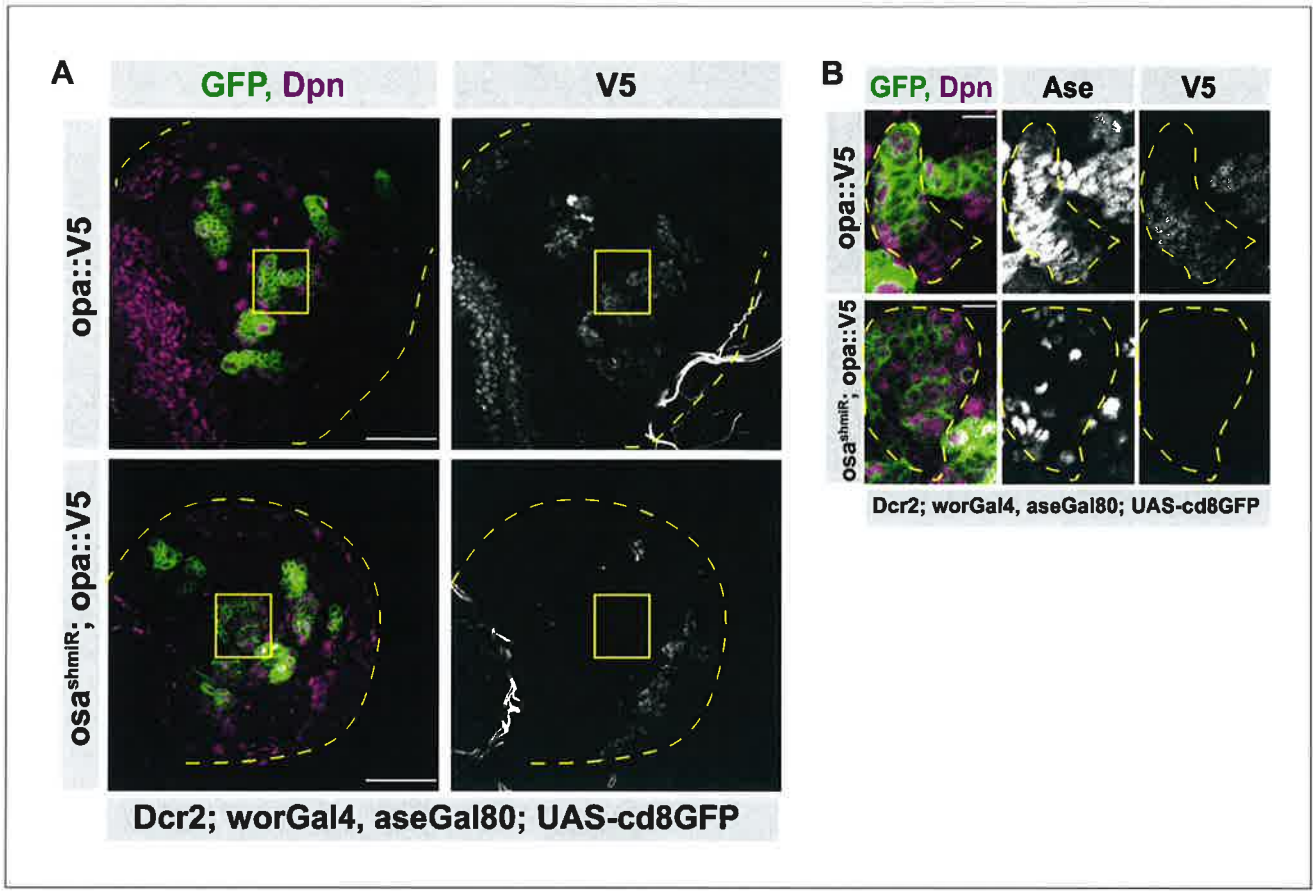

Figure 4—figure supplement 2. Osa initiates the expression of opa in INPs. (**A**) Opa is induced directly by Osa. Overview images of brain lobes expressing opa-V5 alone or along with osa shmiR in type II lineages, stained for Dpn and V5 antibodies, lobes are outlined with yellow dashed lines, scale bar 50 µm, (induced with worGal4, aseGal80, marked with membrane bound GFP). Osa knock-down causes the loss of V5 expression in type II lineages. (**B**) Close-up images of (**A**) marked with yellow square, stained with Dpn, V5 and Ase antibodies. Type II lineage is outlined with yellow dashed lines, scale bar 10 µm, (induced with worGal4, aseGal80, marked with membrane bound GFP). Knock-down of Osa causes higher numbers of Dpn^{+} cells which are $V5^{-}$.

DOI: https://doi.org/10.7554/eLife.46566.024

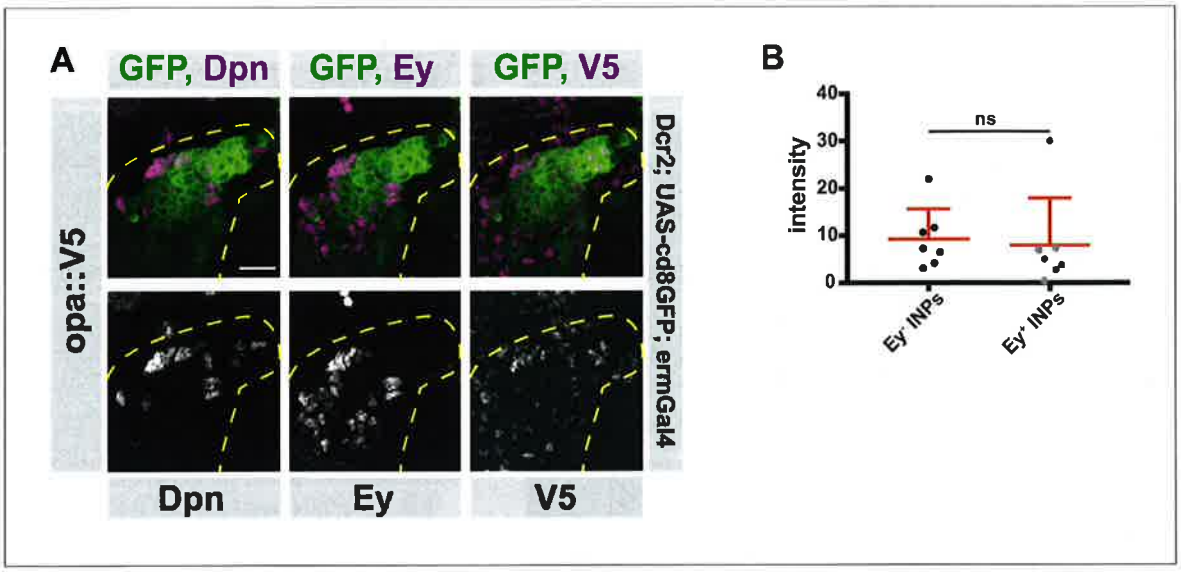

Figure 4—figure supplement 3. Different temporal states have different opa levels. (**A**) Close-up images of fly brains endogenously expressing V5-tagged opa in INPs, stained for V5, Dpn and Ey. Lineages are outlined with yellow dashed line, scale bar 10 µm, (induced with ermGal4, marked with membrane bound GFP). (**B**) Quantifications of opa::V5-signal intensity measurements of Ey^+ vs Ey^- INPs, n = 7, normalized to background intensity. Data represent mean ± SD, not significant, Student's t-test.

DOI: https://doi.org/10.7554/eLife.46566.025

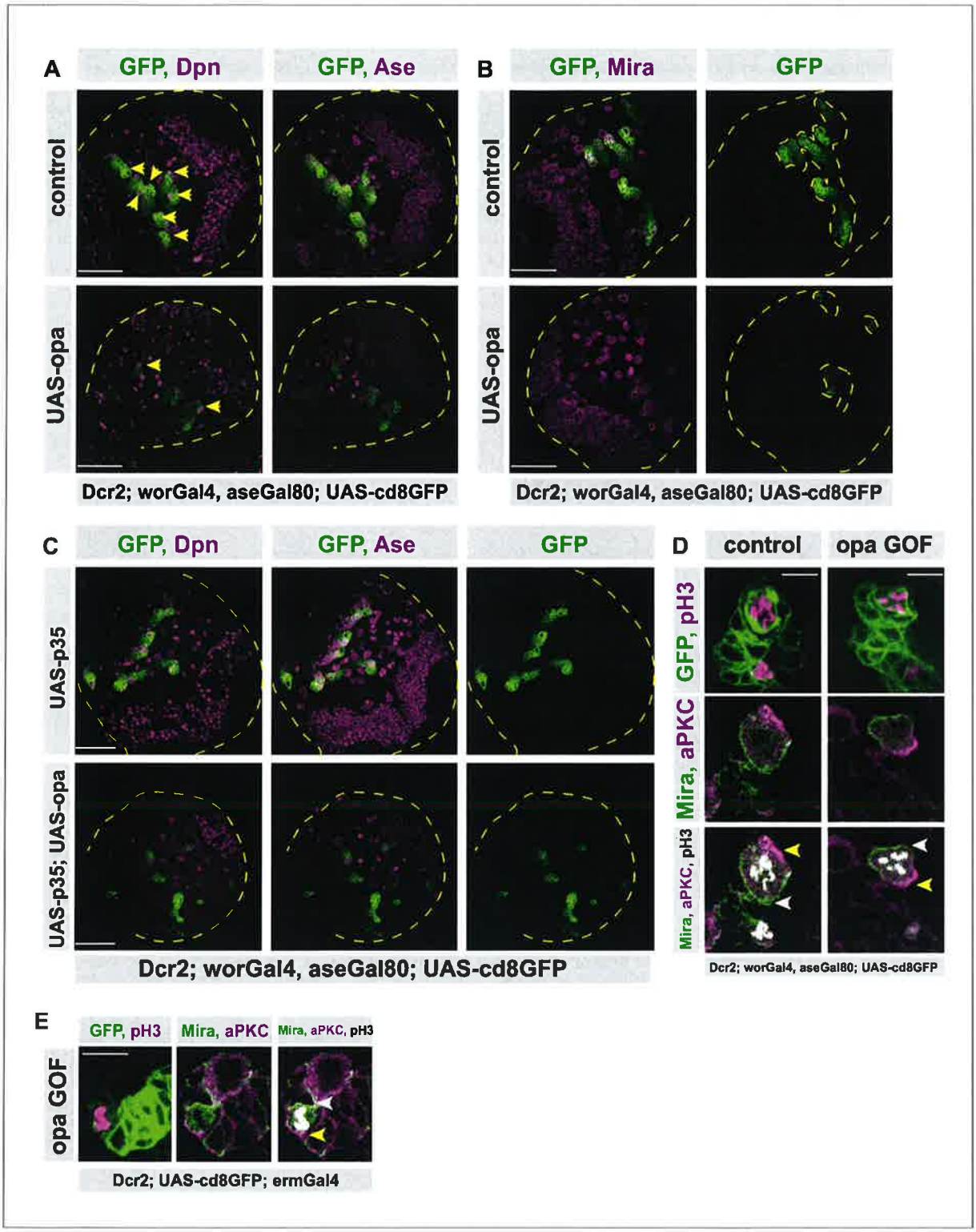

Figure 5—figure supplement 1. Opa overexpression causes shorter type II lineages. (**A**) Overview images of brain lobes, control or type II lineage-specific opa overexpression, stained for Dpn, and Ase antibodies, lobes are outlined with yellow dashed lines, yellow arrowheads mark Dpn positive

Figure 5—figure supplement 1 continued on next page

Figure 5—figure supplement 1 continued

type II NB lineages, one lineage is invisible in this z-plane, scale bar 50 µm, (induced with worGal4, aseGal80, marked with membrane bound GFP). (**B**) Overview images of brain lobes, control or type II lineage-specific opa overexpression, stained for Mira antibody, lobes and type II lineages are outlined with yellow dashed lines, scale bar 50 µm, (induced with worGal4, aseGal80, marked with membrane bound GFP). (**C**) Overexpression of apoptosis inhibitor p35 in type II lineages is not sufficient to prevent type II lineage loss upon opa overexpression. Overview images of brain lobes overexpressing opa alone and together with p35, stained for Dpn and Ase antibodies, lobes are outlined with yellow dashed lines, scale bar 50 µm, (induced with worGal4, aseGal80, marked with membrane bound GFP). (**D**) Close-up images of control and opa overexpressing type II NBs stained for pH3, Mira and aPKC, scale bar 10 µm, the crescents of Mira staining are marked with white arrowhead, and the crescents of aPKC staining are marked with yellow arrowhead, (induced with worGal4, aseGal80, marked with membrane bound GFP). (**E**) Close-up images of larval brains overexpressing opa in INPs, stained for pH3, Mira and aPKC, the crescents of Mira staining are marked with white arrowhead, and the crescents of aPKC staining are marked with yellow arrowhead, scale bar 10 µm, control is in ***Figure 2—figure supplement 2E*** (induced with ermGal4, marked with membrane bound GFP).

DOI: https://doi.org/10.7554/eLife.46566.030

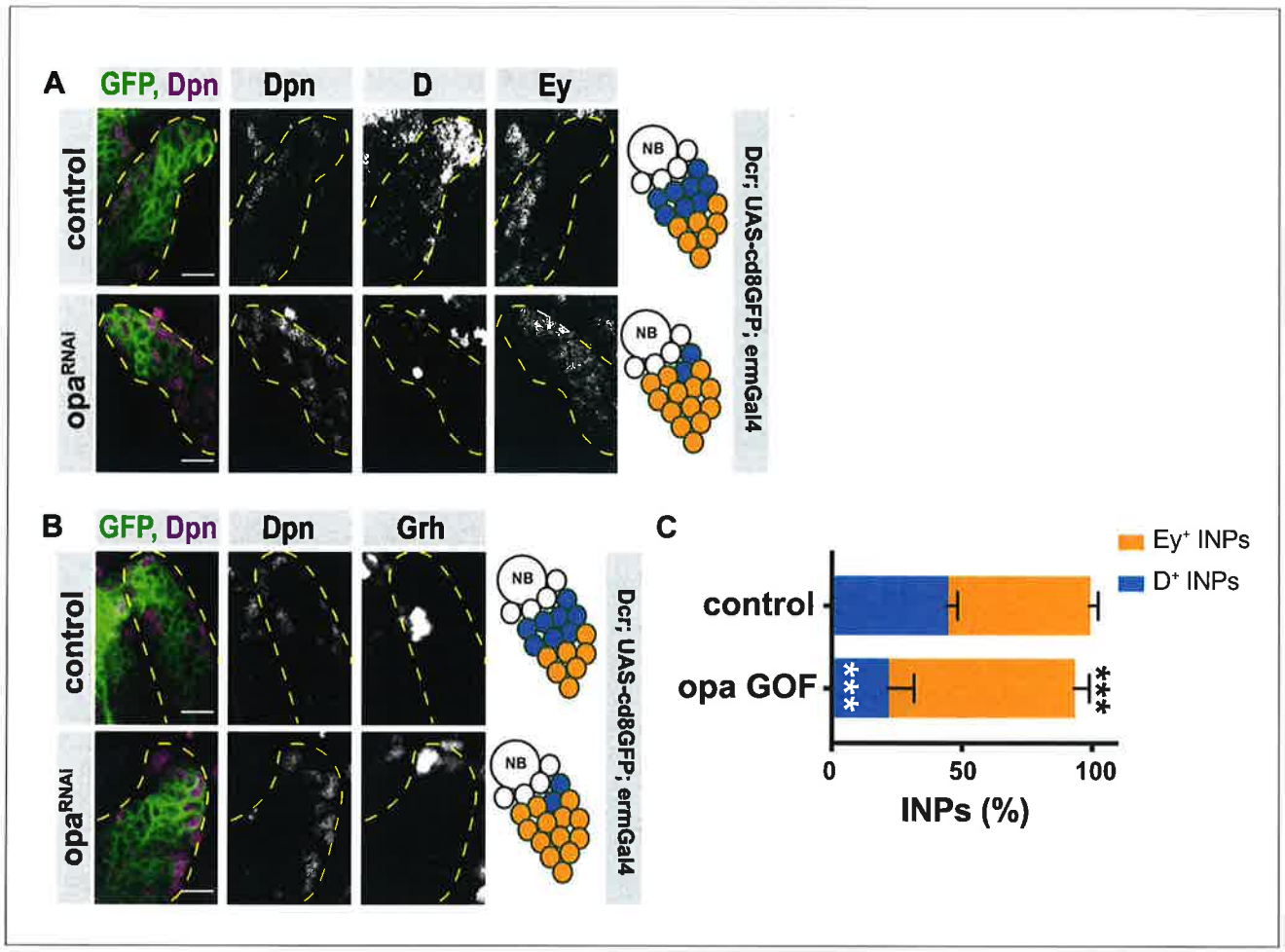

Figure 5—figure supplement 2. Opa overexpression causes loss of D$^+$INPs in DM1 lineages. (**A–B**) Close-up images of larval brains overexpressing opa in type II DM1 lineages, stained for Dpn, D and Ey (**A**), and Dpn and Grh (**B**), lineages are outlined with yellow dashed line, scale bar 10 µm (induced with ermGal4, marked with membrane bound GFP). (**C**) Quantification of Dpn$^+$, D$^+$, and Dpn$^+$, Ey$^+$ INPs in control and opa gain-of-function brains, n = 6, total INP numbers in control were normalized to 100%. Data represent mean ± SD, ***p<=0.001, Student's t-test. (D$^+$ INPs control 11.33 ± 0.42 [n = 6], opa GOF 5.5 ± 1.05 [n = 6], p<0.001; Ey$^+$ INPs control 14 ± 0.36 [n = 6], opa GOF 18.33 ± 0.61 [n = 6], p<0.001).
DOI: https://doi.org/10.7554/eLife.46566.031

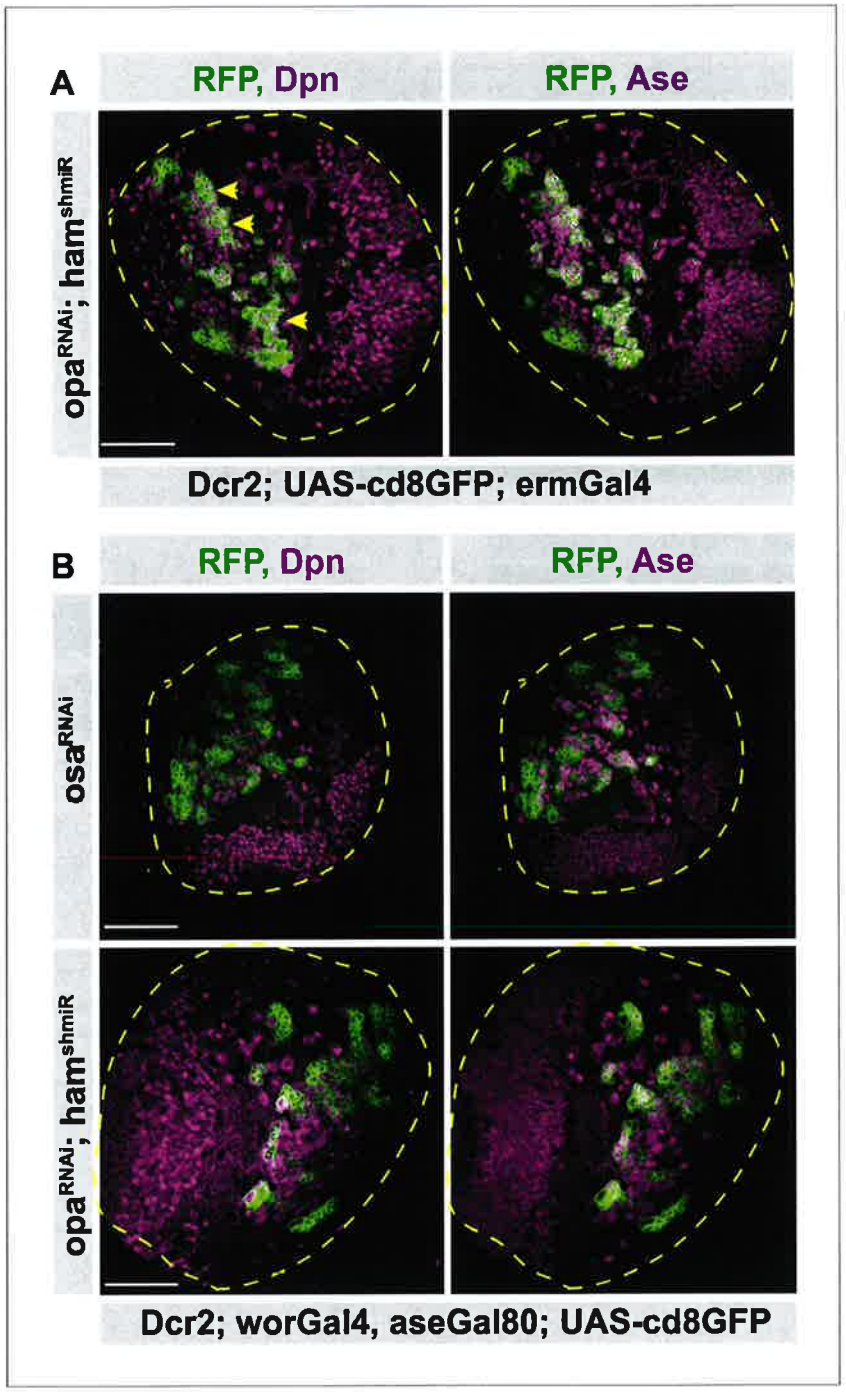

Figure 6—figure supplement 1. Opa and hamlet cannot recapitulate Osa knock-down phenotype. (**A**) Overview images of opa and ham RNAi expressing brains in type II lineages are stained for Dpn and Ase antibodies, brain lobes are outlined with yellow dashed lines, yellow arrowheads mark lineages with overproliferation, scale bar 50 µm, (induced with ermGal4, marked with membrane bound GFP). (**B**) Overview images of osa RNAi, and opa/ham double RNAi expressing brains in type II lineages are stained for Dpn and Ase antibodies, brain lobes are outlined with yellow dashed lines, scale bar 50 µm, (induced with worGal4, aseGal80, marked with membrane bound GFP).
DOI: https://doi.org/10.7554/eLife.46566.036

6. Chapter 2: Dynamics of activating and repressive histone modifications in *Drosophila* neural stem cell lineages and brain tumors

6.1. Prologue

During central nervous system (CNS) development, spatiotemporal gene expression programs mediate specific lineage decisions to generate neuronal and glial cell types from neural stem cells (NSCs). However, little is known about the epigenetic landscape underlying these highly complex developmental events. Here, we perform ChIP-seq on distinct subtypes of *Drosophila* FACS- purified neural stem cells (NSCs) and their differentiated progeny to dissect the epigenetic changes accompanying the major lineage decisions *in vivo*. By analyzing active and repressive histone modifications, we show that stem cell identity genes are silenced during differentiation by loss of their activating marks and not via repressive histone modifications. Our analysis also uncovers a new set of genes specifically required for altering lineage patterns in type II neuroblasts, one of the two main *Drosophila* NSC identities. Finally, we demonstrate that this subtype specification in NBs, unlike NSC differentiation, requires Polycomb-group (PcG)-mediated repression.

This manuscript submitted to Development on August 2nd , 2019 (MS ID#: DEVELOP/2019/183400). It is also posted on biorxiv (MS ID#: BIORXIV/2019/724039, **doi:** https://doi.org/10.1101/724039, https://www.biorxiv.org/content/10.1101/724039v1)

Authors:

Merve Deniz Abdusselamoglu[+], Lisa Landskron[+], Sarah K. Bowman, Elif Eroglu, Thomas Burkard, Robert E. Kingston and Juergen A. Knoblich*

[+] These authors contributed equally to this work

* Corresponding author

Author Contributions:

M.D.A. and L.L. conducted experiments, interpreted data and wrote the manuscript under the supervision of J.A.K. E.E. optimized the chromatin isolation with S.K.B. who performed ChIP-Seq, under the supervision of R.E.K. T.B. performed the analysis on the ChIP-Seq data.

6.2. Introduction

During development of the central nervous system (CNS), neural stem cells (NSCs) divide asymmetrically to generate daughter cells with self-renewing capacity but also complex neurogenic and gliogenic lineages. Regulation of this process requires tightly and highly dynamic control of multiple cell fate decisions. For cells to commit to their ultimate cell identity, spatiotemporal gene expression programs are required. It is assumed that activation of lineage-specific genes and silencing of stem cell genes is accompanied by changes in chromatin states. How histone modifications change over time during neurogenesis *in vivo*, however, is not very well described.

The *Drosophila* larval CNS has become a key model for the fundamental mechanisms underlying brain development and chromatin states (Homem & Knoblich, 2012). The larval CNS is populated by distinct types of NSCs (called neuroblasts in *Drosophila*), which vary in abundance, neuronal output and division mode. Together, these NBs give rise to the majority of the adult brain's neurons (Truman & Bate, 1988). The majority of the central brain NBs are of Type I (NBIs). Each NBI gives rise to another NBI and a ganglion mother cell (GMC), which divides once more to generate two differentiated neurons of glia. Type II neuroblasts (NBIIs) instead are a rare subpopulation with only 8 NBII per brain lobe (Fig. 1A) (Bello, Izergina, Caussinus, & Reichert, 2008; Boone & Doe, 2008; Homem & Knoblich, 2012; Sousa-Nunes, Cheng, & Gould, 2010). Unlike NBIs, NBIIs divide into one NBII and one transit-amplifying cell called intermediate neural progenitors (INPs). They generate many more neurons, because INPs continue to divide

asymmetrically for 5-6 times, each time giving rise to a GMC that divides into two neurons or glia cells. (Bello et al., 2008; Boone & Doe, 2008; Homem & Knoblich, 2012). Other than lineage structure and size, cell markers can also be used to differentiate NB subtypes. While NBIs express both Asense (Ase) and Deadpan (Dpn) (Bowman et al., 2008), NBIIs only express Dpn (Bello et al., 2008). During neurogenesis, both NB subtypes divide asymmetrically to give rise to their respective progeny (Kang & Reichert, 2014). Brain tumors form if the asymmetric segregation of cell fate determinants during NB cell division is disrupted (Betschinger, Mechtler, & Knoblich, 2006; Juergen A Knoblich, 2010). Among these determinants are the TRIM-NHL protein Brain tumor (Brat) and the Notch inhibitor Numb (Arama, Dickman, Kimchie, Shearn, & Lev, 2000; Betschinger et al., 2006; Bowman et al., 2008; Jürgen A Knoblich, Jan, & Jan, 1995; Lee et al., 2006a; Lee, Wilkinson, Siegrist, Wharton, & Doe, 2006b). While Brat-depletion results in the generation of ectopic NBII-like tumor NBs (tNBs) at the expense of differentiated brain cells (Bowman et al., 2008), simultaneous loss of Brat and Numb causes the NBI-like tNBs to overproliferate (see Results).

In many cell types, transitions in chromatin states are regulated by the evolutionary conserved Polycomb (PcG) and Trithorax (TrxG) group proteins. PcG and TrxG have emerged as antagonistic regulators that silence or activate gene expression, respectively (Kingston & Tamkun, 2014; Levine et al., 2002; Schuettengruber, Chourrout, Vervoort, Leblanc, & Cavalli, 2007). These multimeric protein complexes regulate the transcriptional state of genes by post-translationally modifying amino acid residues of histone tails (Kingston & Tamkun, 2014; Levine, King, & Kingston, 2004). PcG proteins exert a repressive activity via two main complexes, the Polycomb repressive complexes 1 and 2 (PRC1 and PRC2). Although PRC1 and PRC2 can exist in various compositions and associate with context-specific accessory proteins, both PRC1 and PRC2 have been shown to contain a specific core set of proteins including subunits with catalytic activity (Bracken, Dietrich, Pasini, Hansen, & Helin, 2006; Simon & Kingston, 2009). Within PRC2, *Enhancer of zeste* (*E(z)* in *Drosophila*, EZH1/2 in mammals) catalyzes the trimethylation of lysine 27 on histone 3 (H3K27me3) (Cao & Zhang, 2004). H3K27me3 is

recognized by PRC1, which in turn includes the histone 2A ubiquityltransferase *Sce* (RING1A/B in mammals) (de Napoles et al., 2004). Histone modifications associated with active transcription are deposited by TrxG proteins (Kassis, Kennison, & Tamkun, 2017), which counteract repressive histone acetylation or methylation marks, in particular by trimethylation of lysine 4 on histone 3 at active promoters (Byrd & Shearn, 2003; Dou et al., 2005; Petruk et al., 2001) (Kim et al., 2005).
Although well-known for their role in long-term transcriptional memory, PcG and TrxG complexes are highly dynamic during development and thus facilitate cellular plasticity (Kwong et al., 2008; Negre et al., 2006). In the last decade, it has been shown that PcG and TrxG complexes are crucial to ensure correct neurogenesis in mammals (Hirabayashi et al., 2009; Lim et al., 2009; Pereira et al., 2010) as well as in *Drosophila* (Bello, Holbro, & Reichert, 2007; Touma, Weckerle, & Cleary, 2012). Despite the strength of genetic *in vivo* experiments, however, global analysis of the histone modifications underlying their function, and therefore target genes, has mainly been performed *in vitro*. This constitutes a real knowledge-gap as recent studies demonstrated that the chromatin states may vary significantly between *in vivo* tissues and their related *in vitro* cell lines, mainly due to culture conditions (R. Xie et al., 2013; Zhu et al., 2013). Given also that epigenetic changes are highly context – and developmental time-dependent, providing *in vivo* datasets to investigate chromatin states of different cell types in complex tissues will increase our understanding of how the epigenetic landscape dynamically defines cellular states.

In recent years, *in vivo* studies made use of *Drosophila* to shed light on the dynamics of chromatin state changes during embryonic neural differentiation (Ye et al., 2016) and during larval stages (Aughey, Estacio-Gómez, Thomson, Yin, & Southall, 2018; Marshall & Brand, 2017). Profiling the binding of chromatin remodelers has highlighted the plasticity of chromatin states during differentiation (Marshall & Brand, 2017). Although binding of chromatin factors is associated with active or repressive chromatin, binding does not necessarily reflect downstream histone modifications. For example, the histone marks can change drastically between parasegments of the

Drosophila embryo while the occupancy of PcG proteins remains unchanged (Bowman et al., 2014). Thus, investigating the dynamics of chromatin states based on chromatin marks is crucial for understanding the functional specialization of cells during development. Moreover, how PcG/TrxG complexes target genes on the chromatin level between different subtypes of progenitor cells during neuronal differentiation, or tumorigenic transformation has remained elusive.

Here, we use the *Drosophila* larval CNS to track *in vivo* changes of histone modifications not only upon differentiation, but also between different populations of neural stem cells and their tumorigenic counterparts. We developed a FACS-based method to sort different cell types and perform ChIP-Seq for the active histone mark, H3K4me3, and the repressive mark, H3K27me3. Our FACS-based approach provides an in vivo dataset that reveals dynamic histone modifications during neuronal differentiation. In particular, we observed that self-renewal and cell division genes are repressed independently of H3K27me3 levels. In contrast, we further show that H3K27me3-mediated repression is crucial for silencing lineage-specific stem cell factors, including known factors as wells as a new set of genes that are specific to NBIIs. Finally, we present genetic evidence for the requirement of these new NBII-specific factors for self-renewal and demonstrate the role of PcG complexes in defining different subtypes of neural stem cells.

6.3. Results

Profiling repressive and active histone modifications of neural stem cells and neurons.

H3K4me3 and H3K27me3 are two major histone modifications associated with TrxG-activated and PcG-repressed states, respectively. However, these histone modifications have not yet been analyzed independently in distinct subtypes of neural stem cells in *Drosophila*. To analyze H3K4me3 and H3K27me3 histone marks in different brain cell types by ChIP-Seq, we combined genetic labeling with a protocol for generating sequencing libraries from picogram quantities of DNA (Bowman et al., 2014).

The NB subtype-specific GAL4 drivers *ase*-GAL4 (NBI lineage-specific) and *wor*-GAL4, *ase*-GAL80 (NBII lineage-specific), allowed us to preferentially label distinct NB lineages with nuclear-localized fluorophores (stinger::GFP or RFP). Indeed, GFP expressed by *ase*-GAL4 exclusively labeled NBI lineages (positive for both Dpn and Ase) and was not expressed in NBIIs (only Dpn+) (Fig. 1B). To amplify the production of rare NBIIs and at the same time generate tumor NBs (tNBs), RNAi constructs against the cell fate determinants *brat* and *numb*, were expressed using the mentioned driver lines. Depletion of *brat* in larval brains with a NBII-specific driver resulted in the overproliferation of NBII-like tNBs, evident by an increase in Dpn+, Ase- cells (Fig. 1C). In contrast, simultaneously depleting *numb* and *brat* by an NBI-specific driver resulted in overgrowth of (Dpn+, Ase+) NBI-like tNBs (Fig. 1B). Therefore, this strategy allowed us to generate fluorescently labeled distinct NB cell types and neurons.

Besides central brain NB lineages, the larval brain consists of embryonic neurons, mushroom body neuroblasts and cells of the optic lobes. To avoid impurities from these structures NBI, neurons and tNBs were isolated according to fluorescence intensity and cell size by flow cytometry (Berger et al., 2012; Harzer, Berger, Conder, Schmauss, & Knoblich, 2013). Purified cell populations were then analyzed by ChIP-seq for H3K27me3 and H3K4me3 histone modifications (Fig. 1D).

The H3K4me3 signal peaked around transcriptional start sites (TSSs), whereas the H3K27me3 signal occurred in broad domains covering gene bodies. For example, in all cell types the ubiquitously expressed gene *RNA polymerase II subunit 215kDa* contained a H3K4me3 peak at the TSS which was devoid of H3K27me3 signal (Fig. S1A). In contrast, the gene *caudal* showed no H3K4me3 peak, but instead high H3K27me3 levels over the gene body (Fig. S1B). This is in accordance with the fact that the function of *caudal* is mostly restricted to the larval digestive system. Moreover, *caudal* is not expressed in the larval CNS (modENCODE data and (Berger et al., 2012)) and has been shown to inhibit neuroblast specification upon misexpression (Birkholz, Vef, Rogulja-Ortmann, Berger, & Technau, 2013).

Figure1

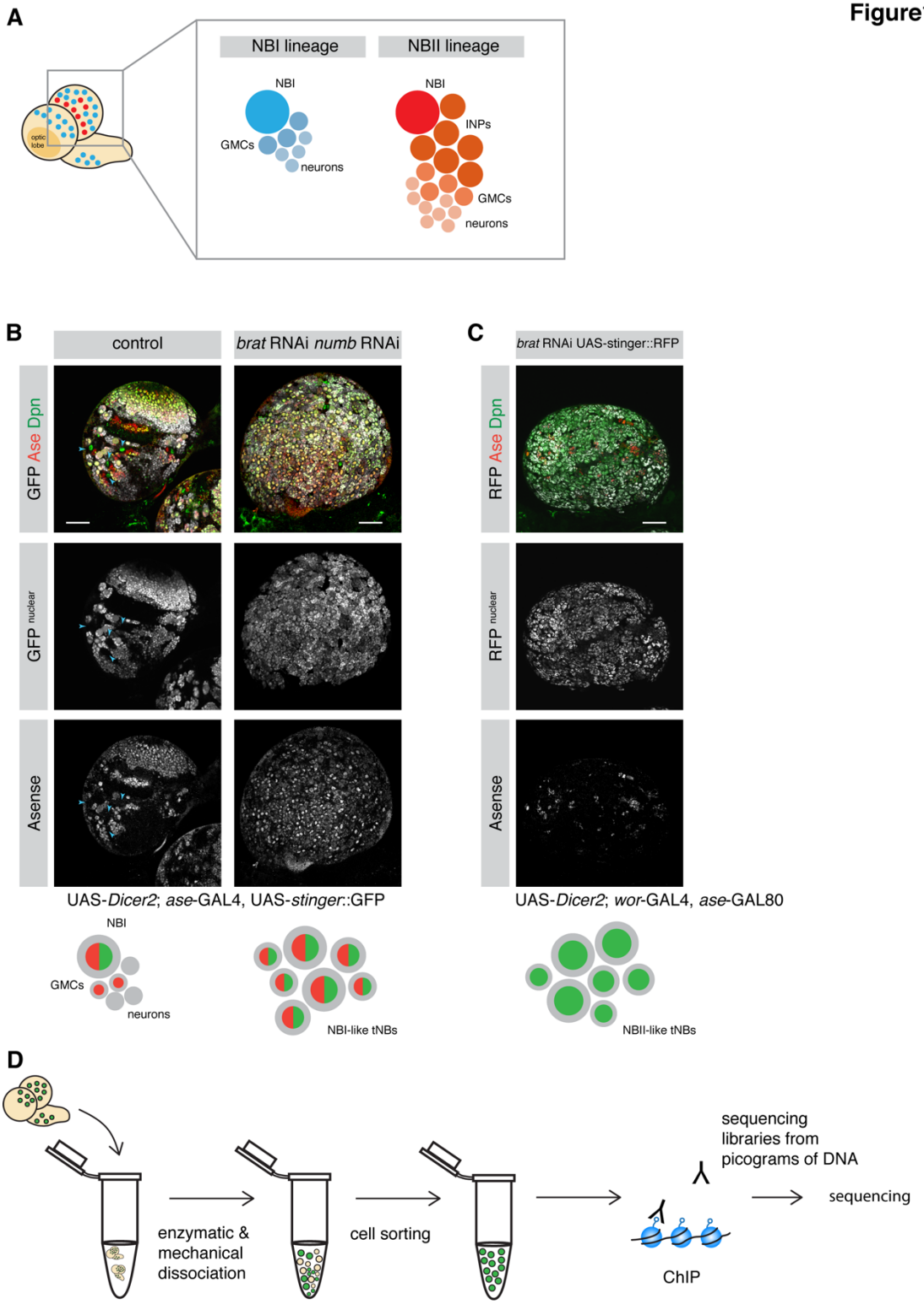

Figure 1. Strategy to investigate histone marks in specific NB lineages.

(A) Cartoon depicting a larval brain with NBI (blue) and NBII (red) lineages. (A and B) Immunostainings with a scalebar = 50µm. (B) The ase-GAL4 driver line marks NBI lineages

with nuclear GFP but not NBII lineages (arrowheads). Combined knockdown of *brat* and *numb* results in ectopic Ase+ Dpn+ tNBs. Dashed line separates optic lobe (OL) and central brain. (C) *brat* depletion with the NBII specific driver line results in mainly Ase- Dpn+ tNBs. (D) Cartoon showing an overview of the ChIP-seq strategy.

Self-renewal and cell cycle genes are repressed during differentiation in a H3K27me3-independent manner

To investigate changes in the epigenetic landscape during neurogenesis, we collected NBIs and neurons as described above in duplicates. We subtracted the individual inputs from their respective samples to generate coverage tracks. The read counts for H3K27me3 localization were analyzed over the whole gene body, but the reads for H3K4me3 were counted 500 bp downstream of the TSS. From this data, regions with differential signals were identified between different cell types. Finally, we performed unsupervised hierarchical clustering analysis on differentially marked genes in NBIs and neurons (Fig. 2A) identifying five distinct groups of genes. Three clusters were dependent on H3K27me3-mediated repression. Cluster 1 showed a decreased H3K27me3 signal upon differentiation, while cluster 3 showed an increased H3K27me3 signal in neurons. These clusters were not enriched for genes of a particular pathway or biological process when analyzed with gene ontology enrichment analysis. Another example of H3K27me3-mediated repression was cluster 5. While cluster 1 and 3 showed changes in H3K27 signal and no or mild changes in H3K4me3, genes in cluster 5 (22 genes) showed a drastic switch from a H3K4me3+ H3K27me3- to a H3K4me3- H3K27me3+ chromatin state upon differentiation. Cluster 5 included the lncRNAs *cherub*, *pncR002:3R* and *sphinx* and transcription factors *nab* and *vvl* (Fig. 2B).

The other two clusters (Cluster 2 and 4) were mainly dependent on changes in H3K4me3 signal. Cluster 2 showed an increase in H3K4me3 levels in neurons, while cluster 4 contained a large number of 318 genes and was characterized by a loss of H3K4me3 upon differentiation. These gene loci had either a small increase in H3K27me3 or were completely devoid of both marks (H3K4me3 and H3K27me3) in neurons (Fig. 2A, C, D). Gene ontology

enrichment analysis (Supplement table 1) showed that cluster 4 genes were enriched for genes involved in self-renewal (e.g. stem cell proliferation p=0,002) and mitosis-related processes (e.g. DNA replication p=3,04E-21), which are both processes that cease upon differentiation. In support of this finding, protein complexes essential for cell division were enriched in cluster 4 (Fig. 2E), whereas *bona fide* NB self-renewal transcription factors such as *vfl*, *klu*, and *dpn* as well as asymmetric cell division regulators (*Gαi, mud, insc, bora*) appeared in cluster 5. This suggests that during differentiation stem cell-promoting genes lack a H3K27me3 mark and that their repression could be mediated through mechanisms independent of PcG. This result is corroborated by previous data indicating that the genes *mira*, *CycE*, *stg* and *dpn* are enriched in HP1-associated chromatin in *Drosophila* neurons (Marshall & Brand, 2017).

Thus, these data suggest that a small group of genes is controlled by H3K27me3-repression upon differentiation, whereas most stem cell–related genes are turned off via an additional mechanism, potentially involving HP1 enrichment. This result is surprising considering H3K27me3 datasets indicate spreading of PcG-repressed regions upon neural differentiation in mammals (Södersten et al., 2018; Zhu et al., 2013) and suggests that different strategies of epigenetic control of neurogenesis have been established across evolution.

Figure 2

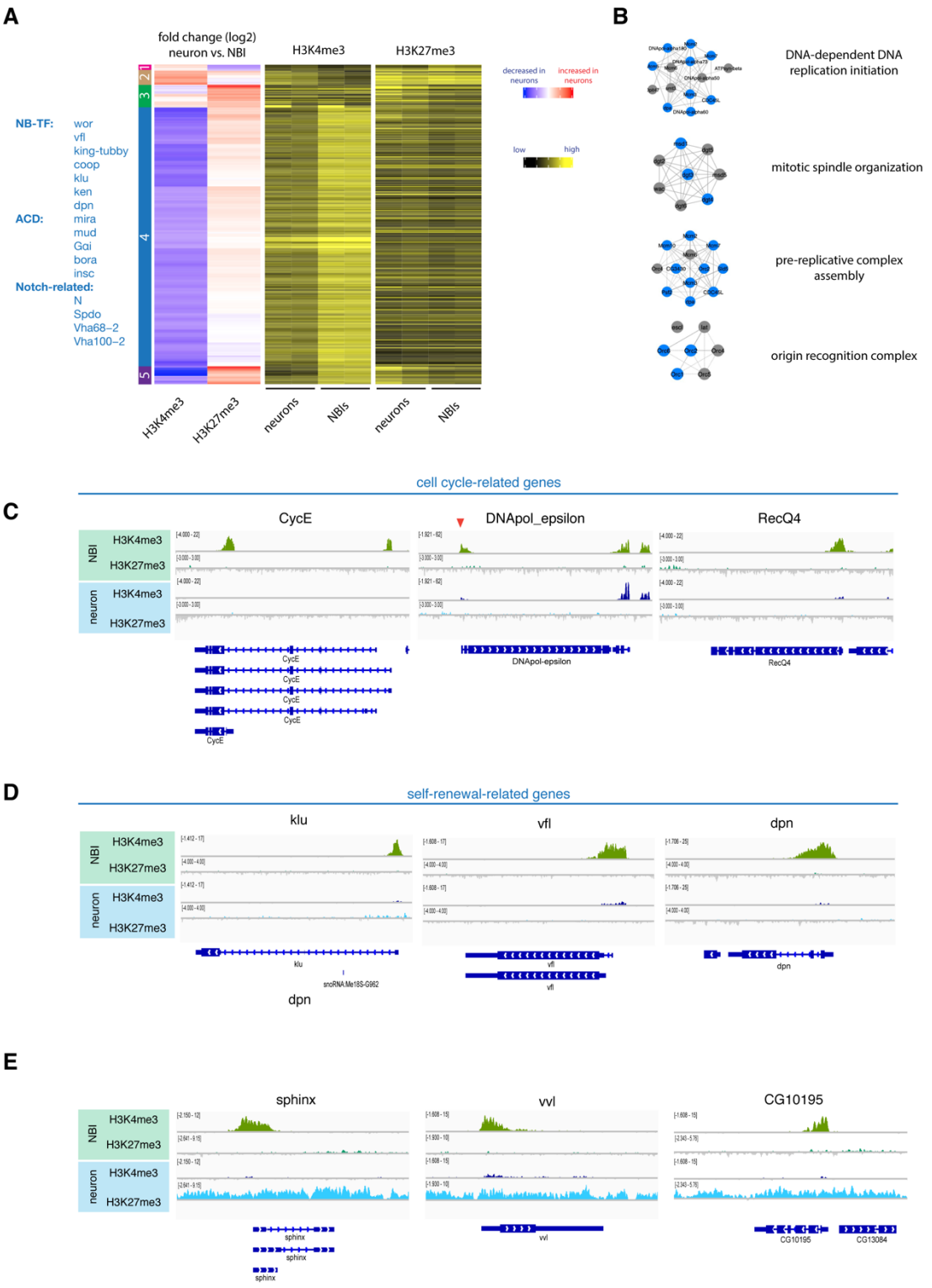

Figure 2. Changes of active and repressive histone modifications upon differentiation.

(A) Unsupervised hierarchical clustering analysis of gene log2 foldchange between NBIs and neurons. NB-related genes of cluster 4 according to literature are indicated blue. (B) ChIP-seq tracks of representative examples for genes of cluster 5. ChIP-seq tracks of representative examples for cell-cycle-related genes (C) and self-renewal-related genes (D). (E) Examples of mitosis related protein complexes. Blue indicates genes found in cluster 4.

Subtype-specific neuroblast genes are controlled by TrxG and PcG

Next, we wanted to address whether alterations of histone modifications can be observed between different types of NB lineages. To this end, we made use of tNBs which are of a different origin. RNAi of both *brat* and *numb* induced tumors made of NBIs while the depletion *brat* alone initiates tumors consisting of NBIIs (Fig. 1B-C). We reasoned that features occurring in NBII-like tNBs but absent in NBI-like tNBs would likely be specific to NBII lineages rather than due to tumorigenesis. We performed hierarchical clustering analysis between NBIs, NBI-like tNBs and NBII-like tNBs as described above and identified two NBII-specific sets of genes (Fig. 3A and Fig. S2). The first cluster of genes showed a decrease in H3K4me3 in NBII-like tNBIIs compared to NBIs and no or only mild changes when compared to NBI-like tNBIs (NBII cluster1). Moreover, these loci showed no or only modest increases in H3K27me3. As a key example, among this set of genes, we found the NBI-specific transcription factor *asense*, which showed clear H3K4me3 signals in NBI and *brat numb* depleted NBI-like tNBs but no signal in NBII-like tNBs (Fig. S3A).

In the second gene cluster (NBII cluster 2), NBII-like tNBIIs showed increased H3K4me3 signal and lower H3K27me3 occupancy. Interestingly, previous genetic evidence has suggested a role of *trithorax* in maintaining different subtypes of neuroblast lineages. In particular, the two loci *buttonhead* and *Sp1* are required to specify NBII from neuroectoderm (Álvarez & Díaz-Benjumea, 2018) and to maintain NBII lineages (Komori, Xiao, Janssens, Dou, & Lee, 2014; Y. Xie et al., 2014). Indeed, both genes are H3K4me3 positive in NBII-like tNBIIs and have reduced intensity of H3K27me3 signal in NBI-derived numb tumors as well as NBIs (Fig. 3B). Our clustering identified additional genes with a similar pattern (Fig. 3A). Two of these H3K4me3

positive NBII-like NBII-specific genes were the homeodomain transcription factor Distal-less (Dll) and the transcriptional coactivator eyes absent (eya). We decided to further focus on and characterize the contribution of these two genes in NBII specification as previous work showed that Dll enhancer was active in NBII lineages (Izergina, Balmer, Bello, & Reichert, 2009) and eya was mainly expressed in NBIIs (which we confirmed by immunostaining (Fig. 3D)). Dll-or eya-depleted brains resulted in smaller NBII cells (Fig. 3E and Fig. S2B) with a reduced number of INPs (Fig. 3F), which indicates reduced stemness (Song & Lu, 2011; Wissel et al., 2018). In contrast, NBI lineages showed normal NB growth and unaffected GMC numbers (Fig. 3G and Fig. S2C). Thus, our data indicate that these two genes are required to maintain NBII lineages. This would further suggest that NB subtype-specific genes are regulated by PcG and TrxG.

Finally, tNB-specific changes were mostly H3K4me3 changes (reduction in tNB cluster 1 and gain in tNB cluster 2+3) (Fig. 3A and Fig. S2) while only minor changes were observed for H3K27me3. This suggests that tumor specific changes are mediated by TrxG proteins rather than PcG.

Figure 3

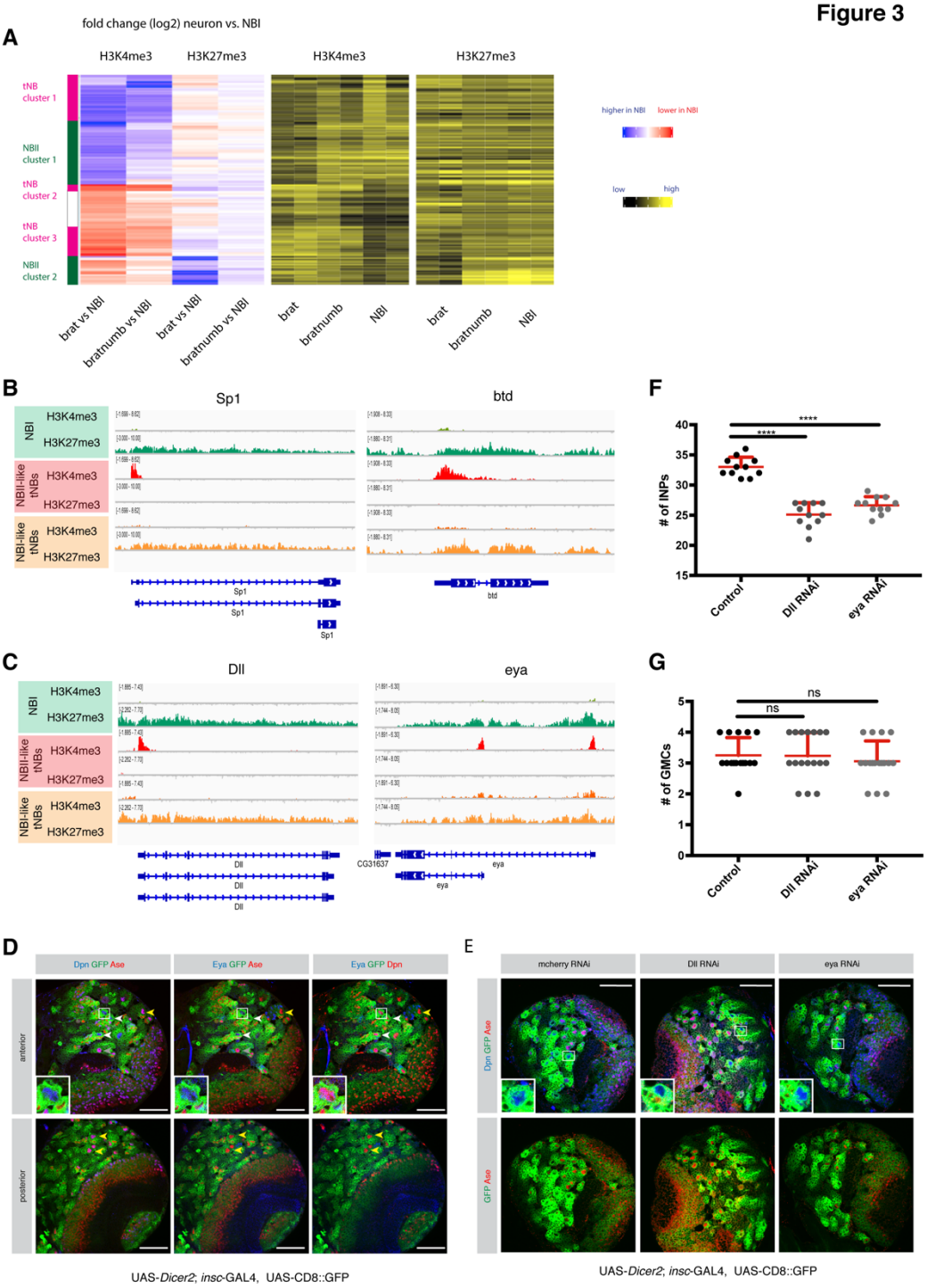

Figure 3. Comparison of different NB subtypes identifies PcG and TrxG-dependent NBII-specific factors.

(A) Unsupervised hierarchical clustering analysis of gene log2 foldchange between NBI, NBI-like tNB and NBII-like tNB (relevant section is shown, for full heatmap see Fig. S5.). ChIP-seq tracks of the known NBII factors *Sp1* and *btd* (B) and novel NBII-specific factors *Dll* and *eya* (C). (D) Eya immunostaining in type I and type II neuroblasts. Scale bar

50 µm. Driver line used was UAS-*dicer2*; *insc*-Gal4, UAS-CD8::GFP. (E) Immunostainings of larval brains expressing RNAi against of Dll or eya show smaller NBIIs (blow-up). Scale bar is 50 µm. Quantification of immediate progenies of NBIIs (F) and NBIs (G). Driver line used was UAS-*dicer2*; *insc*-Gal4, UAS-CD8::GFP. Mean ± SD is shown. (for INPs (F) n=11, control = 33±1.61, *Dll* = 25.09±1.97 and *eya* = 26.64±1.43, and for GMCs (G) control = 3.25±0.57 (n=16), *Dll* = 3.23± 0.75 (n=17) and *eya* = 3.05±0.65 (n=17)). One-way ANOVA test was used and ****p < 0.0001, ns = not significant. n numbers are lineages quantified.

PRC 1 and 2 are required for neuroblast maintenance

Our data suggest that both TrxG and PcG complexes play an important role in maintaining NBI and NBII identities. TrxG-dependent maintenance of NBII identity was shown to rely on the target genes *buttonhead* and *Sp1* (Álvarez & Díaz-Benjumea, 2018; Komori et al., 2014). By contrast, the role of PcG in NB-subtype specification, besides HOX gene repression, remains largely unexplored. During brain development, loss of PcG repression leads to ectopic expression of HOX genes, which in turn induces apoptosis and depletion of both type I and type II NBs (Bello et al., 2007). In accordance with these previous findings, our ChIP-seq data revealed high levels of H3K27me3 at the two HOX gene clusters Antennapedia and Bithorax complex in both NBIs and NBIIs (Fig. S4A).

To investigate whether PRC-mediated repression is only required to prevent HOX gene-induced apoptosis or plays a broader role in neurogenesis, we blocked apoptosis by expressing the baculovirus caspase inhibitor gene P35. To this end, RNAi constructs against components of PRC2 (*E(z), Su(z)12*) or PRC1 (*Sce*) were expressed in NBs using the general NB driver line *insc*-GAL4, which resulted in a great decrease in NBI and NBII cell numbers (Fig. 4A). Upon p35 expression in a PcG-depleted background, GFP+ NB lineages could be restored (Fig. 4B) as previously reported (Bello et al., 2007).

Although RNAi constructs were expressed with the same driver line in NBIs and NBIIs, blocking apoptosis in PRC2-depleted lineages restored NBI but not NBII cell numbers (Fig. 4C, D). In contrast, the number of NBs in PRC1-depleted brains was restored, suggesting PRC1, unlike PRC2, seem to only target the HOX genes and therefore prevent apoptosis of NBs (Fig. 4D).

However, these restored NBIIs still exhibited a smaller cell size (Fig. 4F) than their control NBIIs. These results indicate that in addition to its function as anti-apoptotic in both type I and type II NB, that NBIIs require PRC2 is required specifically in NBIIs to maintain self-renewal potential. These data therefore suggest that PcG-dependent repression targets more genes in addition to the HOX genes to maintain NBII.

PcG proteins prevent premature NB differentiation

Although the number of NBIs was restored in apoptosis-inhibited PcG-depleted conditions, the NBI cell size was reduced (Fig. 4E). NBs must maintain a certain growth rate to maintain their self-renewal potential and prevent differentiation (Song & Lu, 2011). We therefore analyzed these apoptosis-inhibited NBIs and their self-renewal potential. RNAi constructs against PRC1 and PRC2 components were expressed together with P35, and NBs were analyzed at 6h after pupal formation (APF), timepoint at which NB start to exit proliferation (Fig. S4B). While the number of NBI in both PRC1- and PRC2-depleted brains were restored in third instar larval brains upon P35 expression, NB numbers were significantly decreased at 6h APF along with the fact that the diameter of the remaining ones was significantly lower compared to control (Fig. S4C, D). Altogether, these data show that even though the number of NBs were restored in apoptosis-inhibited, PRC-depleted lineages, these NBs fail to maintain their self-renewal potential as reported by their smaller size and early differentiation compared to their wild-type counterparts. These results altogether indicate that PcG proteins are required to maintain stemness both in type I and type II NBs but with different sensitivities.

To address the physiological consequences of premature NB differentiation, we analyzed the viability of PcG-depleted flies. RNAi-mediated knockdown of PcG proteins with and without p35 expression using *insc*-GAL4, led to lethality during development (data not shown). This observation further confirms our previous results that neurogenesis of NBI lineages is not fully restored. However, this approach suffers from the caveat that the *insc* promotor is active in some cells of the larval gut and salivary glands. To

exclude that lethality could originate from abnormal development of other tissues, we next used a brain-restricted NBI lineage-specific driver line *ase*-GAL4. Similar to insc-Gal4, ase-Gal4-mediated loss of PcG proteins led to a decline in NBI numbers and size, which could be rescued by blocking apoptosis (Fig. S5A, B). These phenotypes were nonetheless weaker, which we could explain by the strength of *insc*-Gal4*,* is higher expressed than *ase* in NBIs (Berger et al., 2012). However, immunostainings could confirm that PcG RNAi upon p35 rescue NBI lineages using *ase*-GAL4 still showed a significant decrease in H3K27me3 signal (Fig. S5C). Therefore, these results further confirm that PcG promotes self-renewal beyond preventing apoptosis also in NBI.

When PcG proteins were depleted with *ase*-GAL4 driven RNAi during NBI development, the majority of eggs failed to develop into adult flies (Fig. S5D). Between 3-18% of laid eggs hatched, but flies showed neurological abnormalities, and became stuck in the fly food leading to death. Similarly, preventing apoptosis in these PcG knockdown backgrounds did not rescue the number of viable flies (Fig. S5D). Therefore, NBIs and NBIIs depend on PcG proteins for proper neuron production, although at different sensitivities. In summary, these results suggest that PRC1 and 2 maintain NB neurogenesis by silencing genes that induce apoptosis and genes whose expression leads to differentiation.

Figure 4

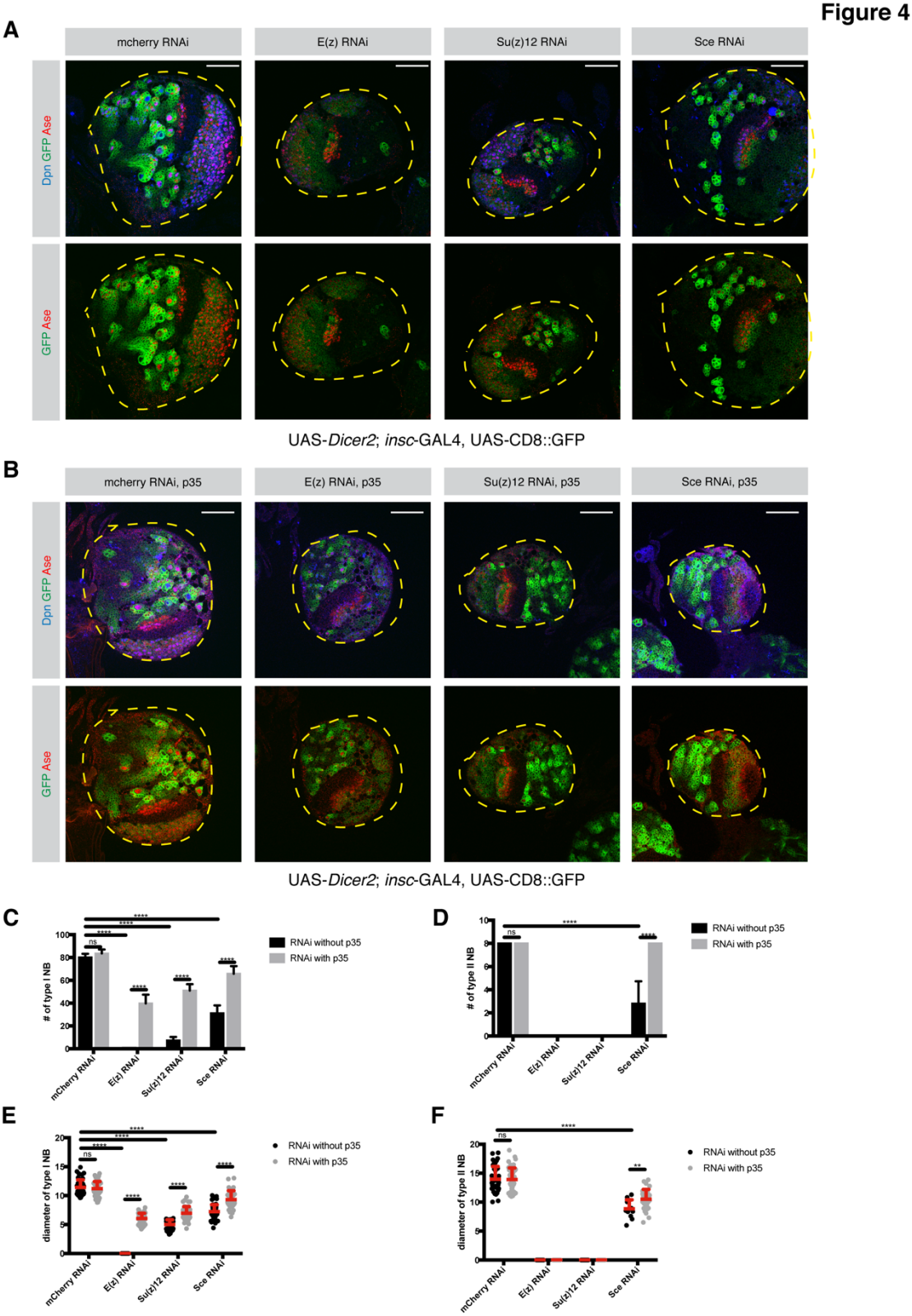
A
mcherry RNAi
E(z) RNAi
Su(z)12 RNAi
Sce RNAi
Dpn GFP Ase
GFP Ase
UAS-Dicer2; insc-GAL4, UAS-CD8::GFP
B
mcherry RNAi, p35
E(z) RNAi, p35
Su(z)12 RNAi, p35
Sce RNAi, p35
Dpn GFP Ase
GFP Ase
UAS-Dicer2; insc-GAL4, UAS-CD8::GFP
C
# of type I NB
RNAi without p35
RNAi with p35
mCherry RNAi
E(z) RNAi
Su(z)12 RNAi
Sce RNAi
D
# of type II NB
RNAi without p35
RNAi with p35
E
diameter of type I NB
F
diameter of type II NB

Figure 4. PRC 1 and 2 are required for NB maintenance

(A) Loss of PRC1 and 2 causes a significant decrease in NB numbers. Larval brain lobes expressing RNAi against mCherry, *E(z), Su(z)12* and *Sce.* Lobes are outlined in yellow dashed lines. Scale bar 50 μm. Driver line used was UAS-*dicer2*; *insc*-Gal4, UAS-CD8::GFP. (B) Larval brains expressing apoptosis inhibitor P35 together with PRC RNAi constructs in (A). Lobes are outlined in yellow dashed lines. Scale bar 50 μm. Driver line used was UAS-*dicer2*; *insc*-Gal4, UAS-CD8::GFP. (C) Quantification of NBI numbers in mCherry, E(z), Su(z)12, and Sce-depleted larval brains with and without P35 expression. n= 5 brain lobes. Mean ± SD (mCherry = 80.2±3.11, mCherry+P35 = 83.6±3.46, *E(z)* = 0.2±0.44, *E(z)*+P35 = 39.8±7.66, *Su(z)12* = 7.4±2.96, *Su(z)12*+P35 = 51±5.61, *Sce* = 31.2±6.83 and *Sce*+P35 = 65.75±6.7). Two-way ANOVA test was used and ****p < 0.0001. (D) Quantification of NBI diameter in mCherry, E(z), Su(z)12, and Sce-depleted larval brains with and without P35 expression. Mean ± SD (mCherry = 10.64±1.6 (n=50), mCherry+P35 = 11.61±1.93 (n=50), *E(z)* = NA, *E(z)*+P35 = 6.05±0.9 (n=50), *Su(z)12* = 6.01±1.14 (n=34), *Su(z)12*+P35 = 6.76±1.3 (n=50), *Sce* = 7.21±1.22 (n=50), and *Sce*+P35 = 9.31±1.54 (n=50)). Two-way ANOVA test was used and ****p < 0.0001. n = NBI numbers quantified. (E) Quantification of NBII numbers in mCherry, E(z), Su(z)12, and Sce-depleted larval brains with and without P35 expression. n= 5 brain lobes. Mean ± SD (mCherry = 8, mCherry+P35 = 8, *E(z)* = NA, *E(z)*+P35 = NA, *Su(z)12* = NA, *Su(z)12*+P35 = NA, *Sce* = 2.8±1.92 and *Sce*+P35 = 8). Two-way ANOVA test was used and ****p < 0.0001. (F) Quantification of NBII diameter in mCherry, E(z), Su(z)12, and Sce-depleted larval brains with and without P35 expression. Mean ± SD (mCherry = 13.96±2.19 (n=40), mCherry+P35 = 13.91±2 (n=40), *E(z)* = NA, *E(z)*+P35 = NA, *Su(z)12* = NA, *Su(z)12*+P35 = NA, *Sce* = 8.85±1.56 (n=12) and *Sce*+P35 = 10.5±1.7 (n=32)). Two-way ANOVA test was used and ****p < 0.0001. n = NBII numbers quantified.

6.4. Discussion

We provide a resource of histone modification datasets for different types of neural stem cells and their differentiated progeny. In combination with chromatin accessibility (Aughey et al., 2018) and binding maps of chromatin remodelers (Marshall & Brand, 2017) of *Drosophila* brain cells, we hope that our dataset will serve as an useful community resource. We show that during differentiation, stem cell identity genes are silenced in a PcG-independent manner, which supports previous findings showing that these genes are silenced through HP1 enriched chromatin (Marshall & Brand, 2017). Additionally, PcG-mediated silencing is unlikely to instruct the stepwise

inactivation of stem cell genes during differentiation as loss of H3K27me3 did not induce ectopic NBs.

Here, we take advantage of *in vivo* genetic labeling to investigate chromatin dynamics of different NB subtypes. As the type II NBs are very lowly abundant, we used tumor NBs of type I and type II origins as a proxy in order to obtain enough material to be able to compare these two cell types. We further validated each change observed by comparing tumor to healthy type I NBs and excluded artifacts due to the tumorigenic state of the cells. Our data show that both TrxG and PcG are required to establish NBII identity. We identify a set of NBII-specific genes, including previously identified *btd* (Komori et al., 2014) and *Sp1* (Álvarez & Díaz-Benjumea, 2018). We further identified *Dll* and *eya* which are specifically required for NBII maintenance. It has been previously described that *btd* acts as an activator of *Dll* in the development of the ventral imaginal discs (Estella, Rieckhof, Calleja, & Morata, 2003). This suggests that in NBII-identity specification the Trithorax-target *btd* could act together with *Dll* and *eya*. Such a mechanism would explain why the loss of *btd* causes a distinct phenotype compared to the loss of *Dll* and *eya*. Interestingly, a NBI to NBII conversion is observed only in 18% of NBIs ectopically over-expressing *btd* indicating that either cofactors are missing or that the chromatin of *btd* targets is inaccessible (Komori et al., 2014). Our data of NB subtype-specific genes being characterized by H3K27me3 repressive chromatin favor the latter. Therefore, as opposed to TrxG-activated stem cell and mitosis genes, the repression of NBII-specific genes is ensured by PcG-mediated H3K27me3 histone modifications suggesting that Polycomb plays a role in defining the diversity of neural stem cell lineages. Moreover, our data indicates that PcG repression is required not only for the silencing of HOX genes but also for the self-renewal capacity of NBs. Unlike TrxG (Komori et al., 2014), the loss of catalytic subunits of PcG complexes did not convert NBIIs to NBIs or vice versa. This suggests that NB subtype-specification cannot be explained solely by an absence of repression but requires a further activation mechanism. Strikingly, loss of PcG complexes caused a significant decrease in the numbers of NBs. Interestingly, across all the cell types, developmental genes such as *cad, eve, peb, scr,* and *slp1*, as

well as genes involved in embryonic NB temporal patterning (*hb, kr, pdm, cas* and *grh*), are heavily marked with H3K27me3. It is therefore possible that PcG-mediated repression is required to silence these developmentally crucial genes in addition to the HOX genes. Thus, the observed reduction in NB stemness might be caused by the de-repression of these genes.

Besides an overall decreased NB maintenance, we observed increased sensitivity of NBII lineages upon reduction of PRC2 activity. Interestingly, *opa* and *ham*, two previously described temporal switch genes in NBII lineages (Abdusselamoglu, Eroglu, Burkard, & Knoblich, 2019), are also enriched with H3K27me3 in NBs. Ectopic expression of these genes limits self-renewal of NBs and causes NBs to disappear (Abdusselamoglu et al., 2019; Eroglu et al., 2014). In the future, investigating the downstream targets of PcG in different NB subtypes could reveal the underlying mechanisms of subtype-specification. In conclusion, our data provide a useful resource to investigate how chromatin state dynamics orchestrate the diversity and correct progression of neural stem cell lineages.

6.5. Materials and Methods

Fly strains

UAS-*Su(z)12* RNAi (BL 31191), UAS-*E(z)* RNAi (BL36068), UAS-*Sce* RNAi (VDRC 106328), UAS-p35 (BL5072, BL5073, both were tested for functionality), UAS-Dll RNAi (VDRC 101750), UAS-eya RNAi (VDRC 108071).

Immunofluorescence

Brains were dissected and fixed for 20 min in PBS with 5% PFA with 0.1% TritonX-100. After three washes with 1XPBS with 0.1% TritonX-100 (PBST), brains were incubated for 1 hour in blocking solution (PBST with 3% Normal goat serum), incubated with blockings solution with primary antibodies and washed again three times with PBST. Secondary antibodies (1:500, goat Alexa Fluor®, Invitrogen) were added for one to two hours and then removed with three PBST washes. Brains were mounted in Vectashield Antifade Mounting Medium (Vector Labs). Primary antibodies used were: rat anti-

Asense (1:500, (Eroglu et al., 2014)), guinea pig anti-Deadpan (1:1000, (Eroglu et al., 2014)), H3K27me3 (1:500, Active Motif 39155).

Microscopy

Images were recorded on Zeiss Confocal 780. Images of different conditions in one panel were recorded using the same settings.

Isolation of NBs using FACS

NB-sized cells were sorted from third instar larval brains according to GFP/RFP signal and cell size as previous described (Berger et al., 2012; Harzer et al., 2013). Briefly, brains were collected in 1X Rinaldini solution and then enzymatically and mechanically dissociated in Schneider's medium supplemented with FBS (10%), PenStrep (2%), Insulin (20 µl/ml), L-Glutamine (20mM), L-Glutathione (40 µg/ml), 20-Hydroxyecdyson (5 µg/ml).

Statistics

Statistical analyses were performed with GraphPad Prism 7. Experiments were not randomized. Sample sizes were estimated depending on the previous experiences with similar setups and the investigator wasn't blinded. Two-way ANOVA was used to assess statistical significance between multiple samples, while unpaired two-tailed Student's *t*-test was used between two samples.

ChIP-Seq

Preparation of soluble chromatin

50000 sorted cells of interest were pelleted by centrifuging at 3000 rpm for 10 min. The cell pellet was resuspended in complete media. Fixation was performed with formaldehyde (final concentration 1%) for 5 min at room temperature. After quenching with glycine (final concentration 125 mM) for 3 min at room temperature, cells were centrifuged at 3000 rpm for 10 min and the supernatant was discarded. Cells then were resuspended in 100 µl 1X PBS with $CaCl_2$ (final concentration: 1mM) and TritonX100 (final

concentration: 0.1%) and incubated with 5 Units micrococcal nuclease (Worthington Biochemical, LS004798) at 37°C for 3 min. After incubation, the sample was immediately transferred on ice and 2.5 µl 0.5 M EDTA, 6.25 µl 0.2 M EGTA and 1.25 µl 1X PBS were added in order to stop the reaction. After adjusting the sample volume to 300 µl with 1X PBS and sonication was performed with a microtip sonicator (OmniZRuptor 250, Omni International; microtip, power output: 20) for 20 seconds in a prechilled metal. Once sonication was over, the sample was snap frozen in liquid nitrogen. Fragment size was assessed using the Agilent High Sensitivity DNA Assay.

Chromatin Immunoprecipitation

The volume of thawed chromatin samples was adjusted to 500 µl with 50 µl 10X lysis buffer (1 mM EDTA, 10 mM Tris-HCl pH8, 0.1% Na-Deoxycholate, 0.5% N-lauroylsarcosine, 1% TritonX100), 140 µl water and 10 µl of 50X complete protease inhibitor. After 5min incubation on ice, samples were spun down at maximum speed for 10 min at 4°C. While supernatant was transferred to fresh tubes, 5 µl was saved as input sample (1%) at 4°C. Samples were incubated with primary antibodies overnight at 4°C. And then, incubated with 10 µl Dynabeads Protein A for 1 hour at 4°C. After 6 washes with lysis buffer containing 100 mM NaCl and 1% TritonX100, ChIP DNA was eluted twice with 125 µl fresh elution buffer (0.2% SDS, 0.1M $NaHCO_3$, 5 mM DTT) at 65°C for 10 min. The input DNA volume was adjusted to 250 µl with elution buffer. To achieve reversal of crosslinking, 1 M Tris-HCl (10 mM final concentration) and 500 mM EDTA (2 mM final concentration) were added to samples. Antibodies used for ChIP were: H3K27me3 (Active Motif, 39155) and H3K4me3 (Millipore 07-473).

Library construction

Library construction was performed as previously described (Bowman et al., 2013). In short, after the ChIP sample volume was adjusted to 37.5 µl, end polishing reaction (50 µl) was performed by incubating the sample with 1X T4 ligase buffer (NEB, Ipswich, MA, USA), 0.4 mM dNTPs, 7.5U T4 Polymerase (NEB), 2.5U Klenow polymerase (NEB), 25U polynucleotide kinase for 30 min at 20°C in a thermocycler. To clean-up the samples, Solid Phase Reversible

Immobilization (SPRI) beads (Agencourt AMPure XP, Beckman Coulter) were used at a 1.8X beads ratio. Once, DNA was eluted with 16.5 µl water, A-tailing reaction (25 µl) was performed. To do so, 16 µl sample with 1X NEB buffer 2, 0.2 mM dATP, 7.5U Klenow 3'-5' exo minus (NEB) were incubated for 30 min at 37°C. SPRI cleanup was performed with 1.8X beads ratio and DNA was eluted with 9.5 µl of water. Adapter ligation reaction (25 µl) was performed by incubating 9 µl of sample with 1X rapid T4 ligase buffer (Enzymatics, Beverly, MA, USA), 0.01 uM annealed universal adapter, 150 U T4 rapid ligase (Enzymatics) for 15 min at room temperature. SPRI cleanup was performed once again with 1.6X beads ratio and DNA was eluted with 10.5 µl water. Finally, library amplification was performed by setting up a PCR reaction (50 µl) with 1X Phusion HF master mix (NEB), 0.2 uM universal primer, 0.2 uM barcoded primer, 1X SYBR Green I (Invitrogen), and 0.5 µl Rox (USB). Then, PCR reaction was performed using an Applied Biosystems 7500 Fast Real-Time PCR System. Program used was as followed: an initial denaturing for 30 seconds at 98°C, followed by multiple cycles of 10 seconds denaturation at 98°C, 20 seconds annealing at 64°C, and 45 seconds extension at 72°C. Reactions were terminated at the end of the extension phase, after SYBR green reported reaction kinetics in the log phase for several cycles.

Bioinformatics

Reads are aligned to dm3 with bowtie2 (v2.2.4) (Langmead & Salzberg, 2012). Coverage tracks are produced with deeptools2 (v2.5.0.1) (Ramirez et al., 2016) by subtracting the respective input (--ratio subract --normalizeTo1x 121400000 -bs 1). Reads of ChIP alignments are counted with multiBamCov of bedtools (v2.25.0) (Quinlan & Hall, 2010). H3K4me3 reads are counted in a 500bp region downstream of the first TSS. H3K27me3 reads are counted over the genebody. Flybase 5.44 is used as annotation. Differential regions are called with DESeq2 (v1.22.2) (Love, Huber, & Anders, 2014). Heatmaps of differential regions are generated with ComplexHeatmaps (v2.1.0) (Gu, Eils, & Schlesner, 2016). The hierarchical tree is based on

log2FC (DEseq2) with method complete and euclidean distance. In addition, log2TPMs are shown.

Accession numbers

The Gene Expression Omnibus accession number for the ChIP-sequencing data reported in this paper is GSE134509.

Enrichment analysis

Gene Ontology (GO) enrichment analysis were performed on www.flymine.org/ with Holm-Bonferroni correction with max p-value 0.05. For analysis of protein complexes the Compleat website (https://www.flyrnai.org/compleat/) was used (Vinayagam et al., 2013).

Acknowledgements

We thank all Knoblich lab members for support and discussions, Francois Bonnay and Joshua A. Bagley for comments on the manuscript, Elke Kleiner, the IMP/IMBA Biooptics Facility for assistance and the Harvard TRiP collection, the Bloomington Drosophila stock center and the Vienna Drosophila Resource Center (VDRC) for reagents.

Author contributions

M.D.A. and L.L. conducted experiments, interpreted data and wrote the manuscript under the supervision of J.A.K. E.E. optimized the chromatin isolation with S.K.B. who performed ChIP-Seq and under the supervision of R.E.K. T.B. performed the analysis on the ChIP-Seq data.

Competing interests

The authors declare no competing financial interests.

Funding

Work in the Knoblich laboratory is supported by the Austrian Academy of Sciences, the Austrian Science Fund (Z_153_B09), and an advanced grant from the European Research Council (ERC).

6.6. REFERENCES

Abdusselamoglu, M. D., Eroglu, E., Burkard, T. R., & Knoblich, J. A. (2019). The transcription factor odd-paired regulates temporal identity in transit-amplifying neural progenitors via an incoherent feed-forward loop. *eLife*, *8*, 450. http://doi.org/10.7554/eLife.46566

Arama, E., Dickman, D., Kimchie, Z., Shearn, A., & Lev, Z. (2000). Mutations in the β-propeller domain of the Drosophila brain tumor (brat) protein induce neoplasm in the larval brain. *Oncogene*, *19*(33), 3706–3716. http://doi.org/10.1038/sj.onc.1203706

Aughey, G. N., Estacio-Gómez, A., Thomson, J., Yin, H., & Southall, T. D. (2018). CATaDa reveals global remodelling of chromatin accessibility during stem cell differentiation in vivo. *eLife*, *7*, 6061. http://doi.org/10.7554/eLife.32341

Álvarez, J.-A., & Díaz-Benjumea, F. J. (2018). Origin and specification of type II neuroblasts in the Drosophila embryo. *Development (Cambridge, England)*, *145*(7), dev158394. http://doi.org/10.1242/dev.158394

Bello, B. C., Izergina, N., Caussinus, E., & Reichert, H. (2008). Amplification of neural stem cell proliferation by intermediate progenitor cells in Drosophila brain development. *Neural Development*, *3*(1), 5. http://doi.org/10.1186/1749-8104-3-5

Bello, B., Holbro, N., & Reichert, H. (2007). Polycomb group genes are required for neural stem cell survival in postembryonic neurogenesis of Drosophila. *Development (Cambridge, England)*, *134*(6), 1091–1099. http://doi.org/10.1242/dev.02793

Berger, C., Harzer, H., Burkard, T. R., Steinmann, J., van der Horst, S., Laurenson, A.-S., et al. (2012). FACS Purification and Transcriptome Analysis of Drosophila Neural Stem Cells Reveals a Role for Klumpfuss in Self-Renewal. *Cell Reports*, *2*(2), 407–418. http://doi.org/10.1016/j.celrep.2012.07.008

Betschinger, J., Mechtler, K., & Knoblich, J. A. (2006). Asymmetric Segregation of the Tumor Suppressor Brat Regulates Self-Renewal in Drosophila Neural Stem Cells. *Cell*, *124*(6), 1241–1253. http://doi.org/10.1016/j.cell.2006.01.038

Birkholz, O., Vef, O., Rogulja-Ortmann, A., Berger, C., & Technau, G. M. (2013). Abdominal-B and caudal inhibit the formation of specific neuroblasts in the Drosophila tail region. *Development (Cambridge, England)*, *140*(17), 3552–3564. http://doi.org/10.1242/dev.096099

Boone, J. Q., & Doe, C. Q. (2008). Identification of Drosophila type II neuroblast lineages containing transit amplifying ganglion mother cells. *Developmental Neurobiology*, *68*(9), 1185–1195. http://doi.org/10.1002/dneu.20648

Bowman, S. K., Deaton, A. M., Domingues, H., Wang, P. I., Sadreyev, R. I., Kingston, R. E., & Bender, W. (2014). H3K27 modifications define segmental regulatory domains in the Drosophila bithorax complex. *eLife*, *3*. http://doi.org/10.7554/eLife.02833

Bowman, S. K., Rolland, V., Betschinger, J., Kinsey, K. A., Emery, G., & Knoblich, J. A. (2008). The Tumor Suppressors Brat and Numb Regulate

Transit-Amplifying Neuroblast Lineages in Drosophila. *Developmental Cell*, *14*(4), 535–546. http://doi.org/10.1016/j.devcel.2008.03.004
Bowman, S. K., Simon, M. D., Deaton, A. M., Tolstorukov, M., Borowsky, M. L., & Kingston, R. E. (2013). Multiplexed Illumina sequencing libraries from picogram quantities of DNA. *BMC Genomics*, *14*(1), 466. http://doi.org/10.1186/1471-2164-14-466
Bracken, A. P., Dietrich, N., Pasini, D., Hansen, K. H., & Helin, K. (2006). Genome-wide mapping of Polycomb target genes unravels their roles in cell fate transitions. *Genes & Development*, *20*(9), 1123–1136. http://doi.org/10.1101/gad.381706
Byrd, K. N., & Shearn, A. (2003). ASH1, a Drosophila trithorax group protein, is required for methylation of lysine 4 residues on histone H3. *Proceedings of the National Academy of Sciences*, *100*(20), 11535–11540. http://doi.org/10.1073/pnas.1933593100
Cao, R., & Zhang, Y. (2004). The functions of E(Z)/EZH2-mediated methylation of lysine 27 in histone H3. *Current Opinion in Genetics & Development*, *14*(2), 155–164. http://doi.org/10.1016/j.gde.2004.02.001
de Napoles, M., Mermoud, J. E., Wakao, R., Tang, Y. A., Endoh, M., Appanah, R., et al. (2004). Polycomb Group Proteins Ring1A/B Link Ubiquitylation of Histone H2A to Heritable Gene Silencing and X Inactivation. *Developmental Cell*, *7*(5), 663–676. http://doi.org/10.1016/j.devcel.2004.10.005
Dou, Y. L., Milne, T. A., Tackett, A. J., Smith, E. R., Fukuda, A., Wysocka, J., et al. (2005). Physical association and coordinate function of the H3K4 methyltransferase MLL1 and the H4K16 acetyltransferase MOF. *Cell*, *121*(6), 873–885. http://doi.org/10.1016/j.cell.2005.04.031
Eroglu, E., Burkard, T. R., Jiang, Y., Saini, N., Homem, C. C. F., Reichert, H., & Knoblich, J. A. (2014). SWI/SNF complex prevents lineage reversion and induces temporal patterning in neural stem cells. *Cell*, *156*(6), 1259–1273. http://doi.org/10.1016/j.cell.2014.01.053
Estella, C., Rieckhof, G., Calleja, M., & Morata, G. (2003). The role of buttonhead and Sp1 in the development of the ventral imaginal discs of Drosophila. *Development (Cambridge, England)*, *130*(24), 5929–5941. http://doi.org/10.1242/dev.00832
Gu, Z., Eils, R., & Schlesner, M. (2016). Complex heatmaps reveal patterns and correlations in multidimensional genomic data. *Bioinformatics*, *32*(18), 2847–2849. http://doi.org/10.1093/bioinformatics/btw313
Harzer, H., Berger, C., Conder, R., Schmauss, G., & Knoblich, J. A. (2013). FACS purification of Drosophila larval neuroblasts for next-generation sequencing. *Nature Protocols*, *8*(6), 1088–1099. http://doi.org/doi:10.1038/nprot.2013.062
Hirabayashi, Y., Suzki, N., Tsuboi, M., Endo, T. A., Toyoda, T., Shinga, J., et al. (2009). Polycomb limits the neurogenic competence of neural precursor cells to promote astrogenic fate transition. *Neuron*, *63*(5), 600–613. http://doi.org/10.1016/j.neuron.2009.08.021
Homem, C. C. F., & Knoblich, J. A. (2012). Drosophila neuroblasts: a model for stem cell biology. *Development (Cambridge, England)*, *139*(23), 4297–4310. http://doi.org/10.1242/dev.080515

Izergina, N., Balmer, J., Bello, B., & Reichert, H. (2009). Postembryonic development of transit amplifying neuroblast lineages in the Drosophila brain. *Neural Development*, *4*(1), 44. http://doi.org/10.1186/1749-8104-4-44

Kang, K. H., & Reichert, H. (2014). Control of neural stem cell self-renewal and differentiation in Drosophila. *Cell and Tissue Research*, *359*(1), 33–45. http://doi.org/10.1007/s00441-014-1914-9

Kassis, J. A., Kennison, J. A., & Tamkun, J. W. (2017). Polycomb and Trithorax Group Genes in Drosophila. *Genetics*, *206*(4), 1699–1725. http://doi.org/10.1534/genetics.115.185116

Kim, T. H., Barrera, L. O., Zheng, M., Qu, C., Singer, M. A., Richmond, T. A., et al. (2005). A high-resolution map of active promoters in the human genome. *Nature*, *436*(7052), 876–880. http://doi.org/10.1038/nature03877

Kingston, R. E., & Tamkun, J. W. (2014). Transcriptional Regulation by Trithorax-Group Proteins. *Cold Spring Harbor Perspectives in Biology*, *6*(10), a019349–a019349. http://doi.org/10.1101/cshperspect.a019349

Knoblich, Juergen A. (2010). Asymmetric cell division: recent developments and their implications for tumour biology. *Nature Reviews. Molecular Cell Biology*, *11*(12), 849–860. http://doi.org/10.1038/nrm3010

Knoblich, Jürgen A, Jan, & Jan, Y. N. (1995). Asymmetric segregation of Numb and Prospero during cell division. *Nature*, *377*(6550), 624–627. http://doi.org/10.1038/377624a0

Komori, H., Xiao, Q., Janssens, D. H., Dou, Y., & Lee, C.-Y. (2014). Trithorax maintains the functional heterogeneity of neural stem cells through the transcription factor Buttonhead. *eLife*, *3*. http://doi.org/10.7554/eLife.03502

Kwong, C., Adryan, B., Bell, I., Meadows, L., Russell, S., Manak, J. R., & White, R. (2008). Stability and dynamics of polycomb target sites in Drosophila development. *PLoS Genetics*, *4*(9), e1000178. http://doi.org/10.1371/journal.pgen.1000178

Langmead, B., & Salzberg, S. L. (2012). Fast gapped-read alignment with Bowtie 2. *Nature Methods*, *9*(4), 357–U54. http://doi.org/10.1038/NMETH.1923

Lee, C.-Y., Andersen, R. O., Cabernard, C., Manning, L., Tran, K. D., Lanskey, M. J., et al. (2006a). Drosophila Aurora-A kinase inhibits neuroblast self-renewal by regulating aPKC/Numb cortical polarity and spindle orientation. *Genes & Development*, *20*(24), 3464–3474. http://doi.org/10.1101/gad.1489406

Lee, C.-Y., Wilkinson, B. D., Siegrist, S. E., Wharton, R. P., & Doe, C. Q. (2006b). Brat is a Miranda cargo protein that promotes neuronal differentiation and inhibits neuroblast self-renewal. *Developmental Cell*, *10*(4), 441–449. http://doi.org/10.1016/j.devcel.2006.01.017

Levine, S. S., King, I. F. G., & Kingston, R. E. (2004). Division of labor in Polycomb group repression. *Trends in Biochemical Sciences*, *29*(9), 478–485. http://doi.org/10.1016/j.tibs.2004.07.007

Levine, S. S., Weiss, A., Erdjument-Bromage, H., Shao, Z., Tempst, P., & Kingston, R. E. (2002). The Core of the Polycomb Repressive Complex Is Compositionally and Functionally Conserved in Flies and Humans.

Molecular and Cellular Biology, *22*(17), 6070–6078. http://doi.org/10.1128/MCB.22.17.6070-6078.2002
Lim, D. A., Huang, Y.-C., Swigut, T., Mirick, A. L., Garcia-Verdugo, J. M., Wysocka, J., et al. (2009). Chromatin remodelling factor Mll1 is essential for neurogenesis from postnatal neural stem cells. *Nature*, *458*(7237), 529–533. http://doi.org/10.1038/nature07726
Love, M. I., Huber, W., & Anders, S. (2014). Moderated estimation of fold change and dispersion for RNA-seq data with DESeq2. *Genome Biology*, *15*(12), 550. http://doi.org/10.1186/s13059-014-0550-8
Marshall, O. J., & Brand, A. H. (2017). Chromatin state changes during neural development revealed by in vivo cell-type specific profiling. *Nature Communications*, *8*(1), 2271. http://doi.org/10.1038/s41467-017-02385-4
Negre, N., Hennetin, J., Sun, L. V., Lavrov, S., Bellis, M., White, K. P., & Cavalli, G. (2006). Chromosomal distribution of PcG proteins during Drosophila development. *PLoS Biology*, *4*(6), e170. http://doi.org/10.1371/journal.pbio.0040170
Pereira, J. D., Sansom, S. N., Smith, J., Dobenecker, M.-W., Tarakhovsky, A., & Livesey, F. J. (2010). Ezh2, the histone methyltransferase of PRC2, regulates the balance between self-renewal and differentiation in the cerebral cortex. *Proceedings of the National Academy of Sciences of the United States of America*, *107*(36), 15957–15962. http://doi.org/10.1073/pnas.1002530107
Petruk, S., Sedkov, Y., Smith, S., Tillib, S., Kraevski, V., Nakamura, T., et al. (2001). Trithorax and dCBP acting in a complex to maintain expression of a homeotic gene. *Science (New York, N.Y.)*, *294*(5545), 1331–1334. http://doi.org/10.1126/science.1065683
Quinlan, A. R., & Hall, I. M. (2010). BEDTools: a flexible suite of utilities for comparing genomic features. *Bioinformatics*, *26*(6), 841–842. http://doi.org/10.1093/bioinformatics/btq033
Ramirez, F., Ryan, D. P., Gruening, B., Bhardwaj, V., Kilpert, F., Richter, A. S., et al. (2016). deepTools2: a next generation web server for deep-sequencing data analysis. *Nucleic Acids Research*, *44*(W1), W160–W165. http://doi.org/10.1093/nar/gkw257
Schuettengruber, B., Chourrout, D., Vervoort, M., Leblanc, B., & Cavalli, G. (2007). Genome regulation by polycomb and trithorax proteins. *Cell*, *128*(4), 735–745. http://doi.org/10.1016/j.cell.2007.02.009
Simon, J. A., & Kingston, R. E. (2009). Mechanisms of Polycomb gene silencing: knowns and unknowns. *Nature Reviews. Molecular Cell Biology*, *10*(10), 697–708. http://doi.org/10.1038/nrm2763
Song, Y., & Lu, B. (2011). Regulation of cell growth by Notch signaling and its differential requirement in normal vs. tumor-forming stem cells in Drosophila. *Genes & Development*, *25*(24), 2644–2658. http://doi.org/10.1101/gad.171959.111
Sousa-Nunes, R., Cheng, L. Y., & Gould, A. P. (2010). Regulating neural proliferation in the Drosophila CNS. *Current Opinion in Neurobiology*, *20*(1), 50–57. http://doi.org/10.1016/j.conb.2009.12.005
Södersten, E., Toskas, K., Rraklli, V., Tiklova, K., Björklund, Å. K., Ringnér, M., et al. (2018). A comprehensive map coupling histone modifications with gene regulation in adult dopaminergic and serotonergic neurons.

Nature Communications, *9*(1), 1226. http://doi.org/10.1038/s41467-018-03538-9

Touma, J. J., Weckerle, F. F., & Cleary, M. D. (2012). Drosophila Polycomb complexes restrict neuroblast competence to generate motoneurons. *Development (Cambridge, England)*, *139*(4), 657–666. http://doi.org/10.1242/dev.071589

Truman, J. W., & Bate, M. (1988). Spatial and temporal patterns of neurogenesis in the central nervous system of Drosophila melanogaster. *Developmental Biology*, *125*(1), 145–157. http://doi.org/10.1016/0012-1606(88)90067-X

Vinayagam, A., Hu, Y., Kulkarni, M., Roesel, C., Sopko, R., Mohr, S. E., & Perrimon, N. (2013). Protein Complex–Based Analysis Framework for High-Throughput Data Sets. *Science Signaling*, *6*(264), rs5–rs5. http://doi.org/10.1126/scisignal.2003629

Wissel, S., Harzer, H., Bonnay, F., Burkard, T. R., Neumueller, R. A., & Knoblich, J. A. (2018). Time-resolved transcriptomics in neural stem cells identifies a v-ATPase/Notch regulatory loop. *Journal of Cell Biology*, *217*(9), 3285–3300. http://doi.org/10.1083/jcb.201711167

Xie, R., Everett, L. J., Lim, H.-W., Patel, N. A., Schug, J., Kroon, E., et al. (2013). Dynamic Chromatin Remodeling Mediated by Polycomb Proteins Orchestrates Pancreatic Differentiation of Human Embryonic Stem Cells. *Cell Stem Cell*, *12*(2), 224–237. http://doi.org/10.1016/j.stem.2012.11.023

Xie, Y., Li, X., Zhang, X., Mei, S., Li, H., Urso, A., & Zhu, S. (2014). The Drosophila Sp8 transcription factor buttonhead prevents premature differentiation of intermediate neural progenitors. *eLife*, *3*. http://doi.org/10.7554/eLife.03596

Ye, Y., Li, M., Gu, L., Chen, X., Shi, J., Zhang, X., & Jiang, C. (2016). Chromatin remodeling during in vivo neural stem cells differentiating to neurons in early Drosophila embryos. *Cell Death and Differentiation*, *24*(3), 409–420. http://doi.org/10.1038/cdd.2016.135

Zhu, J., Adli, M., Zou, J. Y., Verstappen, G., Coyne, M., Zhang, X., et al. (2013). Genome-wide Chromatin State Transitions Associated with Developmental and Environmental Cues. *Cell*, *152*(3), 642–654. http://doi.org/10.1016/j.cell.2012.12.033

6.7. Supplementary Files

Supplement Figure1

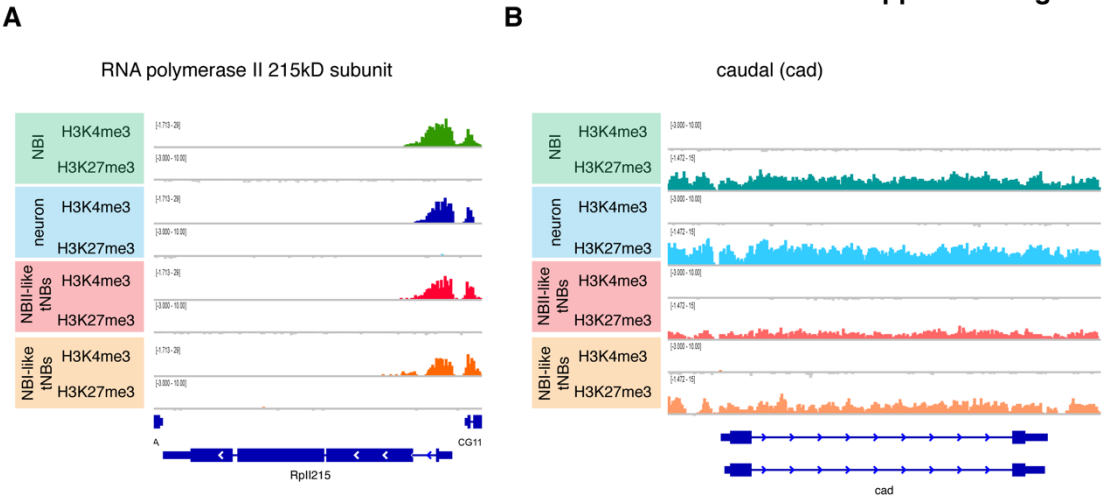

Supplement Figure 1. Examples of H3K4me3 and H3K27me3-dependent gene loci.

H3K4me3 and H3K27me3 distribution of RpLL215 (A), caudal (B).

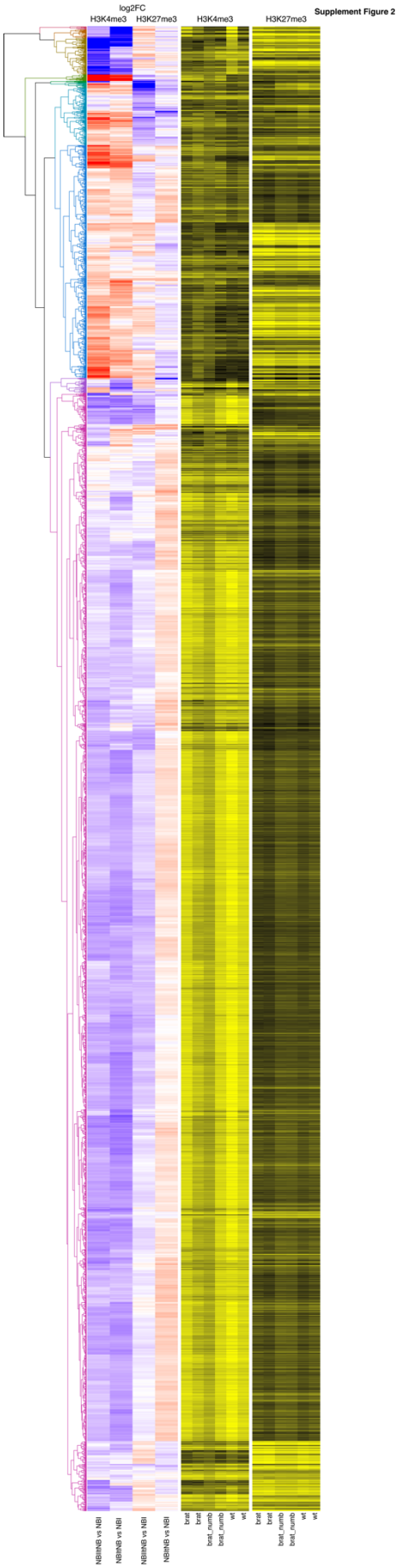
log2FC
H3K4me3
H3K27me3
H3K4me3
H3K27me3
Supplement Figure 2
NBIINB vs NBI
NBIINB vs NBI
NBIINB vs NBI
NBIINB vs NBI
brat
brat
brat_numb
brat_numb
wt
wt
brat
brat
brat_numb
brat_numb
wt
wt

Supplement Figure 2. Full heatmap of H3K4me3 and H3K27me3 changes between NB samples.

Comprehensive hierarchical clustering analysis for NB samples presented in Figure 3.

Supplement Figure 2

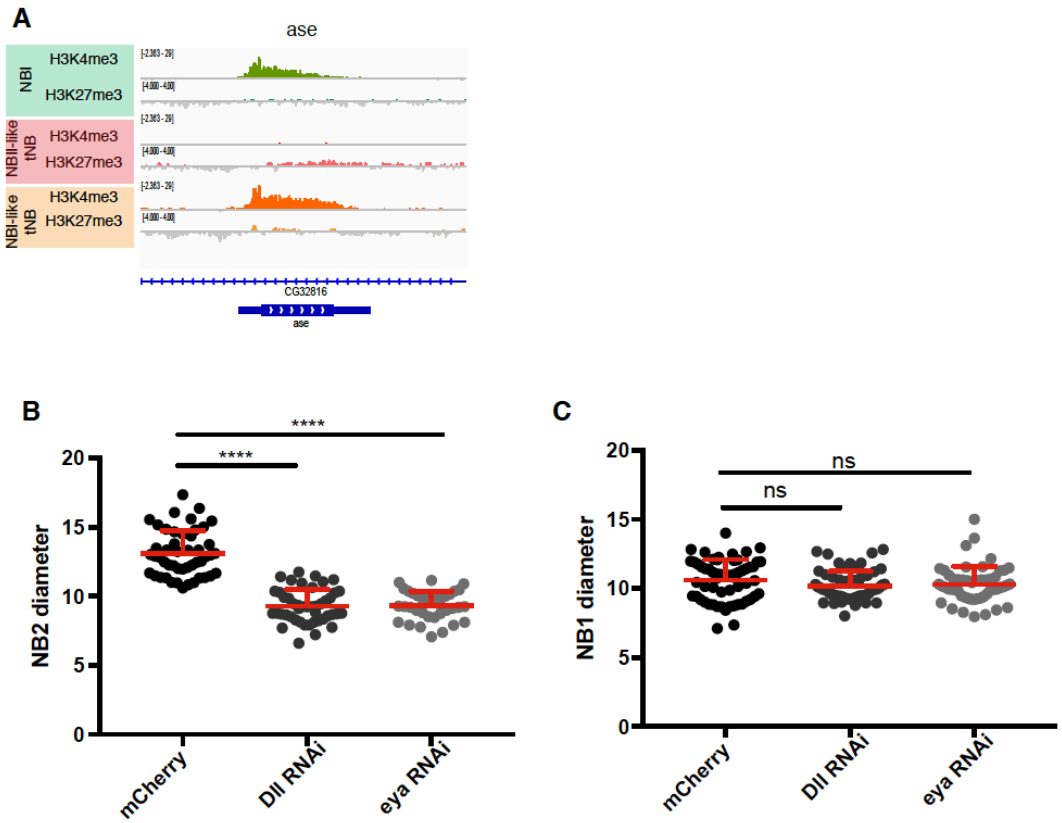

Supplement Figure 3. Dll and eya knockdown affect NBII but not NBI size.

(A) H3K4me3 and H3K27me3 distribution at the *Asense* locus. Measurements of NBII (B) and NBI (C) diameter. Driver line used was UAS-*dicer2*; *insc*-Gal4, UAS-CD8::GFP. Mean ± SD is shown. (for NBII diameter (B) control = 13.09±1.66 (n = 48), *Dll* = 9.29±1.21 (n = 45) and *eya* = 9.34±1.02 (n = 37), and for NBI diameter (C) control = 10.61±1.48 (n=60), *Dll* = 10.17± 1.07 (n=60) and *eya* = 10.28±1.33 (n=52)). One-way ANOVA test was used and ****p < 0.0001, ns = not significant. n numbers are lineages quantified.

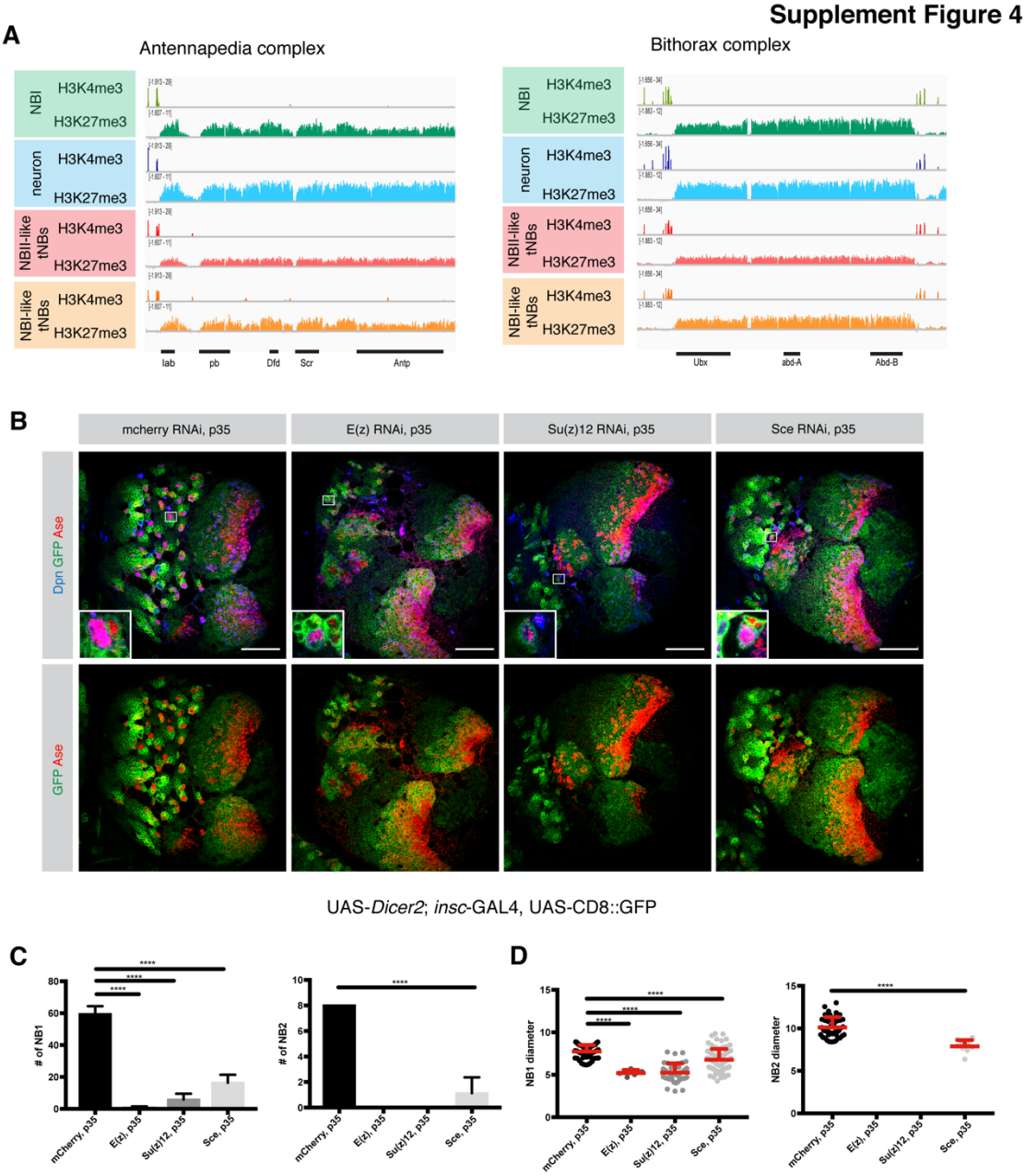

Supplement Figure 4. NBI and NBII neurogenesis depend on PcG with different sensitivity

(A) ChIP-seq tracks of the HOX gene clusters; Antennapedia and Bithorax. (B) Pupal brains expressing apoptosis inhibitor P35 together with mCherry, *E(z), Su(z)* and *Sce* RNAi constructs. PcG loss causes smaller NBI (blow-ups). Scale bar 50 µm. Driver line used was UAS-*dicer2*; *insc*-Gal4, UAS-CD8::GFP. (C) Quantification of NBI and NBII numbers in (B). Mean ± SD is shown (for NBI, mCherry+P35 = 59.43±4.93 (n=7), *E(z)*+P35 = 0.62±0.91 (n=8), *Su(z)12*+P35 = 5.85±3.62 (n=8) and *Sce*+P35 = 16.38±4.98 (n=8) and for NBII, mCherry+P35 = 8 (n=7), *E(z)*+P35 = NA, *Su(z)12*+P35 = NA and *Sce*+P35 = 1.12±1.24 (n=8)). One-way ANOVA test was used and ****p < 0.0001. (D) Quantification of NBI and NBII diameter in (B). Mean ± SD (for NBI, mCherry+P35 = 7.74±0.76 (n=60), *E(z)*+P35 =

5.19±0.37 (n=5), *Su(z)12*+P35 = 5.15±0.92 (n=41) and *Sce*+P35 = 5.74±0.82 (n=80) and for NBII, mCherry+P35 = 10.12±1.2 (n=43), *E(z)*+P35 = NA, *Su(z)12*+P35 = NA and *Sce*+P35 = 7.88±0.73 (n=9)) One-way ANOVA test was used and ****p < 0.0001.

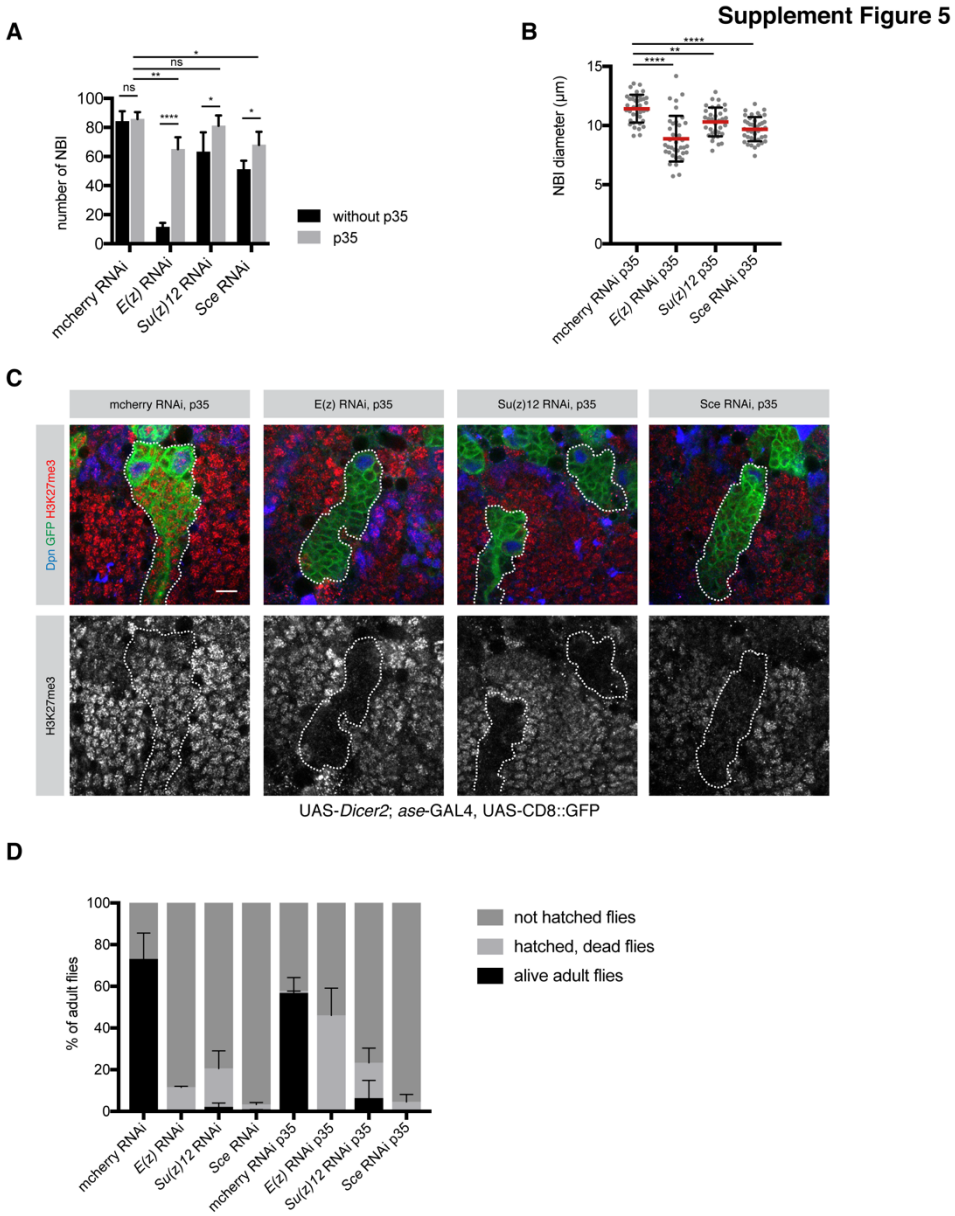

Supplement Figure 5. Blocking apoptosis in PcG depleted NB lineages does not restore neurogenesis.

(A) Number of NBI in L3 larval brains upon RNAi-depletion of PcG genes with and without blocking apoptosis with p35. Mean ± SD. ANOVA test and * p<0.05, ** p<0.005, *** p<0.0005, ns not significant. n= 5 brain lobes, except for *E(z)* RNAi and *Su(z)12* RNAi n=4 brain lobes. Driver line UAS-*dicer2*; *ase*-GAL4, UAS-CD8::GFP was used. (B) Quantification of the NBI cell size of apoptosis-blocked mCherry (n=38), *E(z)* (n=37), *Su(z)12* (n=34), *Sce* (n=41)

RNAi-depleted NBIs. n numbers are NBI numbers, each time from 3 different brain lobes. Driver line used was UAS-*dicer2*; *ase*-GAL4, UAS-CD8::GFP. Mean ± SD. ANOVA test and ** p<0.005, **** p<0.00005. (C) H3K27me3 levels upon the knockdown of PcG genes. Exemplarily NBI lineages are outlined. Driver line used was UAS-*dicer2*; *ase*-GAL4, UAS-CD8::GFP. Scale bar 10µm. (D) Quantification of adult flies that are alive, hatched but dead and did not hatch. For all conditions n=3 independent viability assays. UAS-*dicer2*; *ase*-GAL4. Mean ± SD.

GO-term	**p-value**	**matches**
DNA replication [GO:0006260]	3.05E-21	36
DNA-dependent DNA replication [GO:0006261]	2.49E-19	32
DNA metabolic process [GO:0006259]	2.02E-13	46
cell cycle [GO:0007049]	3.55E-11	69
cell cycle process [GO:0022402]	5.42E-10	59
DNA replication initiation [GO:0006270]	9.46E-08	14
mitotic cell cycle [GO:0000278]	1.36E-07	50
mitotic cell cycle process [GO:1903047]	2.17E-05	39
DNA repair [GO:0006281]	3.23E-03	26
regulation of cell cycle [GO:0051726]	1.90E-02	33
cellular response to DNA damage stimulus [GO:0006974]	1.16E-01	27
regulation of cell cycle process [GO:0010564]	1.57E-01	24
regulation of mitotic cell cycle [GO:0007346]	3.49E+00	23
DNA conformation change [GO:0071103]	4.82E+00	23
DNA recombination [GO:0006310]	6.97E+00	17
DNA-dependent DNA replication maintenance of fidelity [GO:0045005]	8.10E+00	8
positive regulation of cell cycle [GO:0045787]	1.02E+01	14
DNA packaging [GO:0006323]	1.36E+01	21
cellular aromatic compound metabolic process [GO:0006725]	1.63E+01	108
heterocycle metabolic process [GO:0046483]	1.79E+01	106
nuclear division [GO:0000280]	2.81E+01	29
nucleobase-containing compound metabolic process [GO:0006139]	5.94E+01	102
organic cyclic compound metabolic process [GO:1901360]	6.43E+01	108
positive regulation of cell cycle process [GO:0090068]	8.34E+01	11
organelle fission [GO:0048285]	9.15E+01	29
cell cycle DNA replication [GO:0044786]	1.75E+02	10
positive regulation of mitotic cell cycle [GO:0045931]	3.04E+02	10
cell population proliferation [GO:0008283]	6.07E+02	29
chromosome organization [GO:0051276]	6.49E+02	44

meiosis I cell cycle process [GO:0061982]	0.001276	15
organelle organization [GO:0006996]	0.001479	85
microtubule cytoskeleton organization [GO:0000226]	0.001894	27
nucleic acid metabolic process [GO:0090304]	0.002222	89
stem cell proliferation [GO:0072089]	0.002577	15
DNA strand elongation involved in DNA replication [GO:0006271]	0.003373	6
DNA strand elongation [GO:0022616]	0.003373	6
nucleosome assembly [GO:0006334]	0.005838	13
spindle organization [GO:0007051]	0.010199	15
nuclear chromosome segregation [GO:0098813]	0.010349	18
positive regulation of G1/S transition of mitotic cell cycle [GO:1900087]	0.010396	5
microtubule-based process [GO:0007017]	0.011679	31
neuroblast proliferation [GO:0007405]	0.012103	13
positive regulation of mitotic cell cycle phase transition [GO:1901992]	0.013766	7
regulation of cell cycle phase transition [GO:1901987]	0.019088	13
double-strand break repair [GO:0006302]	0.020510	12
cell division [GO:0051301]	0.022294	22
neural precursor cell proliferation [GO:0061351]	0.029439	13
meiotic cell cycle [GO:0051321]	0.030725	20
protein-DNA complex assembly [GO:0065004]	0.031200	15
positive regulation of cell cycle phase transition [GO:1901989]	0.033009	7
microtubule cytoskeleton organization involved in mitosis [GO:1902850]	0.033019	12
meiosis I [GO:0007127]	0.035216	10
cell cycle phase transition [GO:0044770]	0.036278	14
chromosome segregation [GO:0007059]	0.039454	18
chromatin assembly [GO:0031497]	0.040166	13

Supplement Table 1: GO-term analysis of genes with decreased H3K4me3 in neurons compared to NBIs.

GO-term enrichment analysis for genes of cluster 4 (related to Fig. 2).

7. Discussion

Here, in this thesis, we used *Drosophila* neuroblasts as a model system to study different aspects of regulation of stem cell lineages. In chapter 1, we dissected the mechanisms underlying temporal patterning. We proposed a new model for the regulation of temporal patterning. In chapter 2, we have provided a powerful resource and new candidates for NB subtype-specification.

In the future, studying the underlying mechanisms of how these gene networks regulate the neuronal fate decisions would allow us to understand the complexity of brain and its functions. For instance, the incoherent feed-forward loop that we proposed for INP temporal patterning can be investigated in mammalian CNS development. The two-dimensional nature of temporal patterning in type II lineages implicates that fate decisions require different steps of regulation, where each step is more complicated than turn on/off switch system of TFs. With recent advances in single-cell analysis and development of advanced cell culture system as cerebral cortex organoids, one can investigate how the temporal patterning progress in mammalian CNS development.

By studying chromatin states, we can uncover how the cell fate decisions are primed. With investigation of dynamic changes of histone modifications, we can understand how gene expression programs have been initiated and maintained. Understanding how these fate decisions are made will improve our understanding of lineage progression.

In summary, these studies have proven that *Drosophila* is an excellent model system to understand CNS development in depth.

8. References

Arama, E., Dickman, D., Kimchie, Z., Shearn, A., & Lev, Z. (2000). Mutations in the β-propeller domain of the Drosophila brain tumor (brat) protein induce neoplasm in the larval brain. *Oncogene*, *19*(33), 3706–3716. http://doi.org/10.1038/sj.onc.1203706

Artavanis-Tsakonas, S., & Simpson, P. (1991). Choosing a cell fate: a view from the Notch locus. *Trends in Genetics : TIG*, *7*(11-12), 403–408.

Atwood, S. X., & Prehoda, K. E. (2009). aPKC phosphorylates Miranda to polarize fate determinants during neuroblast asymmetric cell division. *Current Biology : CB*, *19*(9), 723–729. http://doi.org/10.1016/j.cub.2009.03.056

Álvarez, J.-A., & Díaz-Benjumea, F. J. (2018). Origin and specification of type II neuroblasts in the Drosophila embryo. *Development (Cambridge, England)*, *145*(7), dev158394. http://doi.org/10.1242/dev.158394

Baumgardt, M., Karlsson, D., Terriente, J., Díaz-Benjumea, F. J., & Thor, S. (2009). Neuronal subtype specification within a lineage by opposing temporal feed-forward loops. *Cell*, *139*(5), 969–982. http://doi.org/10.1016/j.cell.2009.10.032

Bayraktar, O. A., & Doe, C. Q. (2013). Combinatorial temporal patterning in progenitors expands neural diversity. *Nature*, *498*(7455), 449–455. http://doi.org/10.1038/nature12266

Bayraktar, O. A., Boone, J. Q., Drummond, M. L., & Doe, C. Q. (2010). Drosophila type II neuroblast lineages keep Prospero levels low to generate large clones that contribute to the adult brain central complex. *Neural Development*, *5*, 26. http://doi.org/10.1186/1749-8104-5-26

Bello, B. C., Izergina, N., Caussinus, E., & Reichert, H. (2008). Amplification of neural stem cell proliferation by intermediate progenitor cells in Drosophila brain development. *Neural Development*, *3*(1), 5. http://doi.org/10.1186/1749-8104-3-5

Bello, B., Reichert, H., & Hirth, F. (2006). The brain tumor gene negatively regulates neural progenitor cell proliferation in the larval central brain of Drosophila.

Berdnik, D., Török, T., González-Gaitán, M., & Knoblich, J. A. (2002). The endocytic protein alpha-Adaptin is required for numb-mediated asymmetric cell division in Drosophila. *Developmental Cell*, *3*(2), 221–231.

Berger, C., Harzer, H., Burkard, T. R., Steinmann, J., van der Horst, S., Laurenson, A.-S., et al. (2012). FACS Purification and Transcriptome Analysis of Drosophila Neural Stem Cells Reveals a Role for Klumpfuss in Self-Renewal. *Cell Reports*, *2*(2), 407–418. http://doi.org/10.1016/j.celrep.2012.07.008

Betschinger, Joerg, Mechtler, K., & Knoblich, J. A. (2006). Asymmetric Segregation of the Tumor Suppressor Brat Regulates Self-Renewal in Drosophila Neural Stem Cells. *Cell*, *124*(6), 1241–1253. http://doi.org/10.1016/j.cell.2006.01.038

Betschinger, Jörg, Mechtler, K., & Knoblich, J. A. (2003). The Par complex directs asymmetric cell division by phosphorylating the cytoskeletal protein Lgl. *Nature*, *422*(6929), 326–330. http://doi.org/10.1038/nature01486

Bhat, K. M. (1999). Segment polarity genes in neuroblast formation and identity specification during Drosophila neurogenesis. *BioEssays : News and Reviews in Molecular, Cellular and Developmental Biology*, *21*(6), 472–485. http://doi.org/10.1002/(SICI)1521-1878(199906)21:6<472::AID-BIES4>3.0.CO;2-W

Boone, J. Q., & Doe, C. Q. (2008). Identification of Drosophila type II neuroblast lineages containing transit amplifying ganglion mother cells. *Developmental Neurobiology*, *68*(9), 1185–1195. http://doi.org/10.1002/dneu.20648

Bowman, S. K., Neumueller, R. A., Novatchkova, M., Du, Q., & Knoblich, J. A. (2006). The Drosophila NuMA homolog mud regulates spindle orientation in asymmetric cell division. *Developmental Cell*, *10*(6), 731–742. http://doi.org/10.1016/j.devcel.2006.05.005

Bowman, S. K., Rolland, V., Betschinger, J., Kinsey, K. A., Emery, G., & Knoblich, J. A. (2008). The Tumor Suppressors Brat and Numb Regulate Transit-Amplifying Neuroblast Lineages in Drosophila. *Developmental Cell*, *14*(4), 535–546. http://doi.org/10.1016/j.devcel.2008.03.004

Brand, A. H., & Livesey, F. J. (2011). Neural stem cell biology in vertebrates and invertebrates: more alike than different? *Neuron*, *70*(4), 719–729. http://doi.org/10.1016/j.neuron.2011.05.016

Broadus, J., & Doe, C. Q. (1997). Extrinsic cues, intrinsic cues and microfilaments regulate asymmetric protein localization in Drosophila neuroblasts. *Current Biology*, *7*(11), 827–835. http://doi.org/10.1016/s0960-9822(06)00370-8

Brown, J. L., Mucci, D., Whiteley, M., Dirksen, M.-L., & Kassis, J. A. (1998). The Drosophila Polycomb Group Gene pleiohomeotic Encodes a DNA Binding Protein with Homology to the Transcription Factor YY1. *Molecular Cell*, *1*(7), 1057–1064. http://doi.org/10.1016/S1097-2765(00)80106-9

Caussinus, E., & Gonzalez, C. (2005). Induction of tumor growth by altered stem-cell asymmetric division in Drosophila melanogaster. *Nature Genetics*, *37*(10), 1125–1129. http://doi.org/10.1038/ng1632

Ceron, J., Tejedor, F. J., & Moya, F. (2006). A primary cell culture of Drosophila postembryonic larval neuroblasts to study cell cycle and asymmetric division. *European Journal of Cell Biology*, *85*(6), 567–575. http://doi.org/10.1016/j.ejcb.2006.02.006

Chell, J. M., & Brand, A. H. (2010). Nutrition-Responsive Glia Control Exit of Neural Stem Cells from Quiescence. *Cell*, *143*(7), 1161–1173. http://doi.org/10.1016/j.cell.2010.12.007

Choksi, S. P., Southall, T. D., Bossing, T., Edoff, K., de Wit, E., Fischer, B. E., et al. (2006). Prospero Acts as a Binary Switch between Self-Renewal and Differentiation in Drosophila Neural Stem Cells. *Developmental Cell*, *11*(6), 775–789. http://doi.org/10.1016/j.devcel.2006.09.015

Colombani, J., Raisin, S., Pantalacci, S., Radimerski, T., Montagne, J., & Leopold, P. (2003). A nutrient sensor mechanism controls Drosophila growth. *Cell*, *114*(6), 739–749. http://doi.org/10.1016/s0092-8674(03)00713-x

Cotton, M., Benhra, N., & Le Borgne, R. (2013). Numb Inhibits the Recycling of Sanpodo in Drosophila Sensory Organ Precursor. *Current Biology*, *23*(7), 581–587. http://doi.org/10.1016/j.cub.2013.02.020

Couturier, L., Mazouni, K., & Schweisguth, F. (2013). Numb Localizes at Endosomes and Controls the Endosomal Sorting of Notch after Asymmetric Division in Drosophila. *Current Biology*, *23*(7), 588–593. http://doi.org/10.1016/j.cub.2013.03.002

Dessaud, E., McMahon, A. P., & Briscoe, J. (2008). Pattern formation in the vertebrate neural tube: a sonic hedgehog morphogen-regulated transcriptional network. *Development (Cambridge, England)*, *135*(15), 2489–2503. http://doi.org/10.1242/dev.009324

Dillard, C., Narbonne-Reveau, K., Foppolo, S., Lanet, E., & Maurange, C. (2018). Two distinct mechanisms silence chinmo in Drosophila neuroblasts and neuroepithelial cells to limit their self-renewal. *Development (Cambridge, England)*, *145*(2), dev154534. http://doi.org/10.1242/dev.154534

Ding, R., Weynans, K., Bossing, T., Barros, C. S., & Berger, C. (2016). The Hippo signalling pathway maintains quiescence in Drosophila neural stem cells. *Nature Communications*, *7*, 10510. http://doi.org/10.1038/ncomms10510

Doe, C. Q. (2017). Temporal Patterning in the Drosophila CNS. *Annual Review of Cell and Developmental Biology*, *33*(1), 219–240. http://doi.org/10.1146/annurev-cellbio-111315-125210

Dumstrei, K., Wang, F., & Hartenstein, V. (2003). Role of DE-Cadherin in Neuroblast Proliferation, Neural Morphogenesis, and Axon Tract Formation in DrosophilaLarval Brain Development. *The Journal of Neuroscience*, *23*(8), 3325–3335. http://doi.org/10.1523/JNEUROSCI.23-08-03325.2003

Eroglu, E., Burkard, T. R., Jiang, Y., Saini, N., Homem, C. C. F., Reichert, H., & Knoblich, J. A. (2014). SWI/SNF complex prevents lineage reversion and induces temporal patterning in neural stem cells. *Cell*, *156*(6), 1259–1273. http://doi.org/10.1016/j.cell.2014.01.053

Farnsworth, D. R., Bayraktar, O. A., & Doe, C. Q. (2015). Aging Neural Progenitors Lose Competence to Respond to Mitogenic Notch Signaling. *Current Biology*, *25*(23), 3058–3068. http://doi.org/10.1016/j.cub.2015.10.027

Froldi, F., Szuperak, M., Weng, C.-F., Shi, W., Papenfuss, A. T., & Cheng, L. Y. (2015). The transcription factor Nerfin-1 prevents reversion of neurons into neural stem cells. *Genes & Development*, *29*(2), 129–143. http://doi.org/10.1101/gad.250282.114

Fuse, N., Hisata, K., Katzen, A. L., & Matsuzaki, F. (2003). Heterotrimeric G Proteins Regulate Daughter Cell Size Asymmetry in Drosophila Neuroblast Divisions. *Current Biology*, *13*(11), 947–954. http://doi.org/10.1016/S0960-9822(03)00334-8

Gaspard, N., Bouschet, T., Hourez, R., Dimidschstein, J., Naeije, G., van den Ameele, J., et al. (2008). An intrinsic mechanism of corticogenesis from embryonic stem cells. *Nature*, *455*(7211), 351–357. http://doi.org/10.1038/nature07287

Gateff, E. (1994). Tumor suppressor and overgrowth suppressor genes of Drosophila melanogaster: developmental aspects. *The International Journal of Developmental Biology*, *38*(4), 565–590.
Gateff, E., Löffler, T., & Wismar, J. (1993). A temperature-sensitive brain tumor suppressor mutation of Drosophila melanogaster: developmental studies and molecular localization of the gene. *Mechanisms of Development*, *41*(1), 15–31.
Grosskortenhaus, R., Pearson, B. J., Marusich, A., & Doe, C. Q. (2005). Regulation of temporal identity transitions in Drosophila neuroblasts. *Developmental Cell*, *8*(2), 193–202. http://doi.org/10.1016/j.devcel.2004.11.019
Grosskortenhaus, R., Robinson, K. J., & Doe, C. Q. (2006). Pdm and Castor specify late-born motor neuron identity in the NB7-1 lineage. *Genes & Development*, *20*(18), 2618–2627. http://doi.org/10.1101/gad.1445306
Haenfler, J. M., Kuang, C., & Lee, C.-Y. (2012). Cortical aPKC kinase activity distinguishes neural stem cells from progenitor cells by ensuring asymmetric segregation of Numb. *Developmental Biology*, *365*(1), 219–228. http://doi.org/10.1016/j.ydbio.2012.02.027
Harris, R. E., Pargett, M., Sutcliffe, C., Umulis, D., & Ashe, H. L. (2011). Brat Promotes Stem Cell Differentiation via Control of a Bistable Switch that Restricts BMP Signaling. *Developmental Cell*, *20*(1), 72–83. http://doi.org/10.1016/j.devcel.2010.11.019
Holguera, I., & Desplan, C. (2018). Neuronal specification in space and time. *Science (New York, N.Y.)*, *362*(6411), 176–180. http://doi.org/10.1126/science.aas9435
Homem, C. C. F., & Knoblich, J. A. (2012). Drosophila neuroblasts: a model for stem cell biology. *Development (Cambridge, England)*, *139*(23), 4297–4310. http://doi.org/10.1242/dev.080515
Homem, C. C. F., Reichardt, I., Berger, C., Lendl, T., & Knoblich, J. A. (2013). Long-term live cell imaging and automated 4D analysis of drosophila neuroblast lineages. *PloS One*, *8*(11), e79588. http://doi.org/10.1371/journal.pone.0079588
Homem, C. C. F., Steinmann, V., Burkard, T. R., Jais, A., Esterbauer, H., & Knoblich, J. A. (2014). Ecdysone and mediator change energy metabolism to terminate proliferation in Drosophila neural stem cells. *Cell*, *158*(4), 874–888. http://doi.org/10.1016/j.cell.2014.06.024
Ikeshima-Kataoka, H., Skeath, J. B., Nabeshima, Y.-I., Doe, C. Q., & Matsuzaki, F. (1997). Miranda directs Prospero to a daughter cell during Drosophila asymmetric divisions. *Nature*, *390*(6660), 625–629. http://doi.org/10.1038/37641
Ingham, P. W. (1985). A clonal analysis of the requirement for the trithorax gene in the diversification of segments in Drosophila. *Journal of Embryology and Experimental Morphology*, *89*, 349–365.
Isshiki, T., Pearson, B., Holbrook, S., & Doe, C. Q. (2001). Drosophila neuroblasts sequentially express transcription factors which specify the temporal identity of their neuronal progeny. *Cell*, *106*(4), 511–521.
Ito, K., & Hotta, Y. (1992). Proliferation pattern of postembryonic neuroblasts in the brain of Drosophila melanogaster. *Developmental Biology*, *149*(1), 134–148. http://doi.org/10.1016/0012-1606(92)90270-Q

Izergina, N., Balmer, J., Bello, B., & Reichert, H. (2009). Postembryonic development of transit amplifying neuroblast lineages in the Drosophila brain. *Neural Development*, *4*(1), 44. http://doi.org/10.1186/1749-8104-4-44

Izumi, Y., Ohta, N., Hisata, K., Raabe, T., & Matsuzaki, F. (2006). Drosophila Pins-binding protein Mud regulates spindle-polarity coupling and centrosome organization. *Nature Cell Biology*, *8*(6), 586–593. http://doi.org/10.1038/ncb1409

Janssens, D. H., Hamm, D. C., Anhezini, L., Xiao, Q., Siller, K. H., Siegrist, S. E., et al. (2017). An Hdac1/Rpd3-Poised Circuit Balances Continual Self-Renewal and Rapid Restriction of Developmental Potential during Asymmetric Stem Cell Division. *Developmental Cell*, *40*(4), 367–380.e7. http://doi.org/10.1016/j.devcel.2017.01.014

Janssens, D. H., Komori, H., Grbac, D., Chen, K., Koe, C. T., Wang, H., & Lee, C.-Y. (2014). Earmuff restricts progenitor cell potential by attenuating the competence to respond to self-renewal factors. *Development (Cambridge, England)*, *141*(5), 1036–1046. http://doi.org/10.1242/dev.106534

Jennings, B. H. (2011). Drosophila – a versatile model in biology & medicine. *Materials Today*, *14*(5), 190–195. http://doi.org/10.1016/S1369-7021(11)70113-4

Kadoch, C., & Crabtree, G. R. (2015). Mammalian SWI/SNF chromatin remodeling complexes and cancer: Mechanistic insights gained from human genomics. *Science Advances*, *1*(5), e1500447. http://doi.org/10.1126/sciadv.1500447

Kanai, M. I., Okabe, M., & Hiromi, Y. (2005). Seven-up controls switching of transcription factors that specify temporal identities of Drosophila neuroblasts. *Developmental Cell*, *8*(2), 203–213. http://doi.org/10.1016/j.devcel.2004.12.014

Kassis, J. A., Kennison, J. A., & Tamkun, J. W. (2017). Polycomb and Trithorax Group Genes in Drosophila. *Genetics*, *206*(4), 1699–1725. http://doi.org/10.1534/genetics.115.185116

Knoblich, J A, Jan, L. Y., & Jan, Y. N. (1997). The N terminus of the Drosophila Numb protein directs membrane association and actin-dependent asymmetric localization. *Proceedings of the National Academy of Sciences*, *94*(24), 13005–13010. http://doi.org/10.1073/pnas.94.24.13005

Knoblich, Juergen A. (2010). Asymmetric cell division: recent developments and their implications for tumour biology. *Nature Reviews. Molecular Cell Biology*, *11*(12), 849–860. http://doi.org/10.1038/nrm3010

Knoblich, Jürgen A, Jan, & Jan, Y. N. (1995). Asymmetric segregation of Numb and Prospero during cell division. *Nature*, *377*(6550), 624–627. http://doi.org/10.1038/377624a0

Koe, C. T., Li, S., Rossi, F., Wong, J. J. L., Wang, Y., Zhang, Z., et al. (2014). The Brm-HDAC3-Erm repressor complex suppresses dedifferentiation in Drosophila type II neuroblast lineages. *eLife*, *3*, e01906.

Kohwi, M., Lupton, J. R., Lai, S.-L., Miller, M. R., & Doe, C. Q. (2013). Developmentally regulated subnuclear genome reorganization restricts

neural progenitor competence in Drosophila. *Cell*, *152*(1-2), 97–108. http://doi.org/10.1016/j.cell.2012.11.049
Komori, H., Xiao, Q., Janssens, D. H., Dou, Y., & Lee, C.-Y. (2014a). Trithorax maintains the functional heterogeneity of neural stem cells through the transcription factor Buttonhead. *eLife*, *3*. http://doi.org/10.7554/eLife.03502
Komori, H., Xiao, Q., McCartney, B. M., & Lee, C.-Y. (2014b). Brain tumor specifies intermediate progenitor cell identity by attenuating β-catenin/Armadillo activity. *Development (Cambridge, England)*, *141*(1), 51–62. http://doi.org/10.1242/dev.099382
Kraut, R., Chia, W., Jan, L. Y., Jan, Y. N., & Knoblich, J. A. (1996). Role of inscuteable in orienting asymmetric cell divisions in Drosophila. *Nature*, *383*(6595), 50–55. http://doi.org/10.1038/383050a0
Lai, S.-L., & Doe, C. Q. (2014). Transient nuclear Prospero induces neural progenitor quiescence. *eLife*, *3*. http://doi.org/10.7554/eLife.03363
Landskron, L., Steinmann, V., Bonnay, F., Burkard, T. R., Steinmann, J., Reichardt, I., et al. (2018). The asymmetrically segregating lncRNA cherub is required for transforming stem cells into malignant cells. *eLife*, *7*, R106. http://doi.org/10.7554/eLife.31347
Le Borgne, R., Bardin, A., & Schweisguth, F. (2005). The roles of receptor and ligand endocytosis in regulating Notch signaling. *Development (Cambridge, England)*, *132*(8), 1751–1762. http://doi.org/10.1242/dev.01789
Lee, C.-Y., Andersen, R. O., Cabernard, C., Manning, L., Tran, K. D., Lanskey, M. J., et al. (2006a). Drosophila Aurora-A kinase inhibits neuroblast self-renewal by regulating aPKC/Numb cortical polarity and spindle orientation. *Genes & Development*, *20*(24), 3464–3474. http://doi.org/10.1101/gad.1489406
Lee, C.-Y., Robinson, K. J., & Doe, C. Q. (2006b). Lgl, Pins and aPKC regulate neuroblast self-renewal versus differentiation. *Nature*, *439*(7076), 594–598. http://doi.org/10.1038/nature04299
Lee, C.-Y., Wilkinson, B. D., Siegrist, S. E., Wharton, R. P., & Doe, C. Q. (2006c). Brat is a Miranda cargo protein that promotes neuronal differentiation and inhibits neuroblast self-renewal. *Developmental Cell*, *10*(4), 441–449. http://doi.org/10.1016/j.devcel.2006.01.017
Lewis, E. B. (1978). A Gene Complex Controlling Segmentation in <Emphasis Type="Italic">Drosophila</Emphasis>. In *Genes, Development and Cancer* (Vol. 16, pp. 205–217). Boston, MA: Springer, Boston, MA. http://doi.org/10.1007/978-1-4419-8981-9_13
Li, Xiaosu, Xie, Y., & Zhu, S. (2016). Notch maintains Drosophila type II neuroblasts by suppressing the expression of the Fez transcription factor Earmuff. *Development (Cambridge, England)*, dev.136184. http://doi.org/10.1242/dev.136184
Li, Xin, Erclik, T., Bertet, C., Chen, Z., Voutev, R., Venkatesh, S., et al. (2013). Temporal patterning of Drosophila medulla neuroblasts controls neural fates. *Nature*, *498*(7455), 456–462. http://doi.org/10.1038/nature12319
Linford, N. J., Bilgir, C., Ro, J., & Pletcher, S. D. (2013). Measurement of Lifespan in Drosophila melanogaster. *Jove-Journal of Visualized Experiments*, (71), e50068. http://doi.org/10.3791/50068

Liu, K., Shen, D., Shen, J., Gao, S. M., Li, B., Wong, C., et al. (2017). The Super Elongation Complex Drives Neural Stem Cell Fate Commitment. *Developmental Cell*, *40*(6), 537–551.e6. http://doi.org/10.1016/j.devcel.2017.02.022

Liu, Z., Yang, C.-P., Sugino, K., Fu, C.-C., Liu, L.-Y., Yao, X., et al. (2015). Opposing intrinsic temporal gradients guide neural stem cell production of varied neuronal fates. *Science (New York, N.Y.)*, *350*(6258), 317–320. http://doi.org/10.1126/science.aad1886

Lu, B., Rothenberg, M., Jan, L. Y., & Jan, Y. N. (1998). Partner of Numb colocalizes with Numb during mitosis and directs Numb asymmetric localization in Drosophila neural and muscle progenitors. *Cell*, *95*(2), 225–235. http://doi.org/10.1016/s0092-8674(00)81753-5

Marchetti, G., Reichardt, I., Knoblich, J. A., & Besse, F. (2014). The TRIM-NHL Protein Brat Promotes Axon Maintenance by Repressing src64B Expression. *The Journal of Neuroscience*, *34*(41), 13855–13864. http://doi.org/10.1523/JNEUROSCI.3285-13.2014

Maurange, C., Cheng, L., & Gould, A. P. (2008a). Temporal Transcription Factors and Their Targets Schedule the End of Neural Proliferation in Drosophila. *Cell*, *133*(5), 891–902. http://doi.org/10.1016/j.cell.2008.03.034

Maurange, C., Cheng, L., & Gould, A. P. (2008b). Temporal transcription factors and their targets schedule the end of neural proliferation in Drosophila. *Cell*, *133*(5), 891–902. http://doi.org/10.1016/j.cell.2008.03.034

Mettler, U., Vogler, G., & Urban, J. (2006). Timing of identity: spatiotemporal regulation of hunchback in neuroblast lineages of Drosophila by Seven-up and Prospero. *Development (Cambridge, England)*, *133*(3), 429–437. http://doi.org/10.1242/dev.02229

Mummery-Widmer, J. L., Yamazaki, M., Stoeger, T., Novatchkova, M., Bhalerao, S., Chen, D., et al. (2009). Genome-wide analysis of Notch signalling in Drosophila by transgenic RNAi. *Nature*, *458*(7241), 987–992. http://doi.org/10.1038/nature07936

Naka, H., Nakamura, S., Shimazaki, T., & Okano, H. (2008). Requirement for COUP-TFI and II in the temporal specification of neural stem cells in CNS development. *Nature Neuroscience*, *11*(9), 1014–1023. http://doi.org/10.1038/nn.2168

Neumüller, R. A., Richter, C., Fischer, A., Novatchkova, M., Neumüller, K. G., & Knoblich, J. A. (2011). Genome-wide analysis of self-renewal in Drosophila neural stem cells by transgenic RNAi. *Cell Stem Cell*, *8*(5), 580–593. http://doi.org/10.1016/j.stem.2011.02.022

Ogawa, H., Ohta, N., Moon, W., & Matsuzaki, F. (2009). Protein phosphatase 2A negatively regulates aPKC signaling by modulating phosphorylation of Par-6 in Drosophila neuroblast asymmetric divisions. *J Cell Sci*, *122*(Pt 18), 3242–3249. http://doi.org/10.1242/jcs.050955

Otsuki, L., & Brand, A. H. (2018). Cell cycle heterogeneity directs the timing of neural stem cell activation from quiescence. *Science (New York, N.Y.)*, *360*(6384), 99–. http://doi.org/10.1126/science.aan8795

O'Connor-Giles, K. M., & Skeath, J. B. (2003). Numb Inhibits Membrane Localization of Sanpodo, a Four-Pass Transmembrane Protein, to

Promote Asymmetric Divisions in Drosophila. *Developmental Cell*, *5*(2), 231–243. http://doi.org/10.1016/S1534-5807(03)00226-0
Prokop, A., & Technau, G. M. (1991). The origin of postembryonic neuroblasts in the ventral nerve cord of Drosophila melanogaster. *Development (Cambridge, England)*, *111*(1), 79–88.
Read, R. D. (2011). Drosophila melanogaster as a model system for human brain cancers. *Glia*, *59*(9), 1364–1376. http://doi.org/10.1002/glia.21148
Read, R. D., Cavenee, W. K., Furnari, F. B., & Thomas, J. B. (2009). A Drosophila Model for EGFR-Ras and PI3K-Dependent Human Glioma. *PLoS Genetics*, *5*(2), e1000374. http://doi.org/10.1371/journal.pgen.1000374
Rebollo, E., Roldán, M., & Gonzalez, C. (2009). Spindle alignment is achieved without rotation after the first cell cycle in Drosophila embryonic neuroblasts. *Development (Cambridge, England)*, *136*(20), 3393–3397. http://doi.org/10.1242/dev.041822
Rebollo, E., Sampaio, P., Januschke, J., Llamazares, S., Varmark, H., & Gonzalez, C. (2007). Functionally unequal centrosomes drive spindle orientation in asymmetrically dividing Drosophila neural stem cells. *Developmental Cell*, *12*(3), 467–474. http://doi.org/10.1016/j.devcel.2007.01.021
Reichert, H. (2011). <Emphasis Type="Italic">Drosophila</Emphasis> Neural Stem Cells: Cell Cycle Control of Self-Renewal, Differentiation, and Termination in Brain Development. In *Cell Cycle in Development* (Vol. 122, pp. 529–546). Berlin, Heidelberg: Springer, Berlin, Heidelberg. http://doi.org/10.1007/978-3-642-19065-0_21
Rhyu, M. S., Jan, L. Y., & Jan, Y. N. (1994). Asymmetric distribution of numb protein during division of the sensory organ precursor cell confers distinct fates to daughter cells. *Cell*, *76*(3), 477–491.
Rusan, N. M., & Peifer, M. (2007). A role for a novel centrosome cycle in asymmetric cell division. *Journal of Cell Biology*, *177*(1), 13–20. http://doi.org/10.1083/jcb.200612140
San-Juán, B. P., & Baonza, A. (2011). The bHLH factor deadpan is a direct target of Notch signaling and regulates neuroblast self-renewal in Drosophila. *Developmental Biology*, *352*(1), 70–82. http://doi.org/10.1016/j.ydbio.2011.01.019
Santolini, E., Puri, C., Salcini, A. E., Gagliani, M. C., Pelicci, P. G., Tacchetti, C., & Di Fiore, P. P. (2000). Numb Is an Endocytic Protein. *Journal of Cell Biology*, *151*(6), 1345–1352.
Schaefer, M., Petronczki, M., Dorner, D., Forte, M., & Knoblich, J. A. (2001). Heterotrimeric G proteins direct two modes of asymmetric cell division in the Drosophila nervous system. *Cell*, *107*(2), 183–194. http://doi.org/10.1016/s0092-8674(01)00521-9
Schaefer, M., Shevchenko, A., & Knoblich, J. A. (2000). A protein complex containing Inscuteable and the Galpha-binding protein Pins orients asymmetric cell divisions in Drosophila. *Current Biology*, *10*(7), 353–362. http://doi.org/10.1016/s0960-9822(00)00401-2
Schuettengruber, B., Bourbon, H.-M., Di Croce, L., & Cavalli, G. (2017). Genome Regulation by Polycomb and Trithorax: 70 Years and Counting. *Cell*, *171*(1), 34–57. http://doi.org/10.1016/j.cell.2017.08.002

Schuettengruber, B., Chourrout, D., Vervoort, M., Leblanc, B., & Cavalli, G. (2007). Genome regulation by polycomb and trithorax proteins. *Cell*, *128*(4), 735–745. http://doi.org/10.1016/j.cell.2007.02.009

Shan, Z., Tu, Y., Yang, Y., Liu, Z., Zeng, M., Xu, H., et al. (2018). Basal condensation of Numb and Pon complex via phase transition during Drosophila neuroblast asymmetric division. *Nature Communications*, *9*(1), 737. http://doi.org/10.1038/s41467-018-03077-3

Shen, C.-P., Jan, L. Y., & Jan, Y. N. (1997). Miranda Is Required for the Asymmetric Localization of Prospero during Mitosis in Drosophila. *Cell*, *90*(3), 449–458. http://doi.org/10.1016/S0092-8674(00)80505-X

Siegrist, S. E., Haque, N. S., Chen, C.-H., Hay, B. A., & Hariharan, I. K. (2010). Inactivation of both Foxo and reaper promotes long-term adult neurogenesis in Drosophila. *Current Biology : CB*, *20*(7), 643–648. http://doi.org/10.1016/j.cub.2010.01.060

Siller, K. H., Cabernard, C., & Doe, C. Q. (2006). The NuMA-related Mud protein binds Pins and regulates spindle orientation in Drosophila neuroblasts. *Nature Cell Biology*, *8*(6), 594–600. http://doi.org/10.1038/ncb1412

Sipe, C. W., & Siegrist, S. E. (2017). Eyeless uncouples mushroom body neuroblast proliferation from dietary amino acids in Drosophila. *eLife*, *6*, 166. http://doi.org/10.7554/eLife.26343

Skeath, J. B., & Doe, C. Q. (1998). Sanpodo and Notch act in opposition to Numb to distinguish sibling neuron fates in the Drosophila CNS. *Development (Cambridge, England)*, *125*(10), 1857–1865. http://doi.org/10.1126/science.7716513

Skeath, J. B., & Thor, S. (2003). Genetic control of Drosophila nerve cord development. *Current Opinion in Neurobiology*, *13*(1), 8–15. http://doi.org/10.1016/S0959-4388(03)00007-2

Smith, C. A., Lau, K. M., Rahmani, Z., Dho, S. E., Brothers, G., She, Y. M., et al. (2007). aPKC-mediated phosphorylation regulates asymmetric membrane localization of the cell fate determinant Numb. *Embo Journal*, *26*(2), 468–480. http://doi.org/10.1038/sj.emboj.7601495

Song, Y., & Lu, B. (2012). Interaction of Notch signaling modulator Numb with α-Adaptin regulates endocytosis of Notch pathway components and cell fate determination of neural stem cells. *The Journal of Biological Chemistry*, *287*(21), 17716–17728. http://doi.org/10.1074/jbc.M112.360719

Sousa-Nunes, R., Chia, W., & Somers, W. G. (2009). Protein phosphatase 4 mediates localization of the Miranda complex during Drosophila neuroblast asymmetric divisions. *Genes & Development*, *23*(3), 359–372. http://doi.org/10.1101/gad.1723609

Sousa-Nunes, R., Yee, L. L., & Gould, A. P. (2011). Fat cells reactivate quiescent neuroblasts via TOR and glial insulin relays in Drosophila. *Nature*, *471*(7339), 508–. http://doi.org/10.1038/nature09867

Spana, E. P., Kopczynski, C., Goodman, C. S., & Doe, C. Q. (1995). Asymmetric localization of numb autonomously determines sibling neuron identity in the Drosophila CNS. *Development (Cambridge, England)*, *121*(11), 3489–3494.

Syed, M. H., Mark, B., & Doe, C. Q. (2017). Steroid hormone induction of temporal gene expression in Drosophila brain neuroblasts generates neuronal and glial diversity. *eLife*, *6*, e26287. http://doi.org/10.7554/eLife.26287

Tocchini, C., & Ciosk, R. (2015). TRIM-NHL proteins in development and disease. *Seminars in Cell & Developmental Biology*, *47-48*, 52–59. http://doi.org/10.1016/j.semcdb.2015.10.017

Touma, J. J., Weckerle, F. F., & Cleary, M. D. (2012). Drosophila Polycomb complexes restrict neuroblast competence to generate motoneurons. *Development (Cambridge, England)*, *139*(4), 657–666. http://doi.org/10.1242/dev.071589

Truman, J. W., & Bate, M. (1988). Spatial and temporal patterns of neurogenesis in the central nervous system of Drosophila melanogaster. *Developmental Biology*, *125*(1), 145–157. http://doi.org/10.1016/0012-1606(88)90067-X

Viktorin, G., Riebli, N., Popkova, A., Giangrande, A., & Reichert, H. (2011). Multipotent neural stem cells generate glial cells of the central complex through transit amplifying intermediate progenitors in Drosophila brain development. *Developmental Biology*, *356*(2), 553–565. http://doi.org/10.1016/j.ydbio.2011.06.013

Walsh, K. T., & Doe, C. Q. (2017). Drosophila embryonic type II neuroblasts: origin, temporal patterning, and contribution to the adult central complex. *Development (Cambridge, England)*, *144*(24), 4552–4562. http://doi.org/10.1242/dev.157826

Wang, Hengbin, Wang, L., Erdjument-Bromage, H., Vidal, M., Tempst, P., Jones, R. S., & Zhang, Y. (2004a). Role of histone H2A ubiquitination in Polycomb silencing. *Nature*, *431*(7010), 873–878. http://doi.org/10.1038/nature02985

Wang, Hongyan, Ouyang, Y., Somers, W. G., Chia, W., & Lu, B. (2007). Polo inhibits progenitor self-renewal and regulates Numb asymmetry by phosphorylating Pon. *Nature*, *449*(7158), 96–100. http://doi.org/10.1038/nature06056

Wang, Hongyan, Somers, G. W., Bashirullah, A., Heberlein, U., Yu, F., & Chia, W. (2006). Aurora-A acts as a tumor suppressor and regulates self-renewal of Drosophila neuroblasts. *Genes & Development*, *20*(24), 3453–3463. http://doi.org/10.1101/gad.1487506

Wang, L., Brown, J. L., Cao, R., Zhang, Y., Kassis, J. A., & Jones, R. S. (2004b). Hierarchical Recruitment of Polycomb Group Silencing Complexes. *Molecular Cell*, *14*(5), 637–646. http://doi.org/10.1016/j.molcel.2004.05.009

Watson, K. L., Justice, R. W., & Bryant, P. J. (1994). Drosophila in cancer research: the first fifty tumor suppressor genes. *J Cell Sci*, *1994*(Supplement 18), 19–33. http://doi.org/10.1242/jcs.1994.Supplement_18.4

Weng, M., & Lee, C.-Y. (2011). Keeping neural progenitor cells on a short leash during Drosophila neurogenesis. *Current Opinion in Neurobiology*, *21*(1), 36–42. http://doi.org/10.1016/j.conb.2010.09.005

Weng, M., Golden, K. L., & Lee, C.-Y. (2010). dFezf/Earmuff maintains the restricted developmental potential of intermediate neural progenitors in

Drosophila. *Developmental Cell*, *18*(1), 126–135. http://doi.org/10.1016/j.devcel.2009.12.007
White, K., & Kankel, D. R. (1978). Patterns of cell division and cell movement in the formation of the imaginal nervous system in Drosophila melanogaster. *Developmental Biology*, *65*(2), 296–321. http://doi.org/10.1016/0012-1606(78)90029-5
Wirtz-Peitz, F., Nishimura, T., & Knoblich, J. A. (2008). Linking cell cycle to asymmetric division: Aurora-A phosphorylates the Par complex to regulate Numb localization. *Cell*, *135*(1), 161–173. http://doi.org/10.1016/j.cell.2008.07.049
Wright, T. R. F. (1987). The Genetics Of Biogenic Amine Metabolism, Sclerotization, And Melanization In Drosophila Melanogaster. *Advances in Genetics*, *24*, 127–222. http://doi.org/10.1016/S0065-2660(08)60008-5
Wu, P.-S., Egger, B., & Brand, A. H. (2008). Asymmetric stem cell division: Lessons from Drosophila. *Seminars in Cell & Developmental Biology*, *19*(3), 283–293. http://doi.org/10.1016/j.semcdb.2008.01.007
Xiao, Q., Komori, H., & Lee, C.-Y. (2012). klumpfuss distinguishes stem cells from progenitor cells during asymmetric neuroblast division. *Development (Cambridge, England)*, *139*(15), 2670–2680. http://doi.org/10.1242/dev.081687
Xie, Y., Li, X., Zhang, X., Mei, S., Li, H., Urso, A., & Zhu, S. (2014). The Drosophila Sp8 transcription factor buttonhead prevents premature differentiation of intermediate neural progenitors. *eLife*, *3*. http://doi.org/10.7554/eLife.03596
Xu, J., Hao, X., Yin, M.-X., Lu, Y., Jin, Y., Xu, J., et al. (2017). Prevention of medulla neuron dedifferentiation by Nerfin-1 requires inhibition of Notch activity. *Development (Cambridge, England)*, *144*(8), 1510–1517. http://doi.org/10.1242/dev.141341
Yang, C.-P., Samuels, T. J., Huang, Y., Yang, L., Ish-Horowicz, D., Davis, I., & Lee, T. (2017). Imp and Syp RNA-binding proteins govern decommissioning of Drosophila neural stem cells. *Development (Cambridge, England)*, dev.149500. http://doi.org/10.1242/dev.149500
Zacharioudaki, E., Falo Sanjuan, J., & Bray, S. (2019). Mi-2/NuRD complex protects stem cell progeny from mitogenic Notch signalling. *eLife*, *8*. http://doi.org/10.7554/eLife.41637
Zacharioudaki, E., Magadi, S. S., & Delidakis, C. (2012). bHLH-O proteins are crucial for Drosophila neuroblast self-renewal and mediate Notch-induced overproliferation. *Development (Cambridge, England)*, *139*(7), 1258–1269. http://doi.org/10.1242/dev.071779
Zhang, Y., Koe, C. T., Tan, Y. S., Ho, J., Tan, P., Yu, F., et al. (2019). The Integrator Complex Prevents Dedifferentiation of Intermediate Neural Progenitors back into Neural Stem Cells. *Cell Reports*, *27*(4), 987–996.e3. http://doi.org/10.1016/j.celrep.2019.03.089
Zhu, S., Barshow, S., Wildonger, J., Jan, L. Y., & Jan, Y. N. (2011). Ets transcription factor Pointed promotes the generation of intermediate neural progenitors in Drosophila larval brains. *Proceedings of the National Academy of Sciences of the United States of America*, *108*(51), 20615–20620. http://doi.org/10.1073/pnas.1118595109

Zhu, S., Lin, S., Kao, C.-F., Awasaki, T., Chiang, A.-S., & Lee, T. (2006). Gradients of the Drosophila Chinmo BTB-zinc finger protein govern neuronal temporal identity. *Cell*, *127*(2), 409–422. http://doi.org/10.1016/j.cell.2006.08.045